THE UNIVERSITY OF MICHIGAN

INDUSTRY PROGRAM OF THE COLLEGE OF ENGINEERING

OPTIMAL OPERATION OF A TUBULAR CHEMICAL REACTOR

Mark R. Newberger

A dissertation submitted in partial fulfillment
of the requirements for the degree of
Doctor of Philosophy in
The University of Michigan
1968

March, 1968

IP-813

"Whenever you feel like criticizing anyone, just remember that all the people in this world haven't had the advantages that you've had."

F. Scott Fitzgerald

TABLE OF CONTENTS

TABLE OF CONTENTS (CONT'D)

TABLE OF CONTENTS (CONT'D)

ACKNOWLEDGMENTS

I would like to express my sincere gratitude to Professor Robert H. Kadlec, chairman of the doctoral committee, for his interest and help and to the members of the doctoral committee whose cooperation and guidance was invaluable.

Special thanks go to my fellow graduate students for assistance with parts of the experimental work, and for their refreshing discussions.

I am also indebted to the shop personnel of the Department of Chemical and Metallurgical Engineering for their suggestions on practical design of equipment.

I would like to acknowledge the Anaconda American Brass Company for providing reactor materials, and the following organizations for financial support: the Michigan Memorial Phoenix Project, the National Science Foundation, the Shell Oil Company, and the Union Carbide Corporation.

I would also like to thank the University of Michigan, College of Engineering Industry Program for assistance in preparation of the manuscript.

Finally, I will always be grateful to my wife, Sharon, for her patience and forebearance and for her excellent typing of this dissertation.

LIST OF TABLES

LIST OF TABLES (CONT'D)

LIST OF FIGURES

LIST OF FIGURES (CONT'D)

LIST OF APPENDICES

NOMENCLATURE

English Alphabet

A	symbol for diethyl adipate
A_o	area for heat transfer, ft.^{2}
a_o	constant proportional to ratio of heating cost to selling price of component R_1
a_1, a_2, a_3	constants defined in Equation (3.39)
B	symbol for hydroxyl ion
b_2	constant defined by Equation (5.15)
C_{A_i}	reactor inlet concentration of component A , mole/l.
C_A, C_{R_1}, C_B	concentrations of A , R_1 , and B , mole/l.
C_c	circumference of turbulent core in stagnant boundary layer model, ft.
C_i	term in objective function J for Rozonoer's modification of the Maximum Principle
$C_{i_{calc}}$	concentration predicted using mathematical model, mole/l.
$C_{i_{Exp}}$	experimentally measured value of concentration, mole/l.
C_t, C_s, C_w	tube and shell fluid and tube wall heat capacities, BTU/lb./°F
$C_1, \ldots, C_4$	constants defined in Appendix G
D, D_A, D_{R_1}	molecular diffusivities, ft.^{2}/sec.
D_e	effective axial dispersion, ft.^{2}/sec.
D_i, D_o	inside and outside diameters, ft.
EtOH	symbol for ethanol

E_1, E_2, E_3	activation energies in Arrhenius equation, cal./g.mole
f_i	component of $\vec{f}$
$\vec{f}$	vector of right hand sides of state equations
$f(Re)$	graphical function given by Sieder and Tate
F_1, F_2, F_3, F_4	defined in Equations (3.83) - (3.86)
G_{A_o}	molar rate of diester entering reactor, mole/hr.
g	defined in Equation (7.41)
H	Hamiltonian defined in Equation (3.7)
h_i, h_o	heat transfer coefficients of tube and shell, BTU/hr./ft.^{2}/°F
J	objective function for optimization
K_H	quotient K_w'/K_2' in Appendix E
K_w'	equilibrium constant for water hydrolysis in Appendix E
K_2'	equilibrium constant for dissociation of bicarbonate in Appendix E
k	thermal conductivity BTU/hr./ft./°F
k'	distribution coefficient
k_m	mass transfer coefficient, ft./sec.
k_w	thermal conductivity of tube wall, BTU/hr./ft./°F
k_1, k_2, k_3	reaction rate constants, l/g.mole/sec.
$k_{1_o}, k_{2_o}, k_{3_o}$	frequency factor in Arrhenius equation, l/g.mole/sec.
$k_{1_{ext}}$	value of k_1 for which $\frac{\partial H}{\partial k_1} = 0$

k_{1_i}	a value of k_1 lying in the range $k_{1_*} < k_1 < k_1^*$
$k_{1_{optimal}}$	value of k_1 which satisfies conditions of the Maximum Principle
k_1^* and k_{1_*}	upper and lower limits on k_1 corresponding to T^* and T_*
$\vec{k}$	vector $[k_1 , k_2]'$
L	reactor length, ft.
M	the absolute maximum value of H
M_n	nth moment defined in Equation (5.12)
M_n^c	nth central moment defined in Equation (5.14)
N	mass flux, mole/sec/ft.^{2}
Pe	Peclet number
Pr	Prandtl number
Q_{tube}, Q_{shell}	heat transferred by tube and shell fluid, BTU/hr.
q	wall heat flux into reactor, cal./sec./ft.^{2}
q_{ext}	value of q for which $\frac{\partial H}{\partial q} = 0$
$q_{singular}$	value of q which causes H to remain independent of q
q^*, q_*	upper and lower limits on q in idealized reactor problems, cal./sec./ft.^{2}
R	gas constant, cal./g.mole/°K
Re	Reynolds number
R_i, R_o	inner and outer tube radii, ft.

R_1	symbol for monoethyl adipate
R_2	symbol for adipate ion
r	radial coordinate direction, ft.
r_i	volumetric rates of production of species i , mole/sec./l.
S	cross sectional area, $ft.^2$
S_c	Schmidt number
S_o, S_1	manifold of allowable initial and final points for trajectory of $\vec{x}$
T	temperature, units are indicated at point of use
T_{OPT}	optimal inlet temperature
T_T, T_S	tube and shell fluid temperatures
T_w	tube inside wall temperature
T_o, T_1	tangent planes to manifolds S_o and S_1 in statement of the Maximum Principle
T^*, T_*	upper and lower limits on temperature
t	independent variable in general state equations or residence time, sec.
t_f	final residence time, sec.
t_o, t_1	initial and final times in general statement of the Maximum Principle
U	vector space of all possible values of $\vec{u}$
U_L	heat transfer coefficient for loss to surroundings BTU/hr./$ft.^2$/°F
U_o	overall heat transfer coefficient, BTU/hr./$ft.^2$/°F

u_i	component of vector $\vec{u}$
$\vec{u}$	vector of control variables
v	velocity, ft./sec.
W_T, W_S	tube shell flow rate, lb./hr.
X	vector space of all possible values of $\vec{x}$
x_i	general state variable
$\vec{x}$	vector of general state variables
$\vec{x}_o, \vec{x}_1$	initial and final values of $\vec{x}$
Y_B	mole ratio of hydroxyl ion, mole/(mole A entering reactor)
Y_1, Y_A	mole ratio of component A , mole/(mole A entering reactor)
Y_2, Y_{R_1}	mole ratio of component R_1 , mole/(mole A entering reactor)
Y_3	the symbol for temperature when used in state equations
z	distance along reactor axis from inlet, ft.
$\bar{z}$	dimensionless position, z/L

Greek Alphabet

$\alpha_1, \alpha_2, \alpha_3$	constants defined in Equations (7.25)
α	defined in Equation (7.8)
$-\Delta H_{1,2}$	heats of reaction for saponification of diethyl adipate
δ	boundary layer thickness, ft.
θ	dimensionless time
θ_o, θ_i	vectors lying in or parallel to planes T_o and T_1
μ	viscosity centipoise

$\mathcal{M}'$	defined by Equation (5.13)
ρ	density of tube fluid, lb./ft.^{3}
ρ_w	density of tube wall, lb./ft.^{3}
τ	difference between tube fluid and wall temperatures
Ψ_i	component of $\vec{\Psi}$
$\vec{\Psi}$	vector of adjoint variables

Subscripts (if unspecified)

b	bulk fluid
f	final
ext	extermal
i	initial or inside
in	initial
n	highest index on state variables, or total number of data points
o	outside
opt	optimal
s	shell
t	tube
w	at wall

Superscripts (if unspecified)

'	transpose of a vector
.	denotes differentiation with respect to t , i.e. $\frac{d}{dt}$
-	average value or indicating a Laplace Transform

ABSTRACT

A theoretical and experimental study was conducted on the optimal steady state operation of a jacketed tubular reactor in which two consecutive, second order, homogeneous, liquid phase chemical reactions occurred in turbulent flow. The reactor was ten, 15 foot lengths of 0.25 inch O.D. by 0.025 inch wall thickness copper tubing concentric with 0.625 inch O.D. x 0.040 inch wall thickness tubing. Inner tubes were connected in series. Pairs of outer tubes were connected forming five shell sections. Hot water flow through each shell section ranging from 0 to 600 pound/hour controlled reactant temperature. Reactant flow rate was constant at 197 pound/hour. Tube Reynolds and Prandtl numbers varied from 7,800 and 5.7 at 85°F to 18,500 and 2.1 at 185°F. The chemical reaction was the successive saponification of diethyl adipate by sodium hydroxide in aqueous solution. Reactor inlet concentrations for diethyl adipate, monoethyl adipate, and hydroxyl ion were 0.018, 0.002, and 0.053 g.moles/l. respectively.

The plug flow model with the heat transfer correlation of Sieder and Tate satisfactorily predicted reactor performance. Sufficient conditions were established on Reynolds and Schmidt numbers and on reaction activation energies for use of the plug flow model in larger scale reactors. Direct and gradient search methods were employed with the plug flow model to determine hot water flow rates in the shell sections which maximized monoethyl adipate (middle product) yield at

the reactor exit. The yield was maximized with no flow in the first two shell sections, intermediate flow in the third, and maximum flow in the final two sections. The optimal value of the third shell flow rate was sensitive to reactor inlet conditions, but optimal reactor yield was insensitive to shell flow changes.

The Pontryagin Maximum Principle was used to predict temperature profiles and wall heat flux profiles to maximize middle product yield at the reactor exit for first and second order consecutive reactions. The temperature should be at the lowest possible value (28°C) over the first part of the reactor, followed by a jump to the highest possible temperature (85°C).

The predicted yield with the optimal temperature profile was 0.69 moles monoester per mole of diester entering the reactor, compared with 0.67 for the experimental reactor operating optimally, 0.65 for the optimal heat flux problem, and 0.61 for optimal isothermal operation. For the optimal wall heat flux problem, the maximum allowable heat flux was taken as the average heat flux in the experimental reactor which was operating optimally. The optimal policy was to set the inlet temperature at 27.7°C and to use full heating along the entire reactor length.

The optimal temperature profile gives an upper bound on yield in all real reactors. For complex reactions it is easier to determine this upper bound from the optimal heat flux problem with constraints set to include all possible values of heat flux in the real reactor.

Other objective functions were considered to minimize total heating for a given reactor yield, and to maximize more general profit functions.

Over the range 29-85°C frequency factors and activation energies for saponification of diethyl and monoethyl adipate were determined to be:

$k_{1_o} = 4.87 \times 10^6$ l./g.mole/sec. $\quad E_1 = 10080$ cal./g.mole

$k_{2_o} = 3.49 \times 10^3$ l./g.mole/sec. $\quad E_2 = 5965$ cal./g.mole

Measured heats of reaction were 10.8 and 16.3 kcal./g.mole respectively.

Chemical analysis for monoethyl adipate was based on extraction of diethyl adipate using benzene. The equilibrium distribution of monoethyl adipate between benzene and water at 25°C is in the ratio of 0.0033:1.

1. INTRODUCTION

A natural application of high speed computation in chemical engineering has been the optimal design and operation of processing equipment. In recent years, application of variational techniques as well as numerical "search" methods have shown that the performance of many chemical reactors may be improved by operating in a non-isothermal fashion. These studies have for the most part been confined to mathematical models and computer simulation. "Optimal" solutions have been found for idealized reactors with major emphasis on the optimization technique rather than an accurate model of the physical reactor.

The main objectives of this research were twofold. A class of optimization problems was solved for first and second order consecutive reactions occurring in a plug flow tubular reactor. For these idealized models, the Pontryagin Maximum Principle was employed. In most cases, the objective of the problem was to maximize the exit concentration of middle product. In addition, other objective functions were considered which took into account the cost of operation. Next, the saponification of diethyl adipate with sodium hydroxide was studied in a jacketed tubular reactor. The jacket was divided into five sections so that reactant temperature and reaction rate could be controlled by varying the flow rates of hot water in the jacket sections. A mathematical model of this reactor was developed. The model predicted reactor performance within experimental uncertainty. It was then used to predict the jacket flow rates required to produce optimal operation.

The idealized reactor amenable to study by the Maximum Principle and the reactor used in this study were related by comparing the results of optimal operation in the two cases. Finally, sensitivity of the exit concentration to perturbations in jacket flow rates was predicted and compared with experimental results.

In the course of this research, several other mathematical models were tried to account for boundary layer effects. This work provides a basis for scaleup to larger diameter reactors and higher Reynolds numbers.

2. LITERATURE SURVEY

A literature survey in the field of chemical reactor modeling and optimization covers many related areas in the engineering and mathematics literatures. This survey has been divided into six topics in an attempt to logically organize this diverse literature.

A. General Literature Surveys

Several authors have attempted to organize various phases of the literature in much greater detail than is done here. Wilhelm[127] in "Progress Towards the A Priori Design of Chemical Reactors," gives several hundred references on all phases of reactor design and modeling. This work contains a commentary on what could and could not be accurately predicted in 1962 and the author's opinions on important areas of research. Professor Denbigh's newest book Chemical Reactor Theory [38] also is a survey of the current state of the art. It gives excellent insight in a qualitative manner on factors which improve operation in various types of reactors. J. Beek[13] has surveyed the literature on packed catalytic reactors. His discussion of the mathematical complexities and difficulties in modeling this type of reactor is highly recommended. Levenspiel and Bischoff[83] present a similar survey on "Patterns of Flow in Chemical Process Vessels." They concentrated in the area of mixing effects and non-ideal reactors. The need for more experimental evidence to support mathematical models is clearly brought out. A comprehensive survey on many phases of reactor design, also considering dynamic operation has been given by Simpkins.[111] A bibliography in the broad area of "Reaction Engineering" has been prepared by Hoelscher.[57]

It contains 584 references divided into 43 areas. Finally, many references to the mathematical theory of optimization and optimal control are cited by Tou.[116]

B. Experimental Tubular Reactor Studies

There have been quite a few experimental studies of tubular reactor performance. In general, only exit compositions were measured. Havorka and Kendall[53] have studied the saponification of ethyl acetate at low flow rates (laminar flow). They significantly increased conversion by using baffles to promote mixing. Weger and Hoelscher[121] studied the catalytic hydrogenation of olefins over palladium black catalyst. Lloyd and Amundson[84] studied the reduction of ferric oxide in a tubular reactor. Their article presents a good discussion of complications and gives many useful suggestions for successful reactor operation. Baron et al.[11] have described the catalytic oxidation of sulpher dioxide in a tubular reactor. Recently Raines and Corrigan[96] reported using the axial diffusion model to describe experimental data in packed reactors. Pauls et al.[91] and Simpkins[111] have performed experimental dynamic response studies on tubular reactors. Batten[12] has described the possibility of obtaining erroneous results when measuring rate constants in tubular reactors with constricted entrance and exit sections. There are no concentration profile data for consecutive reactions occurring in tubular reactors.

C. Kinetics of Consecutive Reactions

A comprehensive survey of theoretical and experimental studies concerning the determination of reaction rate constants for consecutive

reactions is given by Friedman.[48] His work contains twenty-five references on this subject. Texts such as that of Frost and Pearson[49] and Hougen et al.[61] present discussions on consecutive reactions but numerical values of rate constants are generally lacking. Ingold,[62] Frost and Schwemer,[50] and Westheimer et al.[125] give experimentally determined values of the rate constants for the saponification of diethyl adipate with sodium hydroxide, the system used in this study. These authors studied many diesters at a single temperature to obtain the effect of various substituents on reaction rates. Ball and Groenweghe[10] in a recent paper described a general procedure for obtaining rate constants for complex systems. Several numerical examples for consecutive reactions are presented. They utilized the non-linear regression technique also employed in this study. No mention is given to the serious effect of small experimental errors in applying this method.

D. Heat Transfer and Axial Mixing

The large amount of data on heat transfer coefficients in pipes is summarized by the correlation of Sieder and Tate.[110] Texts such as that of Bird et al.[17] present a complete discussion and important references on this subject. Of historical interest, the work of Colburn[31] first showed how an effective overall heat transfer coefficient might be obtained when the local coefficient varied along the tube. Smith et al.[112] have recently presented complete radial temperature profile data for turbulent flow in pipes heated at the wall.

The mathematical model required to describe the effects of axial dispersion on tubular reactor performance has received a great deal of study. Dankwerts[35] first described the effects of incomplete mixing

and concentration gradients on yields in homogeneous reactors. G. I. Taylor[114] showed that a radial velocity profile and radial mixing yielded the same residence time distribution as an effective axial dispersion model. The proper boundary conditions to use with an axial dispersion model have been discussed by Dankwerts,[35] Wehner and Wilhelm,[122] Fan and Ahn,[44] and finally and most clearly by Bischoff.[19] Fan and Bailie[45] presented calculated isothermal profiles for several orders of chemical reactions. Levenspiel and Bischoff[83] present calculated profiles for first and second order reactions. This was extended by Douglass and Bischoff[41] to include variable density effects. Recently, Weinstein and Adler[124] proposed a model which takes account of micromixing effects in continuous reactors.

The available data on effective axial dispersion for flow in straight pipes is correlated by Levenspiel.[82] However, Carter and Bir[27] measured axial diffusivities in a high pressure ethylene reactor containing twelve 180° bends, and obtained values on the order of three times those given by Levenspiel. Bischoff[18] has postulated that straight pipe and mixer sections could be used to approximate reactor bends but could not be quantitative for lack of sufficient experimental data. Tichacek[115] and Hawthorn[54] have given modifications of Taylor's analysis to account for variations in fluid properties. Carberry[25] has shown that for first order isothermal reactions occurring in packed beds with practical (L/D) ratios, the dispersion number (reciprocal Peclet number) is so small that axial dispersion has a negligible effect on conversion. Coste et al.[32] applied the axial dispersion model to a reactor with a highly exothermic reaction. They considered dispersion

of both heat and mass and found that forward integration led to unstable solutions. A cell model approximation did, however, yield a stable solution which satisfied the original equations integrated backwards in time. Carberry and Wendel[26] used a finite difference solution to avoid this difficulty.

There has been only one work describing an unpacked tubular reactor in which axial dispersion was important. This work of Spencer[113] was designed to verify the axial dispersion model. The reactor consisted of a stationary inner tube and an outer tube rotating at high speed. Reaction took place in the annular space. Radial gradients were shown to be negligible so that only axial diffusion was important. The axial dispersion model was found to fit experimental data. However, this reactor in no way resembled a conventional tubular reactor where axial dispersion is due to radial diffusion and a non-uniform radial velocity profile (Taylor Diffusion).

Kramers and Westerterp[73] have discussed the effect of dispersion on conversion to middle product for consecutive reactions. Tichacek[115] has calculated the effect for first and second order consecutive reactions. Hoelscher[56] gives the effect of a non-flat velocity profile on conversion for first order consecutive reactions.

E. Mathematical Theory of Optimization and Optimal Control

In the past ten years the mathematical literature in the areas of optimization and optimal control has greatly expanded. This was due in part to the advent of high speed computers, for all recent developments require high speed computation for their ultimate usefulness.

Coutie and Box[33] were one of the first to describe numerical exploration of complex response surfaces. Many efficient search techniques have been developed to locate maxima in complex response surfaces. These include the gradient method described by Zellnick et al.,[129] and Boas,[21] the direct search of Hooke and Jeeves,[59] the rotating coordinate method of Rosenbrock,[100,101] and quadratically convergent methods of Powell[95] and Fletcher and Reeves.[46] Dynamic programming developed by Bellman[14] has been used successfully for staged systems. The agrange multiplier technique is generally used when equality constraints cannot be eliminated. However, an interesting illustration of a case in which the Lagrange multiplier technique fails was given by Roberts.[98] An optimization of a nitric oxide plant considering sixteen variables was described by Chu et al.[30]

Until the late 1950's, the only available theory for the determination of optimal trajectories was based on the calculus of variations. The work of Pontryagin et al.[94] published in 1958 in Russian and in 1962 in English helped reawaken interest in this area of research. It is the primary reference on the Maximum Principle. Rozonoer[105] very clearly summarized the Maximum Principle and has shown some interesting applications. A geometric interpretation was given by Roxin.[104]

Marcus and Lee[87] proved several existence theorems for optimal controls. Kipiniak[69] and Lawden[76] have used the calculus of variations to solve optimal trajectory problems. Neustadt,[89] and Chen and Ceaglske[29] have applied the discrete Maximum Principle, while Katz[67] used a numerical method based on the calculus of variations to optimize staged systems. Jackson[63] has given a variational treatment

for optimization of complex systems. Denn et al.[39] have applied the ideas of the Maximum Principle to optimize distributed parameter systems. The works of Lee,[79] and Chang[28] treat optimal control problems with constrained state variables. Krasovskii[74] has comprehensively reviewed the Soviet literature.

For complex systems, the Maximum Principle and the calculus of variations are often too difficult to apply. An alternative termed the gradient technique in function space is described by Bryson and Denham[23] and also employed by Kelly.[68] Breakwell[22] formulated the necessary conditions for the problems considered by Bryson and Denham. Rothenberger,[102,103] and Lee[81] have employed quasilinearization to solve the two point boundary value problems obtained from the Maximum Principle and the gradient technique, whereas Freeman and Houghton[47] used a singular perturbation method. Summaries and comparisons of the different methods are described by Rosenbrock and Storey[101] and by Parker.[90]

F. Modeling and Optimization of Tubular Chemical Reactors

Denbigh was one of the first to show that controlled temperature profiles in reactors could lead to improved performance. This was clearly verified by Aris in his exposition on optimal reactor design via dynamic programming.[9] Katz[66] determined optimal temperature profiles for some first order reactions occurring in plug flow reactors using the calculus of variations. The pioneering work considering consecutive reactions was that of Bilous and Amundson.[15] They employed functional differentiation to obtain necessary equations for optimal temperature profiles. They also first showed the possibility of instability in

tubular reactors due to perturbations in feed compositions and wall heat transfer coefficient.[16] Aris[8,9] employed dynamic programming, as well as the Maximum Principle to obtain optimal temperature profiles for consecutive first order reactions, whereas Horn[60] used the calculus of variations for consecutive and more complex reactor optimization. Shatkhan[107] utilized the Maximum Principle for parallel reactions. Lee[78] used the gradient technique to find optimal temperature profiles for first order consecutive reactions, and in a later work[79] solved the same problem using the Maximum Principle on the analog computer. Mah and Aris[86] considered consecutive reversible reactions. Siebenthal and Aris[109] applied the Maximum Principle for batch and tubular reactor studies. Van de Vusse and Voetter[118] determined optimum pressure and concentration gradients along a tubular reactor. Ahlgen and Stevens have considered the very practical problem of optimization in the presence of errors.[3]

Adler and Vortmeyer[1,2] considered the effect of axial dispersion on optimum yields for first order reversible reactions. Ahn[4] has also considered the axial dispersion model as well as several other models and applied optimization theory to each. Jackson[64] used the Maximum Principle to obtain the optimal startup procedure for an autothermic reaction. His problem contained two control variables and also illustrated the case of intermediate or "singular" control being the optimal control. This article is highly recommended for its logical clarity. Gray[52] found optimal wall heat flux profiles for a packed reactor modeled by partial differential equations.

There are several descriptions in the literature of the optimization of industrial reactors. Annable[6] has given a partial optimization of an ammonia catalytic reactor. Calderbank[24] found optimal temperature profiles for a sulfur dioxide converter, and Johnson[65] has determined the optimal temperature profile for the hydrogenation of carbon in a moving bed reactor.

3. THE PONTRYAGIN MAXIMUM PRINCIPLE AND APPLICATIONS

In this chapter the main theorems of the Pontryagin Maximum Principle are stated using the notation of Pontryagin et al.[94] Proofs of these theorems are omitted, since they are quite lengthy and have been dealt with fully by several authors.[94,104,105] It is shown that in certain cases, a somewhat different but exactly equivalent statement of the Maximum Principle due to Rozonoer is more directly applied.

A. The Maximum Principle

Consider that the state of a dynamic system may be described by a set of first order ordinary differential equations:[94]

$$\frac{dx_i}{dt} = f_i(x_1, x_2, \ldots, x_n, u_1, u_2, \ldots u_r) \quad i=1,\ldots n \tag{3.1}$$

or in vector form:

$$\frac{d\vec{x}}{dt} = \vec{f}(\vec{x}, \vec{u}) \tag{3.2}$$

"t" represents the independent variable of the system. To simplify this discussion, "t" is referred to as time, but it may just as well represent position or another independent variable. $\vec{x}$ represents a set of dependent variables describing the condition of the system. The x_i's may represent concentrations, temperature, velocity, etc., and are called "state variables." $\vec{u}$ represents a set of independent variables which may be manipulated in order to guide the system from a given state $\vec{x}_0$ at time t_0 to some final state $\vec{x}_1$ at time t_1.

The set $\vec{u}$ are called "control variables." The vector $\vec{x}$ is defined in the vector space X and $\vec{u}$ in U. The functions $\vec{f}$ must be continuous and have continuous partial derivatives with respect to the x_i.

The control $\vec{u}(t)$ is said to be "optimal" if the functional:

$$J = \int_{t_0}^{t_1} f_0(\vec{x}, \vec{u})\, dt \tag{3.3}$$

is minimized.

Now define the new variable x_0 by:

$$\frac{dx_0}{dt} = f_0(\vec{x}, \vec{u}) \quad , \quad x_0(t_0) = 0 \tag{3.4}$$

The system of Equations (3.1) may therefore be extended to include x_0, Equation (3.4). Notice that $\vec{f} = (f_0, f_1, \ldots, f_n)'$ does not depend on x_0. Equation (3.4) may be rewritten in the form:

$$x_0(t) = \int_{t_0}^{t} f_0(\vec{x}, \vec{u})\, dt$$

When $t = t_1$, the final time, we have:

$$x_0(t_1) = \int_{t_0}^{t_1} f_0(\vec{x}, \vec{u})\, dt = J \tag{3.5}$$

Thus, if $\vec{x}$ must begin in the region (manifold) S_0 of the space X at time t_0 and end in S_1 at time t_1, then the optimal control is one which takes $\vec{x}$ from S_0 to S_1 at time t_1 and minimizes $x_0(t_1)$.

Now also consider an additional set of variables, $\vec{\psi} = (\psi_0, \psi_1, \ldots \psi_n)'$ called adjoint variables and defined by:

$$\frac{d\psi_i}{dt} = -\sum_{j=0}^{n} \frac{\partial f_j}{\partial x_i} \cdot \psi_j \quad , \quad i = 0, 1, \ldots, n \tag{3.6}$$

Notice that Equation (3.6) represents a system of linear equations, homogeneous in $\vec{\psi}$. Define the function H which is analogous to the Hamiltonian of classical mechanics as the dot product of the vectors $\vec{\psi}$ and $\vec{f}$:

$$H = \vec{\psi} \cdot \vec{f} = \sum_{j=0}^{n} \psi_j f_j(\vec{x}, \vec{u}) \tag{3.7}$$

Equations (3.1), (3.4), and (3.6) may now be compactly written in terms of the Hamiltonian as:

$$\begin{aligned} \frac{dx_i}{dt} &= \frac{\partial H}{\partial \psi_i} \\ \frac{d\psi_i}{dt} &= -\frac{\partial H}{\partial x_i} \end{aligned} \qquad i = 0, 1, \ldots n \tag{3.8}$$

For given values of $\vec{\psi}$ and $\vec{x}$, let

$$M = \underset{\vec{u} \in U}{\text{abs. max.}} H(\vec{\psi}, \vec{x}, \vec{u}) \tag{3.9}$$

the statement $\vec{u} \in U$ indicating that $\vec{u}$ is chosen in the allowable region U . The following theorem is then the necessary condition for optimality:

Theorem 1.

Let $\vec{u}(t)$, $t_0 \leq t \leq t_1$, be a permissible control such that the corresponding trajectory $\vec{x}(t)$ departing at time t_0 from S_0 passes at the instant t_1 through S_1 . A necessary condition for the control

$\vec{u}(t)$ and trajectory $\vec{x}(t)$ to be optimal is that there exists a non-zero vector function:

$\vec{\psi}(t) = (\psi_0(t), \psi_1(t), \ldots, \psi_n(t))'$ corresponding to the functions $\vec{u}(t)$ and $\vec{x}(t)$ given above, such that:

1. Given any t, $t_0 \leq t < t_1$, the function $H(\vec{\psi}(t), \vec{x}(t), \vec{u}(t))$ of the variable $\vec{u} \in U$ attains a maximum at $\vec{u} = \vec{u}(t)$:

$$H(\vec{\psi}(t), \vec{x}(t), \vec{u}(t)) = \mathcal{M}(\vec{\psi}(t), \vec{x}(t)) \tag{3.10}$$

2. At the final instant t_1 (t_1 not fixed in advance) the following relationships are satisfied:

$$\psi_0(t_1) \leq 0 \tag{3.11}$$

$$\mathcal{M}(\vec{\psi}(t_1), \vec{x}(t_1)) = 0 \tag{3.12}$$

Furthermore, as shown in Appendix A, consequences of $\vec{\psi}(t)$ and $\vec{x}(t)$ satisfying the Hamiltonian Equations (3.8) are that the functions $\psi_0(t)$ and $\mathcal{M}(\vec{\psi}(t), \vec{x}(t))$ of the variable t prove to be constant. Hence, verification can be carried out at any instant $t_0 \leq t \leq t_1$, and not necessarily at t_1.

3. For a fixed final time, t_1, the condition in Equation (3.12) no longer holds.

4. For movable end points of the trajectory constrained to lie in manifolds S_0 and S_1, the vector $\vec{\psi}(t)$ must be orthogonal to the manifold of allowable end points, at t_0 and t_1. This is called the transversality condition, and has the following geometric meaning:

Let $\vec{X}(t_0) \in S_0$ and $\vec{X}(t_1) \in S_1$ be the beginning and end of the trajectory $\vec{X}(t)$. Let T_0 and T_1 be tangent planes to S_0 and S_1 respectively at points $\vec{X}(t_0)$ and $\vec{X}(t_1)$. Then every vector $\vec{\theta}_0$ (or θ_1) lying in or parallel to T_0 (or T_1) is orthogonal to $\vec{\psi}(t_0)$ (or $\vec{\psi}(t_1)$).

$$\vec{\psi}(t_0) \cdot \vec{\theta}_0 = 0 \tag{3.13}$$

$$\vec{\psi}(t_1) \cdot \vec{\theta}_1 = 0 \tag{3.14}$$

If a particular component $X_i(t_1)$ is fixed, then the corresponding component θ_i in $\vec{\theta}$ will equal zero. Hence, $\psi_i(t_1)$ will be free. On the other hand, if a particular component $X_i(t_1)$ is completely unconstrained, then $\vec{\psi}(t_1)$ can be orthogonal to $\vec{\theta}$ only if $\psi_i(t_1) = 0$. If the functional J given in Equation (3.3) is to be maximized rather than minimized, it is only necessary to minimize instead of maximize the Hamiltonian, $H(\vec{\psi}, \vec{X}, \vec{u})$. All other statements of the theorem remain unchanged.

B. Rozonoer's Modification

When it is required to minimize or maximize a linear combination of the state variables $\vec{X}$ at $t = t_1$, then the need for defining X_0 is not present since the differential equation defining X_0 will not be independent of the other state equations. Rozonoer[105] suggested the following equivalent formulation:

Suppose it is required to minimize the function

$$J = \sum_{i=1}^{n} C_i X_i(t_1) \tag{3.15}$$

at the final time t_1 . Then the values of the adjoint variables at time t_1 are given by:

$$\psi_i(t_1) = -c_i \quad , \quad i = 1, 2, \ldots, n \tag{3.16}$$

Neither x_0 nor ψ_0 is ever introduced. The remainder of the necessary condition is identical to Pontryagin's formulation. When applicable, Rozonoer's formulation has been found somewhat simpler to use than the original more general theorem.

C. Application of the Maximum Principle to Tubular Reactor Optimization

In the following sections, the Maximum Principle will be applied to optimize operation of a plug flow tubular reactor of fixed length in which simultaneous, consecutive, second order, liquid phase chemical reactions occur. Temperature and heat flux along the reactor are taken as control variables. The numerical values used for reaction activation energies and frequency factors in the Arrhenius rate constant expression are of the order of those for the saponification of diethyl adipate. Although not exact, these values permit adequate representation of the form of the optimal solutions. In later chapters where comparisons with reactor performance are made, optimal solutions using the more exact numerical values are presented.

For this reaction system, the activation energy of the first reaction is higher than that of the second. As shown by Aris,[9] when reactor length is chosen along with the temperature profile, the middle product yield will be maximized by operating a very short reactor at

the highest possible temperature. However, when the reactor length is fixed this policy is no longer optimal, since the peak in middle product concentration will not necessarily occur at the reactor exit.

Six related problems are considered here. The first two determine the temperature and heat flux profiles for a series of two first order reactions which maximize the middle product concentration at the reactor exit. These problems were found to be necessary prerequisites to an understanding of the more difficult third and fourth problems, similar to the first two, but considering simultaneous consecutive second order reactions. The fifth and sixth problems apply different criteria for optimization. The fifth determines the heat flux along the reactor to produce a given yield of middle product while minimizing the total heating along the reactor. The final problem considers maximizing a function of middle product yield and cost of operation.

D. Optimal Temperature Profile for First Order Consecutive Reactions

Consider a plug flow tubular reactor in which the following first order liquid phase reactions occur at steady state:

$$A \xrightarrow{k_1} R_1 \xrightarrow{k_2} R_2 \tag{3.17}$$

The rate constants follow an Arrhenius temperature dependence:

$$k_i = k_{i_0} \exp\left\{-E_i/RT\right\} \quad , \quad i = 1,2 \tag{3.18}$$

and $E_1 > E_2$. The reaction mixture is considered dilute so that the

effect of concentration on total density may be neglected. Furthermore, density is assumed to be independent of temperature. The plug flow assumption as used here assumes that axial velocity and all fluid properties are independent of radial position and that axial as well as radial diffusion may be neglected. Mass balances on components A and R_1 and division by the inlet concentration of component A yield:

$$\frac{dY_1}{dt} = -k_1 Y_1 \tag{3.19}$$

$$\frac{dY_2}{dt} = k_1 Y_1 - k_2 Y_2 \tag{3.20}$$

where Y_1 and Y_2 are moles of A and R_1 per mole of A entering the reactor, and t is residence time, equal to axial position, z, divided by fluid velocity, v. The problem in question may now be stated as follows:

How shall the fluid temperature be held along the reactor to maximize the yield of component R_1 at the reactor exit, $t = t_f$? The temperature is constrained according to:

$$T_* \leq T \leq T^* \tag{3.21}$$

Utilizing Rozonoer's modification of the Maximum Principle, maximize:

$$J = \sum_{i=1}^{2} c_i Y_i = 0\, Y_1(t_f) + 1\, Y_2(t_f) \tag{3.22}$$

whereby:

$$\psi_1(t_f) = 0 \,, \quad \psi_2(t_f) = -1 \tag{3.23}$$

The Hamiltonian has the form:

$$H = \vec{\psi} \cdot \vec{f} = -\psi_1 k_1 Y_1 + \psi_2 (k_1 Y_1 - k_2 Y_2)$$
$$= k_1 Y_1 (\psi_2 - \psi_1) - \psi_2 k_2 Y_2 \qquad (3.24)$$

The adjoint equations are:

$$\frac{d\psi_1}{dt} = -\frac{\partial H}{\partial Y_1} = -k_1 (\psi_2 - \psi_1) \qquad (3.25)$$

$$\frac{d\psi_2}{dt} = -\frac{\partial H}{\partial Y_2} = k_2 Y_2 \qquad (3.26)$$

By solving each of Equations (3.18) for temperature, T, and equating the two expressions, k_2 may be written in terms of k_1, and temperature eliminated. The result is:

$$k_2 = k_2 (k_1) = k_{2_0} (k_1 / k_{1_0})^{E_2/E_1} \qquad (3.27)$$

Since k_1 is a single valued function of temperature, k_1 may be considered the new control variable. Combining Equation (3.24) and (3.27) to eliminate k_2:

$$H = k_1 Y_1 (\psi_2 - \psi_1) - \psi_2 k_{2_0} (k_1 / k_{1_0})^{E_2/E_1} \qquad (3.28)$$

Now choose k_1 in $k_{1_*} \leq k_1 \leq k_1^*$ to <u>minimize</u> H. If H attains a minimum value with $k_1 = k_{1_i}$, an interior point in $k_{1_*} < k_1 < k_1^*$, then:

$$\left.\frac{\partial H}{\partial k_1}\right|_{k_1=k_{1i}} = 0$$

$$\left.\frac{\partial^2 H}{\partial k_1^2}\right|_{k_1=k_{1i}} > 0$$

$$H(k_{1i}) \leq H(k_1) \;,\; k_{1*} \leq k_1 \leq k_1^* \tag{3.29}$$

If the conditions of Equation (3.29) cannot be fulfilled, then H attains an absolute minimum value on the boundary of the allowable region, in this case at either k_{1*} or k_1^* .

Differentiating Equation (3.24) with respect to k_1 :

$$\frac{\partial H}{\partial k_1} = \gamma_1(\psi_2-\psi_1) - \gamma_2\psi_2 \frac{k_{20}}{(k_{10})^{E_2/E_1}} \cdot \frac{E_2}{E_1} \cdot k_1^{(E_2-E_1)/E_1} \tag{3.30}$$

$$\frac{\partial^2 H}{\partial k_1} = \frac{\gamma_2\psi_2 k_{20}}{(k_{10})^{E_2/E_1}} \cdot \frac{E_2}{E_1} \cdot \frac{E_1-E_2}{E_1} \cdot k_1^{\left(\frac{E_2}{E_1}-2\right)} \tag{3.31}$$

All factors of Equation (3.31) except for ψ_2 are known, <u>a priori</u>, to be positive. Consequently, the sign of ψ_2 determines whether H has a maximum, minimum or point of inflection at $\frac{\partial H}{\partial k_1} = 0$. To ascertain the character of ψ_2 , the adjoint variables need be examined in the phase space shown on the next page:

The following arguments center about the adjoint Equations (3.25) and (3.26) and known final conditions (3.23), which are repeated below:

$$\frac{d\psi_1}{dt} = k_1(\psi_1-\psi_2) \tag{3.25}$$

$$\frac{d\psi_2}{dt} = k_2\psi_2 \tag{3.26}$$

$$\psi_1(t_f) = 0 \;,\; \psi_2(t_f) = -1 \tag{3.23}$$

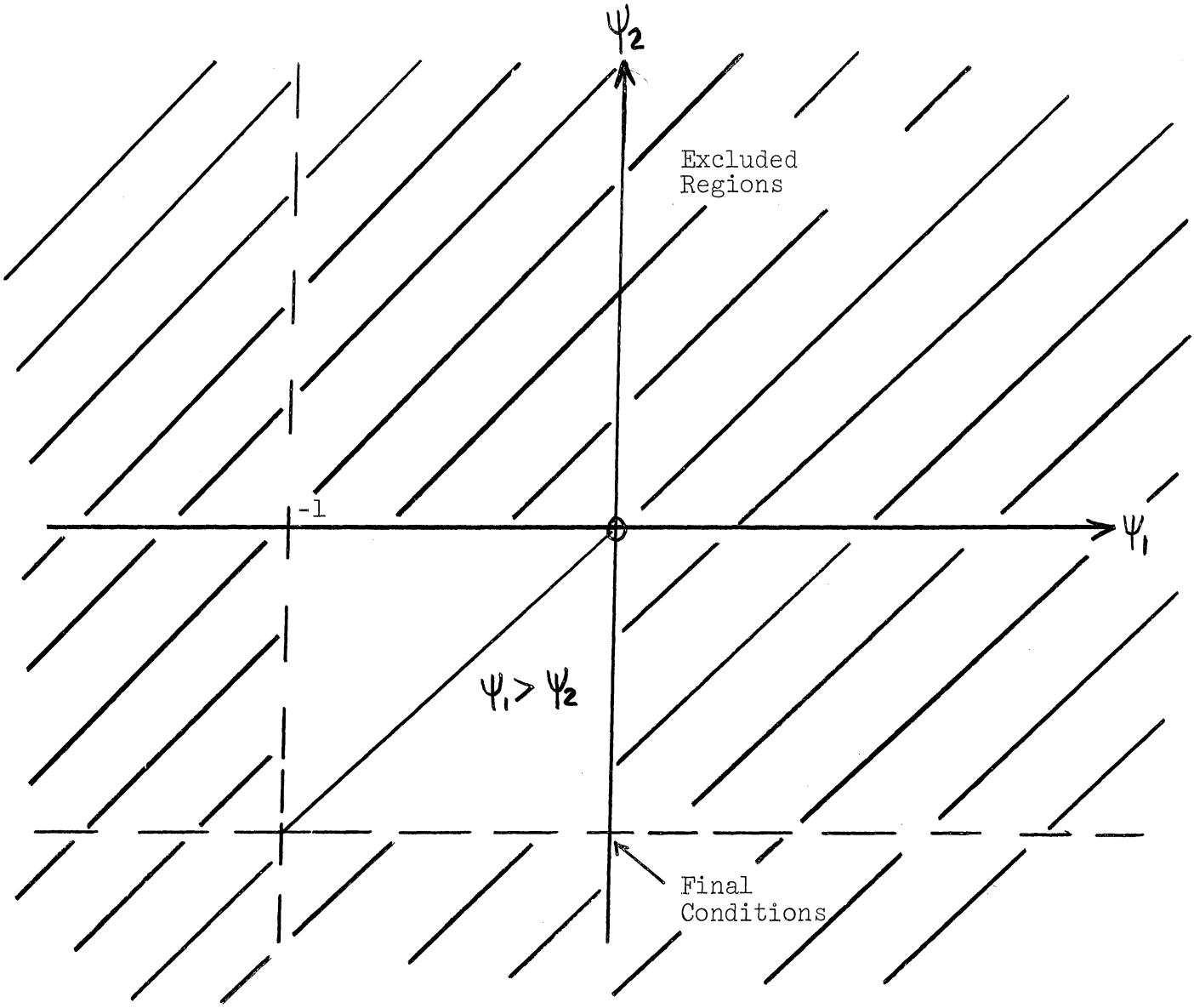

Figure 3.1. Adjoint Variable Phase Space.

From Equation (3.26), when ψ_2 is negative, $\dot{\psi}_2 = \frac{d\psi_2}{dt}$ is also negative, so that ψ_2 must approach $\psi_2(t_f) = -1$ from above. If ψ_2 is ever less than - 1 , it could never reach $\psi_2(t_f) = -1$, since $\dot{\psi}_2$ would remain negative. Therefore the region $\psi_2 < -1$ is excluded. Similarly the region $\psi_2 > 0$ must be excluded for in that region, ψ_2 and $\dot{\psi}_2$ are positive and ψ_2 again would not reach $\psi_2(t_f) = -1$. Finally ψ_2 cannot equal zero for it would then remain zero throughout the time period.

Now consider Equation (3.25). Since we have established that $-1 \leq \psi_2 < 0$, (3.25) may be written:

$$\dot{\psi}_1 = k_1 \psi_1 + (\text{positive term}) \tag{3.32}$$

If ψ_1 is ever positive it would then remain positive and could never arrive at $\psi_1(t_f) = 0$. Therefore, we exclude the region $\psi_1 > 0$. Suppose ψ_1 is less than -1. Since $\psi_2 \geq -1$, ψ_1 will always be less than ψ_2 and consequently from Equation (3.25), $\dot{\psi}_1$ will remain negative. Then we must exclude the region $\psi_1 < -1$, for the final value $\psi_1(t_f) = 0$ could not be reached.

So far we have established that $\vec{\psi}$ behaves according to:

$$\begin{aligned} -1 < \psi_1 \leq 0 \\ -1 \leq \psi_2 < 0 \end{aligned} \tag{3.33}$$

Two more facts are helpful in establishing the nature of the extremal of H. Consider $\psi_1 > \psi_2$. Then according to Equation (3.25), $\dot{\psi}_1 > 0$. But $\dot{\psi}_2 < 0$. Therefore if ψ_1 is ever greater than ψ_2, ψ_1 remains greater. Next, setting $\frac{dH}{dk_1} = 0$ in Equation (3.30) and solving for $k_1 = k_{1\,\text{extremal}}$, we obtain:

$$k_{1\,ext} = \left\{ \frac{\gamma_2}{\gamma_1} \cdot \frac{\psi_2}{(\psi_2 - \psi_1)} \cdot \frac{E_2}{E_1} \cdot \frac{k_{20}}{k_{10}^{E_2/E_1}} \right\}^{E_1/(E_1 - E_2)} \tag{3.34}$$

Only in a special case would the exponent of Equation (3.34), $E_1/(E_1 - E_2)$ have an integral value. Since ψ_2 is negative, and all other factors are positive, ψ_1 must be greater than ψ_2 for $k_{1\,\text{extremal}}$ to be real.

Otherwise Equation (3.34) yields an imaginary value, and H does not possess a real extremal.

The sign of the second partial derivative of H in Equation (3.31) may now be examined to determine the character of any extremal in H. All factors are positive except for ψ_2 which has been shown to be negative. For all values of state and adjoint variables $\frac{\partial^2 H}{\partial k_1^2} < 0$, indicating that all possible extremals of H are minima, not the required maxima. The absolute maximum of H will then be found at one of the boundaries k_{1*} or k_1^*. It is necessary merely to calculate $H(k_{1*})$ and $H(k_1^*)$ and to compare them to find which control satisfies the necessary condition of Theorem 1. However, the following analysis shows that this calculation is not always necessary:

For $\psi_1 < \psi_2$, H does not possess a real extremal, which means that $\frac{\partial H}{\partial k_1}$ does not change sign. Thus only examination of the sign of $\frac{\partial H}{\partial k_1}$ is necessary.

If $\frac{\partial H}{\partial k_1} > 0$, then $k_{1\,\text{optimal}} = k_{1*}$

If $\frac{\partial H}{\partial k_1} < 0$, then $k_{1\,\text{optimal}} = k_1^*$

From Equation (3.30), when $\psi_1 \leq \psi_2$, $\frac{\partial H}{\partial k_1} > 0$, except when $\psi_1 = \psi_2$ and $\gamma_2 = 0$. This is of no significance, for it could only occur at a single instant at the beginning of a trajectory.

For $\psi_1 > \psi_2$, it is not apparent from the expression for H, Equation (3.28), whether k_{1*} or k_1^* will minimize H. For this case we simply calculate both values and compare them. The complete optimal policy may now be stated:

$$\begin{aligned}
&\text{For } \psi_1 \leq \psi_2 \text{ , let } k_1 = k_1^* \\
&\text{For } \psi_1 > \psi_2 \text{ , calculate } H(k_1^*) \text{ and } H(k_{1*}) \\
&\text{If } H(k_1^*) > H(k_{1*}), \text{ let } k_1 = k_{1*} \\
&\text{If } H(k_1^*) < H(k_{1*}), \text{ let } k_1 = k_1^*
\end{aligned} \tag{3.35}$$

Finally, consider the possibility of "singular control" when H is independent of the control value for a finite period of time. From Equation (3.28) H will be independent of k_1 only if:

$$\begin{aligned}
&(1) \quad \psi_2 = \psi_1 \quad \text{or} \quad Y_1 = 0 \\
&\qquad\qquad\quad \text{and} \\
&(2) \quad \psi_2 = 0 \quad \text{or} \quad Y_2 = 0
\end{aligned} \tag{3.36}$$

Neither Y_1 nor Y_2 can equal zero for a finite time, and in the previous analysis, we have excluded the possibility $\psi_2 = 0$ even for an instant. Hence, we may dispense with the possibility of "singular control."

It should be noted that "singular control" does satisfy the necessary conditions of the Maximum Principle and is in fact the optimal control in certain very realistic problems. The required analysis for such a situation is given in the next section, but a very lucid treatment, recommended by this author is given by R. Jackson.(64)

Equations (3.35) give the optimal control as a function of state and adjoint variables. A two point boundary value problem still remains to relate the optimal control to residence time or reactor position. That is, the state equations possess known initial conditions, whereas the adjoint equations have known final conditions.

$$\frac{dY_1}{dt} = -k_1 Y_1 \quad , \quad Y_1(0) = 1$$

$$\frac{dY_2}{dt} = k_1 Y_1 - k_2 Y_2 \quad , \quad Y_2(0) = Y_{2_i}$$

$$\frac{d\psi_1}{dt} = k_1 (\psi_1 - \psi_2) \quad , \quad \psi_1(t_f) = 0$$

$$\frac{d\psi_2}{dt} = k_2 \psi_2 \quad , \quad \psi_2(t_f) = -1$$

These equations were solved in an IBM 7090 digital computer using the Runge-Kutta, fourth order method. Final values of the state variables were guessed. The equations were then integrated backwards, choosing k_1 according to the optimal policy (3.35) each time the derivatives were calculated (four times per step). k_2 was then given by Equation (3.27). The deviations of $Y_1(0)$ and $Y_2(0)$ from the known initial conditions, 1 and Y_{2_i} were used to correct the guesses on the state variables. This process was mechanized using both gradient and direct search methods.[21,59]

The trajectories which satisfy the Maximum Principle are shown in Figure 3.2. Pertinent numerical values in all problems of this chapter are given in Table 3.1. Convergence of the Y_1 and Y_2 trajectories to the known initial conditions required precise location of the jump discontinuity in temperature. Therefore, when the jump was located using the coarse step (0.5 seconds), a "homing in" routine was called in which used a modification of the half-interval method to locate the jump to within 10^{-4} seconds. Integration then continued to $t = 0$ using the 0.5 second step size.

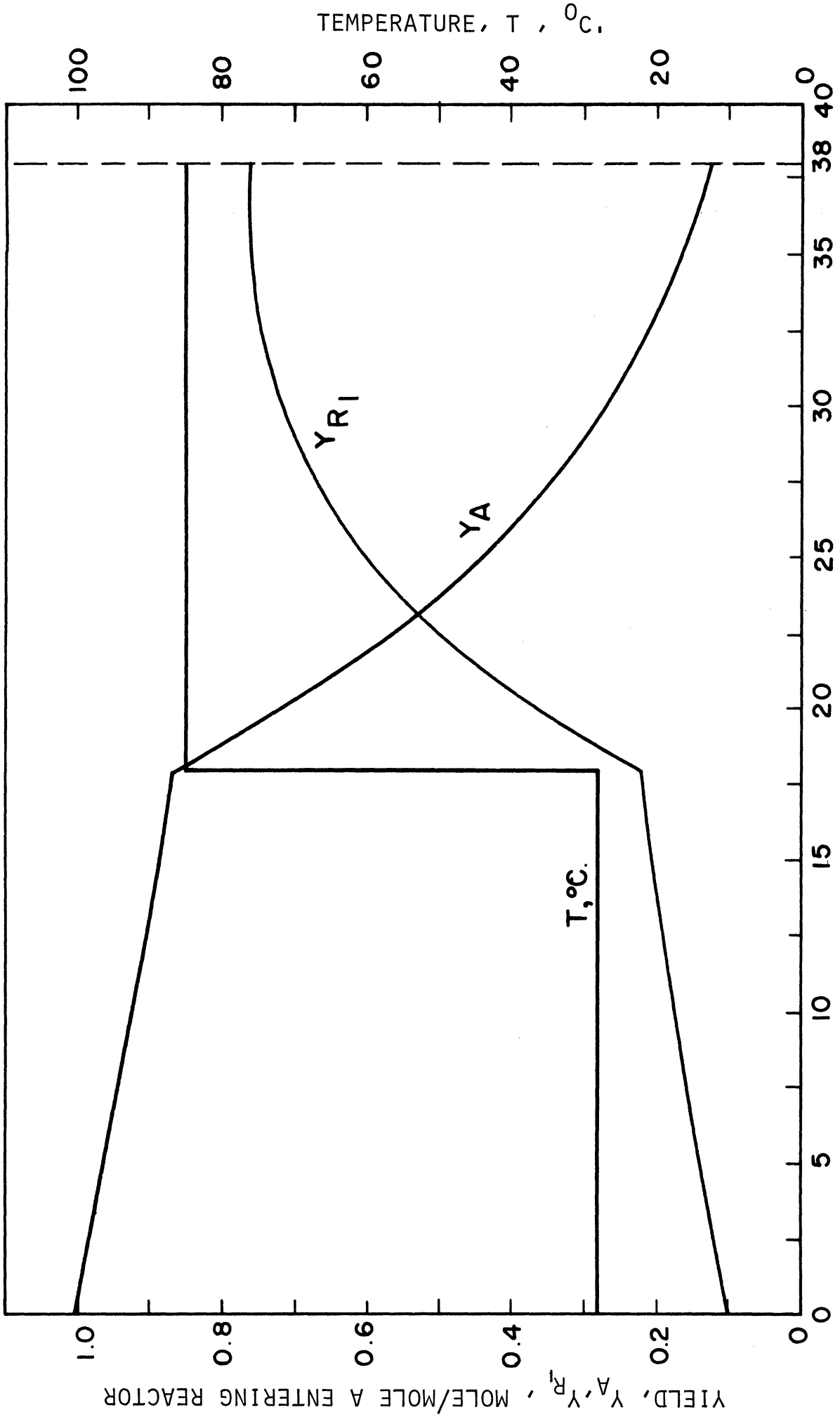

Figure 3.2. Optimal Trajectories for Bounded Temperature Control First Order Consecutive Reactions.

TABLE 3.1

VALUES OF NUMERICAL CONSTANTS FOR PROBLEMS OF CHAPTER 3

Reactor Residence Time = 38 seconds
Initial Conditions

C_{A_o} = 0.0175 mole/l .

$Y_1(0)$ = 1.0 mole/mole A entering the reactor

$Y_2(0)$ = 0.1 mole/mole A entering the reactor

$Y_3(0)$ = 30°C, 50°C or free

Y_B = 3.0 mole/mole A entering the reactor

For First Order Reactions Y_B = 2.5 = constant along reactor

Kinetic Parameters for Arrhenius Equation

$$k_i = k_{i_o} \exp \{-E_i/RT\}$$

$k_{1_o}^{**}$ = 1.172 x 10^6 l./(mole sec.) E_1/R^{**} = 4720.7°K

$k_{2_o}^{**}$ = 2.457 x 10^3 l./(mole sec.) E_2/R^{**} = 3140.8°K

** These were preliminary estimates for the kinetics of diethyl adipate, and yield rate constants 20-50 percent too low. They were adequate, however, for illustrating the forms of optimal trajectories. Corrected values of activation energies and frequency factors are given in Equation (5.5).

The Maximum Principle is only a necessary condition for optimality in general, but for linear systems it is also sufficient. However, even for the non-linear systems, the folowing argument may be used to prove that trajectories which satisfy the Maximum Principle are indeed optimal.

If the trajectory satisfying the Maximum Principle is unique and an optimal solution to the stated problem exists, then this trajectory must be optimal trajectory.

There are two reasons for performing the integrations backwards. We can make much better guesses of the final values of the state variables than of initial values of the adjoint variables. In this problem we were able to ascertain the allowable range of $\vec{\psi}$ before attempting the integration. In more complicated problems, this cannot be done. In addition, attempts to match the final conditions on the adjoint variables would produce only one optimal trajectory, the final one which matched the known final conditions on $\vec{\psi}$. In matching the initial conditions on the state variables by backward integration, each trial produces a trajectory, optimal for a different set of state variable initial conditions. Hopefully, this set converges to the given initial conditions. Then the problem is solved for the required initial conditions, and we get an added bonus, a family of optimal trajectories about the given initial values.

E. Optimal Wall Heat Flux for First Order Consecutive Reactions

Let us again consider the system described in the previous section, and ask how the optimal temperature profile is generated.

If by a wall heat flux, then clearly a jump discontinuity in temperature would be impossible to attain, requiring an infinite heat flux. Therefore, a more realistic optimal control scheme is sought whereby the wall heat flux, $q(t)$ may be varied along the reactor between minimum and maximum values. Specifically, heat flux into the fluid is considered positive. The minimum q is taken as adiabatic operation. Thus choose the wall heat flux (BTU/hr.ft.^{2}) such that:

$$0 \leq q \leq q^* \tag{3.37}$$

and the yield of middle product at the reactor exit is again to be maximized.

State Equations for $Y_1(t)$ and $Y_2(t)$ are again given by Equations (3.19) and (3.20), and reaction rate constants by Equation (3.18). A differential heat balance is needed to relate fluid temperature to the control, q :

$$\frac{dY_3}{dt} = a_1 k_1 Y_1 + a_2 k_2 Y_2 + a_3 q \tag{3.38}$$

where:

$$a_1 = \frac{(-\Delta H_1) C_{Ai}}{\rho C_t}$$

$$a_2 = \frac{(-\Delta H_2) C_{Ai}}{\rho C_t}$$

$$a_3 = \frac{4}{D_i \rho C_t} \tag{3.39}$$

Omitting ψ_0 from the Hamiltonian, since we are using Rozonoer's modification, we obtain from Equation (3.7) after simple rearrangement:

$$H = k_1 Y_1 (-\psi_1 + \psi_2 + \psi_3 a_1) + k_2 Y_2 (-\psi_2 + \psi_3 a_2) + \psi_3 a_3 q \quad (3.40)$$

The adjoint equations are now somewhat different from those of Section D:

$$\frac{d\psi_1}{dt} = k_1 (\psi_1 - \psi_2 - a_1 \psi_3) \quad (3.41)$$

$$\frac{d\psi_2}{dt} = k_2 (\psi_2 - a_2 \psi_3) \quad (3.42)$$

$$\frac{d\psi_3}{dt} = \frac{1}{Y_3^2} \left\{ Y_1 (\psi_1 - \psi_2 - a_1 \psi_3) \left(\frac{E_1}{R}\right) k_1 + Y_2 (\psi_2 - a_2 \psi_3) \left(\frac{E_2}{R}\right) k_2 \right\} \quad (3.43)$$

The functional J to be maximized at $t = t_f$ will now be:

$$J = \sum_{i=1}^{3} c_i Y_i = 0 \cdot Y_1 + 1 \cdot Y_2 + 0 \cdot Y_3 \quad (3.44)$$

Hence final conditions on the adjoint variables are:

$$\psi_1(t_f) = 0 \,, \quad \psi_2(t_f) = -1 \,, \quad \psi_3(t_f) = 0 \quad (3.45)$$

Initial conditions on Y_1 and Y_2 are known

$$Y_1(0) = 1 \,, \quad Y_2(0) = Y_{2i} \quad (3.46)$$

The initial condition for Y_3, the fluid temperature may either be fixed or allowed to be free. In the latter case, $q(t)_{\text{optimal}}$ is a function of the inlet temperature. Thus, we ask for the optimal inlet temperature and optimal heat flux profile to go along with this inlet temperature such that $Y_2(t_f)$ is maximized when compared with $Y_2(t_f)$ produced by all other heat flux profiles and inlet temperatures. The heat flux is constrained according to Equation (3.37). We place no constraint on the allowable value of $Y_3(0)$. According to

Equation (3.13),

$$\psi_3(0) = 0 \tag{3.47}$$

As usual, the two point boundary value problem has taken shape. (Initial conditions are known for γ_1, γ_2, ψ_3, and final conditions are known for ψ_1, ψ_2, ψ_3).

Now let us find the control q_f in $0 \leq q_f < q_f^*$ which minimizes the Hamiltonian (3.40). Since q_f enters linearly and a_3 is positive, the optimal control is given by:

$$\begin{aligned} &\text{If } \psi_3 > 0, \text{ Let } q_f = 0 \\ &\text{If } \psi_3 < 0, \text{ Let } q_f = q_f^* \end{aligned} \tag{3.48}$$

If $\psi_3 = 0$ over a finite period of time, then the Hamiltonian is independent of the control, and q_f can take on any value in its allowable region. This is a case of "singular control" mentioned in the previous section where any value of the control satisfies the Maximum Principle. ψ_3 must equal zero at the beginning and end of the optimal trajectory, so that the possibility of "singular control" as a candidate for the optimal control is very real. Fortunately, there is a way out of this dilemma.

"Singular control" may occur when ψ_3 and $\dot{\psi}_3$ are simultaneously zero. Since the control does not directly enter the adjoint equation for ψ_3, the values of state and adjoint variables must be such that $\dot{\psi}_3 = 0$ when $\psi_3 = 0$. From Equation (3.43) this requires:

$$\gamma_1 (\psi_1 - \psi_2) E_1 k_1 + \gamma_2 \psi_2 E_2 k_2 = 0 \tag{3.49}$$

$$\psi_3 = 0$$

For ψ_3 to remain zero over a finite time, $\dot{\psi}_3$ must remain zero. This requires that $\ddot{\psi}_3$ remain zero. The solution of our problem has now been found. As an alternate possibility for an optimal control after $\psi_3 = \dot{\psi}_3 = 0$, choose q such that $\ddot{\psi}_3$ remains zero. If this cannot be done in the allowable control region $0 \leq q \leq q^*$, then ψ_3 will become different from zero and the optimal control will again be given by Equation (3.48).

Before deriving the required relationships for $\ddot{\psi}_3 = 0$, let us consider the case of $\psi_3 = 0$, $\dot{\psi}_3 \neq 0$. Keeping in mind that integration is proceeding backwards in time, if $\dot{\psi}_3 > 0$, ψ_3 will decrease as t decreases, whereas when $\dot{\psi}_3 < 0$, ψ_3 will increase in the next instant. The optimal control is then:

$$\begin{aligned} \psi_3 = 0 \,,\ \dot{\psi}_3 > 0 \quad &: \quad q = q^* \\ \psi_3 = 0 \,,\ \dot{\psi}_3 < 0 \quad &: \quad q = 0 \end{aligned} \tag{3.50}$$

Now consider the case of $\psi_3 = \dot{\psi}_3 = 0$ over a finite period of time. This requires that $\ddot{\psi}_3$ be held null with the proper control. From Equation (3.43) $\dot{\psi}_3 = \dot{\psi}_3(\vec{Y}, \vec{\psi}, \vec{k}(Y_3))$ so that:

$$\ddot{\psi}_3 = \frac{d}{dt}\dot{\psi}_3 = \frac{\partial \dot{\psi}_3}{\partial \vec{Y}} \cdot \frac{d\vec{Y}}{dt} + \frac{\partial \dot{\psi}_3}{\partial \vec{\psi}} \cdot \frac{d\vec{\psi}}{dt} + \frac{\partial \dot{\psi}_3}{\partial \vec{k}} \cdot \frac{\partial \vec{k}}{\partial Y_3} \cdot \frac{dY_3}{dt} \tag{3.51}$$

where the ordinary derivatives in Equation (3.51) are given by the state and adjoint equations. The control q, enters in the term $\frac{dY_3}{dt}$, the heat balance. Performing the required substitutions and solving for q, the result after considerable simplification is:

$$q = q_{singular} = -\left(\frac{k_1 Y_1}{a_3}\right)\left\{\frac{Y_3^2}{\left(\frac{E_2}{R}\right)Y_2} + a_1 + \frac{a_2 k_2 Y_2}{k_1 Y_1}\right\} \qquad (3.52)$$

Equation (3.52) always yields a negative value for $q_{singular}$, which is outside the allowable control limits of Equation (3.37). Furthermore, it turns out that within the allowable limits on q, $\ddot{\psi}_3$ is always positive. Therefore $\dot{\psi}_3$, becomes negative as t decreases. "Singular control" is therefore ruled out and the complete optimal policy is established:

(1) For $\psi_3 > 0$, let $q = 0$

(2) For $\psi_3 < 0$, let $q = q^*$

(3) For $\psi_3 = 0$, Examine $\dot{\psi}_3$ (3.53)

a. For $\dot{\psi}_3 > 0$, let $q = q^*$

b. For $\dot{\psi}_3 \leq 0$, let $q = 0$

In principle the problem is solved. We must guess Y_1, Y_2 and Y_3 at $t = t_f$, with the known final conditions (0, -1, 0) on $\vec{\psi}$. By adjusting these guesses, convergence to the known initial conditions $Y_1 = 1$, $Y_2 = Y_{2i}$, $\psi_3 = 0$ should eventually be obtained.

The solution to this problem was obtained, but not as easily as for the problem of the previous section. The difficulties and how they were overcome should prove instructive, and are described below. An attempt was first made to match the three initial conditions using both direct and gradient search procedures. Specifically, $Y_1(t_f)$, $Y_2(t_f)$, and $Y_3(t_f)$ were chosen to minimize the function:

$$J = \left(Y_1(0) - 1\right)^2 + \left(Y_2(0) - Y_{2i}\right)^2 + \left(\psi_3(0) - 0\right)^2 \qquad (3.54)$$

For an initial attempt using $y_{2i}=0$, the search converged to:

$$y_1(0) = 0.9989$$
$$y_2(0) = -1.427 \times 10^{-4}$$
$$\psi_3(0) = -1.238 \times 10^{-3}$$

ψ_3 started at $\psi_3(t_f)=0$, decreased to a minimum of -1.362×10^{-3} and then increased again to $\psi_3(0)$. A sketch of the ψ_3 trajectory is shown in Figure 3.3.

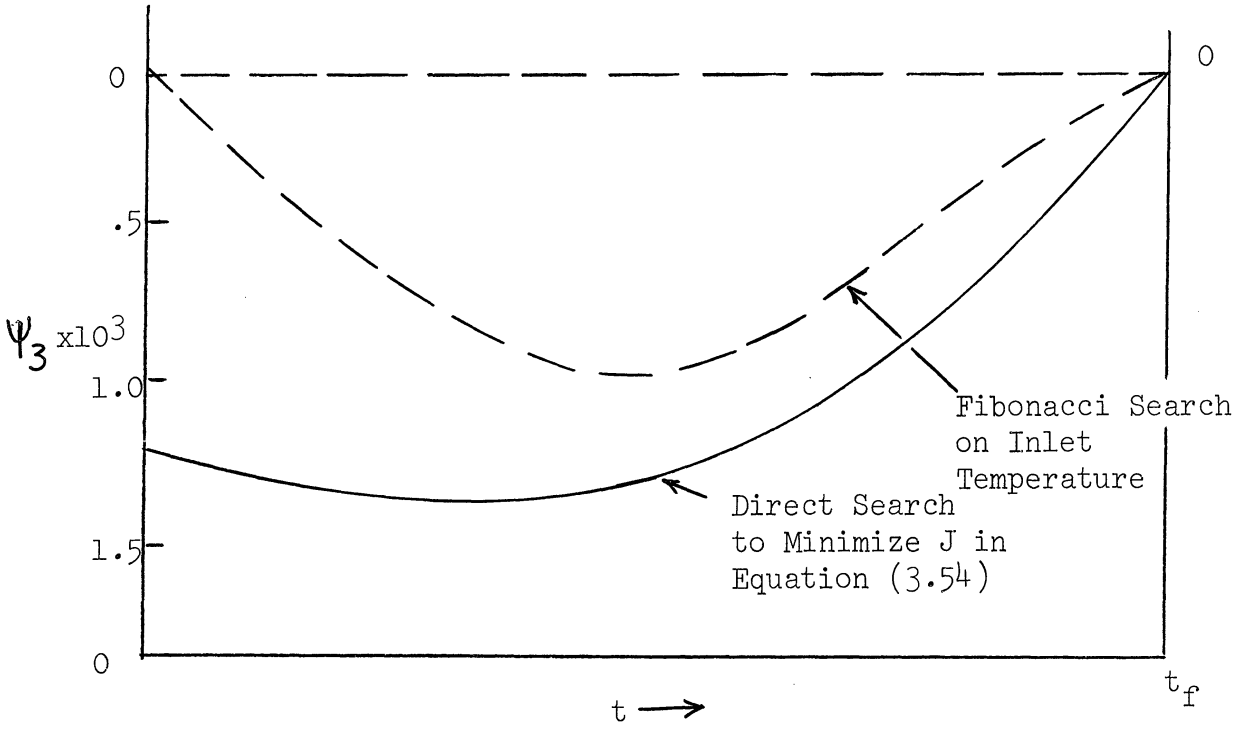

Figure 3.3. Sketch of ψ_3 Trajectory Using Multivariable Search and Fibonacci Search on Inlet Temperature.

As shown, convergence was poor on $\psi_3(0)=0$, indicating that the optimal inlet temperature was not located precisely. Convergence was only slightly improved by decreasing the minimum step size for ending the search. Computing time mounted, however, to 3.5 minutes compared with 1.5 minutes for the two variable search in the previous section. To obtain much better convergence of ψ_3 , the following observations were made:

Although good convergence was not achieved, the "best" trajectory obtained up to that point indicated that the optimal control should be maximum heating along the entire reactor length. This was a consequence of Figure 3.3 and Equation (3.53). This suggested that the optimal policy might be also one of full heating, and that ψ_3 was very sensitive to the inlet temperature. Consequently a much simpler problem was considered.

With known initial conditions, on y_1 and y_2, choose the initial temperature $y_3(0)$ to maximize the exit concentration $y_2(t_f)$. Full heating was used along the entire reactor length $(q_f = q_f^*)$. A Fibonacci search was used to efficiently locate the optimal inlet temperature. Integration was only performed on the state equations, and the search was on only one variable. Hence, computing time was reduced to only 30 seconds. The final conditions obtained from this trajectory were then used to integrate backwards the complete set of state and adjoint equations. The optimal control was determined from Equation (3.53). Sure enough, this control satisfied the necessary conditions for optimality, and excellent convergence on $\psi_3 = 0$ was obtained. The optimal trajectories are shown in Figure 3.4.

The technique used here points up one of the more important ways to make use of the Maximum Principle. Candidates for optimal controls are determined from theoretical analysis and preliminary computation using the Maximum Principle. These controls are then improved much more efficiently without the Maximum Principle and the final results checked against the necessary conditions for optimality. This idea is most often applicable to systems which possess "bang-bang"

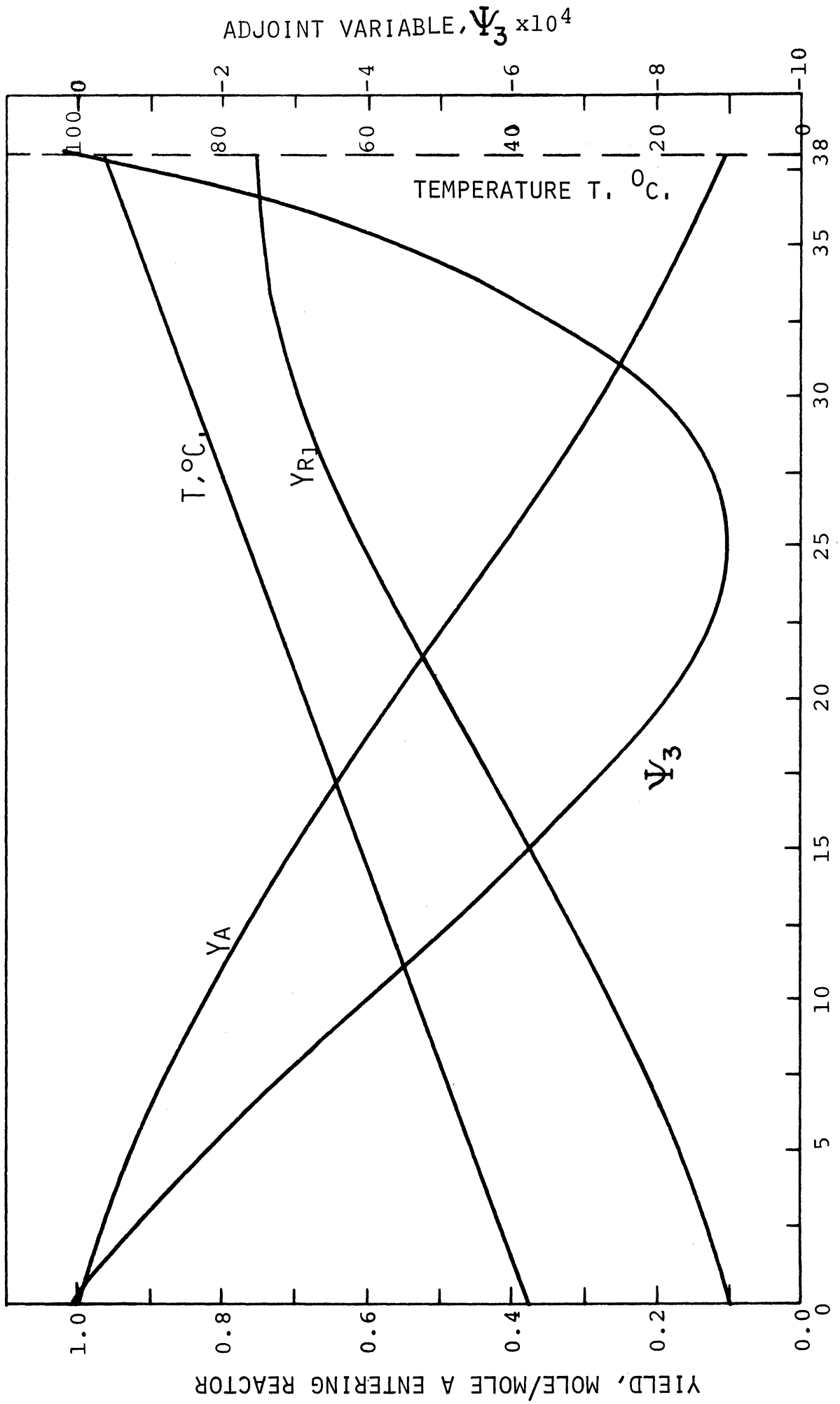

Figure 3.4. Optimal Trajectories for Bounded Heat Flux Control - First Order Reactions, Optimal Inlet Temperature.

optimal controls, that is, controls which remain on the boundaries of the allowable region except at points of discontinuity. As with the previous section, detailed discussion of the "optimal controls" will be delayed until after second order systems are considered.

F. Optimal Temperature Profile for Second Order Consecutive Reactions

With insight obtained from treating first order reactions, the second order system which models the saponification of diethyl adipate is considered. The kinetic model is given by:

$$A + B \xrightarrow{k_1} R_1 + EtOH$$

$$R_1 + B \xrightarrow{k_2} R_2 + EtOH \qquad (3.54)$$

where A = diethyl adipate

B = sodium hydroxide

R_1 = monoethyl adipate

R_2 = adipate ion

$EtOH$ = ethanol

The plug flow assumptions of Section D are again made, and the reaction kinetics again follow the Arrhenius temperature dependence (3.18) with $E_1 > E_2$. Component mass balances and division by the inlet concentration of diethyl adipate yield the state equations:

$$\frac{dY_1}{dt} = -k_1 Y_1 C_B \qquad (3.55)$$

$$\frac{dY_2}{dt} = (k_1 Y_1 - k_2 Y_2) C_B \qquad (3.56)$$

Y_1, and Y_2 refer to mole ratios of components A, and R_1 (mole/mole A entering the reactor), and C_B is the concentration of component B (mole/l). As before, we ask for the temperature profile along the reactor such that:

$$T_* \leqslant T \leqslant T^* \tag{3.21}$$

and Y_2 is maximized at the reactor exit. Although an additional state equation could be written for C_B, it would be redundant. C_B at any reactor position can be obtained from an overall mass balance.

$$C_B(t) = C_{B_i} + \left\{ Y_2(t) + 2Y_1(t) - (Y_{2_i} + 2) \right\} C_{A_i} \tag{3.57}$$

Y_{2_i} is the inlet mole ratio of R_1. C_{A_i} and C_{B_i} are inlet concnetrations of A and B. The Hamiltonian is of the form:

$$H = \vec{\psi} \cdot \vec{f} = \left\{ -\psi_1 k_1 Y_1 + \psi_2 (k_1 Y_1 - k_2 Y_2) \right\} C_B \tag{3.58}$$

Following Equations (3.15), (3.16) and (3.8), and noting that $\frac{dH}{dC_B} = \frac{H}{C_B}$, the adjoint equations may be written in fairly concise form:

$$\frac{d\psi_1}{dt} = C_B k_1 (\psi_1 - \psi_2) - 2H/C_B \tag{3.59}$$

$$\frac{d\psi_2}{dt} = k_2 \psi_2 C_B - H/C_B \tag{3.60}$$

with the final conditions:

$$\psi_1(t_f) = 0, \quad \psi_2(t_f) = -1 \tag{3.61}$$

The Hamiltonian (3.58) must now be examined to ascertain the optimal control, but this time it must be done without <u>a priori</u> knowledge of the bounds on $\vec{\psi}$. We again write k_2 as a function of k_1 and seek k_1 in $k_{1_*} \leqslant k_1 \leqslant k_1^*$ along the trajectory such that H is minimized.

Following the analysis for the first order system, $\frac{\partial H}{\partial k_1}$, $\frac{\partial^2 H}{\partial k_1^2}$, and $k_{1\,\text{extremal}}$ (solution of $\frac{\partial H}{\partial k_1} = 0$) are calculated:

$$\frac{\partial H}{\partial k_1} = \left\{ \gamma_1(\psi_2 - \psi_1) - \gamma_2 \psi_2 \frac{k_{20}}{(k_{10})^{E_2/E_1}} \cdot \frac{E_2}{E_1} \cdot k_1^{\frac{E_2 - E_1}{E_1}} \right\} C_B \qquad (3.62)$$

$$\frac{\partial^2 H}{\partial k_1^2} = \left\{ \frac{\gamma_2 \psi_2 k_{20}}{(k_{10})^{E_2/E_1}} \cdot \frac{E_2}{E_1} \cdot \frac{E_1 - E_2}{E_1} \cdot k_1^{(E_2 - 2E_1)/E_1} \right\} C_B \qquad (3.63)$$

$$k_{1\,EXT} = \left\{ \frac{\gamma_2}{\gamma_1} \cdot \frac{\psi_2}{(\psi_2 - \psi_1)} \cdot \frac{E_2}{E_1} \cdot \frac{k_{20}}{(k_{10})^{E_2/E_1}} \right\}^{E_1/(E_1 - E_2)} \qquad (3.64)$$

Referring to Equations (3.62) through (3.64), H will be minimized systematically for all values of $\vec{\psi}$:

a. $\psi_2 > 0$, $\psi_2 > \psi_1$

$k_{1\,\text{extremal}}$ is real and single valued, and $\frac{\partial^2 H}{\partial k_1^2} > 0$.

Therefore H has a minimum at $k_1 = k_{1\,\text{extremal}}$. This minimum may fall in different positions as shown below:

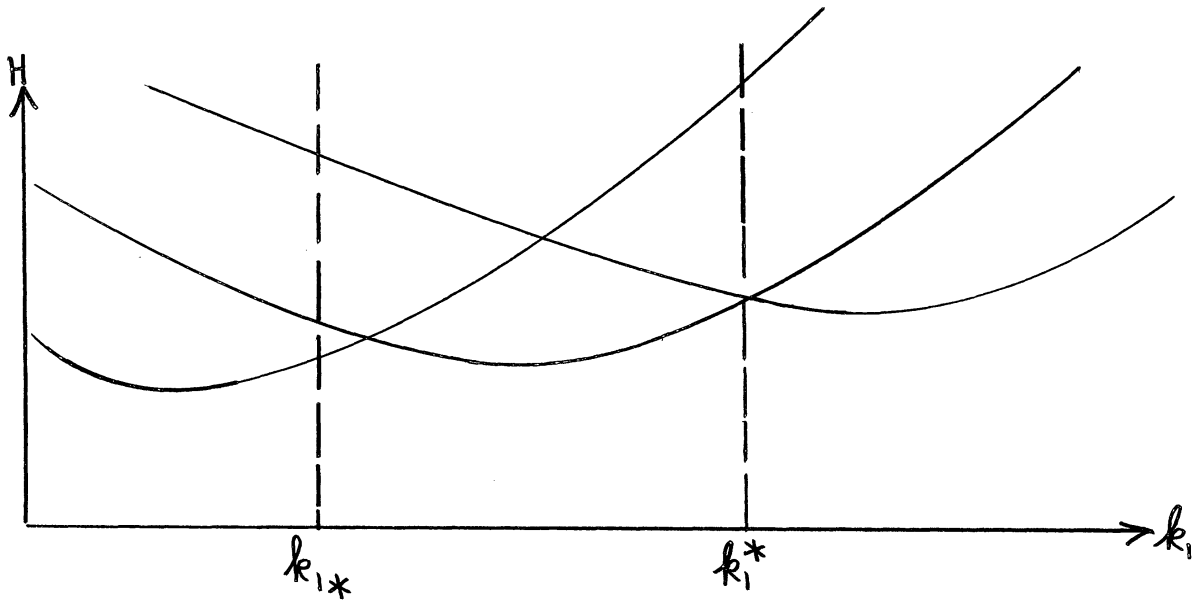

Figure 3.5. Possibilities for Position of H_{minimum} .

From Figure (3.5) the optimal control is apparent.

Compute $k_{1\,\text{extremal}}$ from Equation (3.64).

If $k_{1*} \leq k_{1EXT} \leq k_1^*$ Let $k_1 = k_{1\,\text{extremal}}$

If $k_{1EXT} < k_{1*}$ Let $k_1 = k_{1*}$

If $k_{1EXT} > k_1^*$ Let $k_1 = k_1^*$ (3.65)

b. $\Psi_2 > 0, \ \Psi_2 < \Psi_1$

$k_{1\,\text{extremal}}$ has no real solution, and from Equation (3.62) $\frac{\partial H}{\partial k_1} < 0$. Therefore the optimal control for this case is:

$$k_1 = k_1^* \tag{3.66}$$

c. $\Psi_2 > 0, \ \Psi_2 = \Psi_1$

Equation (3.64) for $k_{1\,\text{ext}}$ is not valid for this case. $\frac{\partial H}{\partial k_1}$ is negative. Therefore:

$$k_1 = k_1^* \tag{3.67}$$

d. $\Psi_2 < 0, \ \Psi_2 > \Psi_1$

$k_{1\,\text{ext}}$ has no real solution, and $\frac{\partial H}{\partial k_1}$ is positive. Therefore set:

$$k_1 = k_{1*} \tag{3.68}$$

e. $\Psi_2 < 0, \ \Psi_2 < \Psi_1$

$k_{1\,\text{extremal}}$ has a real solution. As with the first order system $\frac{\partial^2 H}{\partial k_1^2} < 0$ so that $k_{1\,\text{ext}}$ produces a maximum in H. Thus, calculate $H(k_{1*})$, and $H(k_1^*)$.

If $H(k_1^*) < H(k_{1*})$, Let $k_1 = k_1^*$

If $H(k_1^*) > H(k_{1*})$, Let $k_1 = k_{1*}$ (3.69)

f. $\Psi_2 < 0, \ \Psi_2 = \Psi_1$

Since $\frac{\partial H}{\partial k_1} > 0$, set:

$$k_1 = k_{1*} \tag{3.70}$$

g. $\Psi_2 = 0, \ \Psi_1 > \Psi_2$

$\frac{\partial H}{\partial k_1} < 0$ so that:

$$k_1 = k_1^* \tag{3.71}$$

h. $\Psi_2 = 0, \ \Psi_1 < \Psi_2$

$\frac{\partial H}{\partial k_1} > 0$ so that:

$$k_1 = k_{1*} \tag{3.72}$$

i. $\Psi_2 = \Psi_1 = 0$

This is impossible for then $\dot{\vec{\psi}} = 0$ and the required final conditions could not be reached (See (3.58) - 3.60)).

To complete the investigation, we must finally look for the possibility of "singular control". From (3.58) H will be independent of k_1 only if $\Psi_1 = 0$ or $\gamma_1 = 0$ and $\Psi_2 = 0$ or $k_1\gamma_1 = k_2\gamma_2$ and consequently $H = 0$. At $t = t_f$, $\Psi_1 = 0$, $\Psi_2 \neq 0$, but it is possible that $k_1\gamma_1 = k_2\gamma_2$. $\dot{\Psi}_1 \neq 0$ so that at $t = t_f^-$, Ψ_1 becomes non-zero. Surely $\gamma_1 \neq 0$ for t_f finite H becomes a function of k_1 and singular control is not possible.

The complete optimal control is given by the set of Equations (3.65) through (3.72). The two point boundary value problem of state and adjoint Equations (3.55), (3.56), (3.59), (3.61) with known initial conditions on $\vec{Y}$ was then attempted in the same manner as that of the first order system of Section D. Convergence was not quite as good as with the first order system, but the "optimal control" was similar: Hold the temperature at $T = T_*$ followed by a jump to $T = T^*$ for the remainder of the reactor. It was not unexpected that the controls for first and second order systems would be similar since NaOH concentration changed only by 40 percent of C_{Bi} . The "optimal control" is shown in Figure 3.6.

G. Optimal Wall Heat Flux for Second Order Consecutive Reactions

The Maximum Principle is applied in this section to determine the wall heat flux to maximize production of monoethyl adipate from diethyl adipate in a tubular reactor of fixed length. After completing the previous three sections, this problem may seem fairly straight forward. This is certainly due to the insight gained from the simpler problems. Concerning the present problem, application of the Maximum Principle to determine non-singular control follows closely the treatment for the first order system. For the case of "singular control" the situation is more complicated. We could not definitely dispose of the possibility of "singular control" or establish that it would occur. The required course of action was therefore stated in the computer program. However, it never occurred for the conditions of this reaction system. The results are stated, nevertheless, since another reaction system may require "singular control" for optimal operation.

For the chemical reactions shown in Equation (3.54) we seek the wall heat flux (BTU/hr. ft.^{2}) into the reactor as a function of position to maximize the exit concentration of monoethyl adipate (R_1) . Conventions and nomenclature are consistent with the previous sections. The control $q_f(t)$ is sought in $0 \leq q_f \leq q^*$ such that $Y_2(t_f)$ is maximized. State equations for Y_1 and Y_2 and the algebraic representation of the NaOH concentration, C_B are shown in Equations (3.55) through (3.57). A differential heat balance on the reactor yields:

$$\frac{dT}{dt} = \frac{dY_3}{dt} = (a_1 k_1 + a_2 k_2 Y_2) C_B + a_3 q_f \qquad (3.73)$$

$a_1 - a_3$ are given in Equation (3.39)

The Hamiltonian is given by:

$$H = \left\{k_1 Y_1 \left(-\psi_1 + \psi_2 + a_1 \psi_3\right) + k_2 Y_2 \left(-\psi_2 + a_2 \psi_3\right)\right\} C_B + \psi_3 a_3 q_f \qquad (3.74)$$

and the adjoint equations are:

$$\frac{d\psi_1}{dt} = k_1 C_B \left(\psi_1 - \psi_2 - a_1 \psi_3\right) - \frac{2}{C_B}\left(H - \psi_3 a_3 q_f\right) \qquad (3.75)$$

$$\frac{d\psi_2}{dt} = k_2 C_B \left(\psi_2 - a_2 \psi_3\right) - \frac{\left(H - \psi_3 a_3 q_f\right)}{C_B} \qquad (3.76)$$

$$\frac{d\psi_3}{dt} = \frac{C_B}{R Y_3^2}\left\{k_1 E_1 Y_1 \left(\psi_1 - \psi_2 - a_1 \psi_3\right) + k_2 E_2 Y_2 \left(\psi_2 - a_2 \psi_3\right)\right\} \qquad (3.77)$$

The objective function to be maximized at t_f is given in Equation (3.44) so that final conditions on $\vec{\psi}$ are:

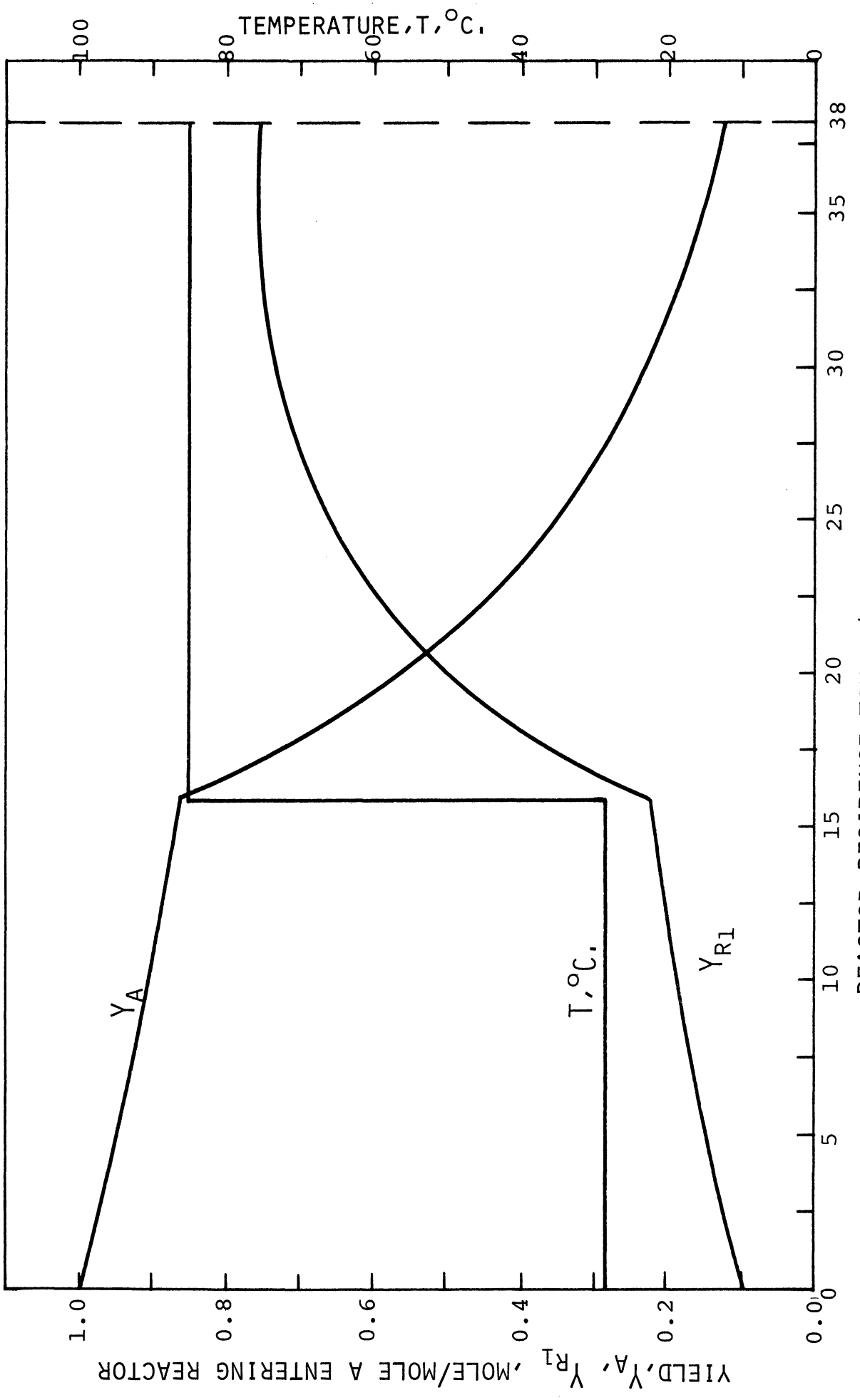

Figure 3.6. Optimal Trajectories for Bounded Temperature Control - Second Order Consecutive Reactions.

$$\psi_1(t_f) = 0 \;,\; \psi_2(t_f) = -1 \;,\; \psi_3(t_f) = 0 \qquad (3.78)$$

Initial conditions on Y_1 and Y_2 are 1 and Y_{2i}, and as in Section E, $Y_3(0)$ may be fixed or allowed to be free in which case $\psi_3(0) = 0$. The initial conditions come into the final two point boundary value problem and are not needed to establish the optimal control. The optimal control policy is therefore established generally at first. Optimal trajectories are then established for both free and fixed inlet temperatures.

Since q_f enters the Hamiltonian linearly, the non-singular control which minimizes H is apparent:

$$\begin{aligned} &\text{If } \psi_3 > 0 && \text{Let } q_f = 0 \\ &\text{If } \psi_3 < 0 && \text{Let } q_f = q_f^* \end{aligned} \qquad (3.79)$$

If $\psi_3 = 0$ and $\dot{\psi}_3 > 0$, then on integrating backwards ψ_3 will become negative. Therefore:

$$\text{Let } \quad q_f = q_f^* \qquad (3.80)$$

Similarly if $\psi_3 = 0$ and $\dot{\psi}_3 < 0$

$$\text{Let } \quad q_f = 0 \qquad (3.81)$$

The Case of Singular Control

If $\psi_3 = \dot{\psi}_3 = 0$, then q_f may be chosen at will in the allowable region. In general, this will cause ψ_3 to immediately become non-zero and the control given above will apply. Therefore, no change in the trajectories would be apparent due to this instantaneous

switching, except that the optimal control might be steered to one of the control boundaries. An alternative is to choose $q_f = q_{singular}$ such that $\ddot{\psi}_3$ remains zero thereby keeping ψ_3 zero. This will be possible only if $0 \leq q_{singular} \leq q_f^*$. $q_{singular}$ is termed the "singular control".

To determine $q_{singular}$, $\ddot{\psi}_3$ is differentiated as in Equation (3.51) and the result set equal to zero. This expression is then solved for $q_f = q_{singular}$. The result is:

$$q_{SINGULAR} = -(F_2 + F_3 + F_4)/F_1 \tag{3.82}$$

$$F_1 = \left\{ \frac{\psi_2}{\gamma_2} \cdot \frac{(\psi_2 - \psi_1)\, a_3}{C_B} + \frac{(2\psi_2 - \psi_1)\, \psi_3\, a_3}{C_B^2} \right\} \tag{3.83}$$

$$F_2 = \frac{\psi_2}{\gamma_2} \cdot (\psi_2 - \psi_1)\left\{ k_1\gamma_1 - k_2\gamma_2 + k_1\gamma_2 - \frac{(E_1 - E_2)}{R\gamma_3^2}\,(a_1 k_1 \gamma_1 + a_2 k_2 \gamma_2) \right\} \tag{3.84}$$

$$F_3 = \left\{ \psi_2 k_1 (\psi_1 - \psi_2 - a_1\psi_3) - \psi_1 k_2 (\psi_2 - a_2\psi_3) \right\} \tag{3.85}$$

$$F_4 = \frac{H}{C_B^2}\,(\psi_1 - 2\psi_2) \tag{3.86}$$

The value of H is easily calculated at $t = t_f$ since $\psi_1 = \psi_3 = 0$. The result is:

$$H = H(t_f) = C_B (k_2\gamma_2 - k_1\gamma_1)\Big|_{t=t_f} \tag{3.87}$$

Consider the case of $\psi_3 = \dot{\psi}_3 = 0$, and q_f in the allowable control region to keep $\dot{\psi}_3$ zero. Then the control may be held singular or may jump to either boundary to resume the optimal policy given by

Equation (3.79) through (3.81). Results are now stated which give allowable ways to leave singular control. They are based on the equation $\ddot{\psi}_3 = 0$ and consider the direction in which $\ddot{\psi}_3$ would move if q were made greater or less than $q_{singular}$.

Case 1. $\psi_2 < 0$

For the case of $\psi_2 < 0$, once q is set equal to $q_{singular}$ with $0 < q_{singular} < q^*$, the control must remain singular until $q_{singular}$ reaches a boundary. The reasoning is as follows: When $0 < q_{singular} < q^*$, letting q jump from $q_{singular}$ to 0 causes $\ddot{\psi}_3$ to become negative. This in the next instant causes $\dot{\psi}_3$ to become positive and ψ_3 to become negative. Then according to Equation (3.79) the optimal control should be full heating, q^*. This switch will cause $\ddot{\psi}_3$ to become positive requiring another switch. Hence, rapid switching and instability of the integration will insue. A similar phenomenon would occur if q were switched from $q_{singular}$ to q^*. We must therefore conclude that for $\psi_2 < 0$, once singular control begins, it must be continued until $q_{singular}$ leaves the allowable control region.

Case 2. $\psi_2 > 0$

For $\psi_2 > 0$, switches to either 0 or q^* from $q_{singular}$ are allowed. The optimal control then coincides with the chosen value, 0 or q^* and no cycling occurs. However, should the control remain singular until $q_{singular}$ reaches a boundary, an immediate jump to the opposite boundary will occur.

Case 3. $\psi_2 = 0$

ψ_2 could not equal zero at the same time that $\psi_3 = \dot{\psi}_3 = 0$. From Equation (3.77) this would require that $\psi_1 = 0$. This impossibility may be explained by noting that the adjoint equations are homogeneous in $\vec{\psi}$. Since $\vec{\psi}$ is non-zero at $t = t_f$, it could never become zero in a finite time. (See equations (3.74) - (3.77)).

Solution of the Two Point Boundary Value Problem

The complete optimal control policy as determined was applied first with a free initial condition on y_3. That is, the optimal inlet temperature was required with the accompanying optimal heat flux profile, which would maximize $y_2(t_f)$ compared with all other possible inlet temperatures and heat flux profiles. The complete set of initial and final conditions are then:

initial conditions $y_1(0) = 1$, $y_2(0) = y_{2_i}$, $\psi_3(0) = 0$

final conditions $\psi_1(t_f) = \psi_3(t_f) = 0$, $\psi_2(t_f) = -1$

As in the previous problems, guesses were made on $\vec{y}(t_f)$ the complete set of state and adjoint equations then being integrated backwards employing the optinal policy. Convergence was again poor on $\psi_3(0) = 0$ but the control for the closest match was one of full heating along the reactor. As described in Section E, the inlet temperature to maximize $y_2(t_f)$ with full heating along the reactor was found using a Fibonacci search. This trajectory was then found to satisfy the necessary conditions for optimality. Convergence on $\psi_3(0) = 0$ was quite good as shown in Figure 3.7.

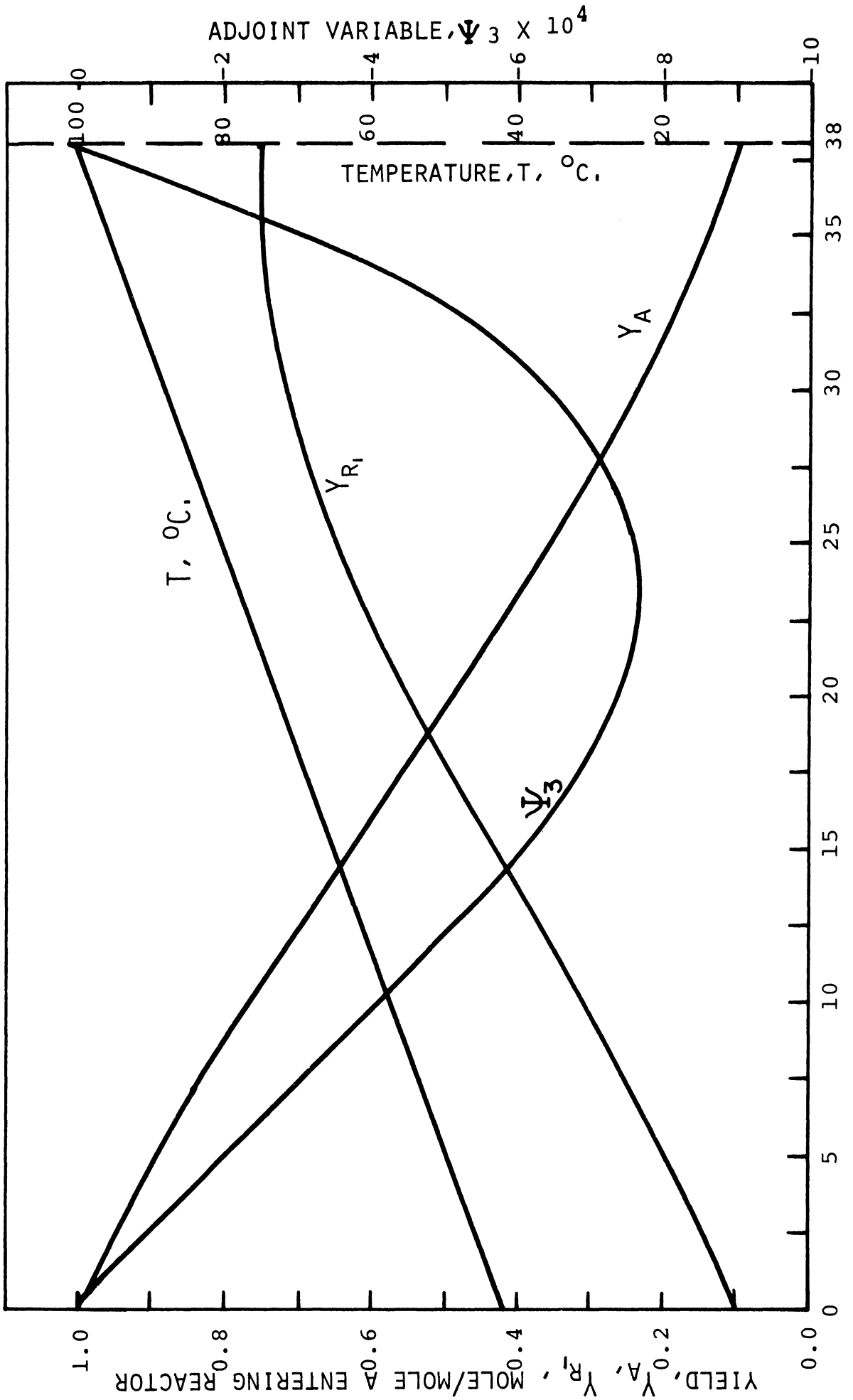

Figure 3.7. Optimal Trajectories for Bounded Heat Flux Control - Optimal Inlet Temperature = 41.43°C.

As shown, the trajectory for monoethyl adipate, Y_2 , peaks at $t=t_f$ at its maximum value. From this fact, guesses at the optimal controls for fixed inlet temperature may be made. Denote by T_{opt} , the inlet temperature shown in Figure 3.7, which should produce the maximum $Y_2(t_f)$ compared with all other inlet temperatures. If $T(0) < T_{opt}$, and full heating is again used along the entire reactor, the maximum $Y_2(t_f)$ will again occur at t_f , but this time Y_2 will still be increasing. Further increase in the reaction rate would then give an ever higher value of $Y_2(t_f)$. However, no higher reaction rate is possible since the heating rate is already at its maximum. Therefore it would seem that the optimal control for $T(0) < T_{opt}$ is also one of full heating, $q = q^*$ for all t . Full heating control was substantiated, satisfying the necessary conditions for optimality. The complete set of trajectories are shown in Figure 3.8.

Finally the case in which $T(0) > T_{opt}$ was considered. Again looking at the trajectories with $T(0) = T_{opt}$, Figure 3.7, if $T(0)$ is increased and the control is held constant at full heating, Y_2 would reach a peak before t_f , and therefore $Y_2(t<t_f) > Y_2(t_f)$ in the neighborhood of t_f . Decreasing the heat flux in some section along the reactor would have the effect of lowering the average reaction rate and of shifting the peak to higher t . Therefore at first guess, at least one switch between $q = q^*$ and $q = 0$ was expected. Only after this problem was solved with the aid of the Maximum Principle was the usual "hindsight" applied and the results were somewhat apparent.

As shown in Figure 3.9, the optimal control for $T(0) > T_{opt}$ is one of adiabatic operation followed by a final section of full heating.

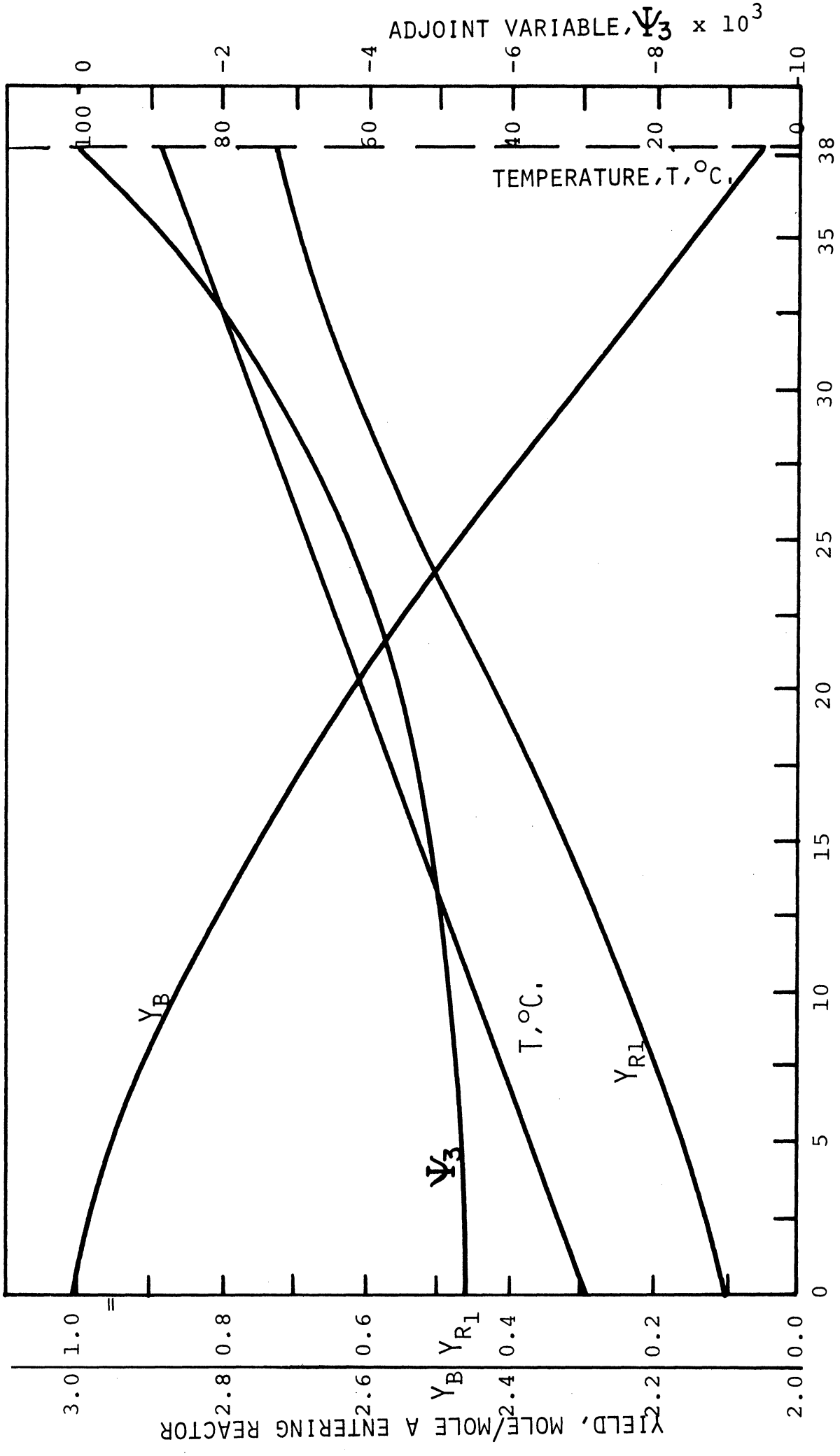

Figure 3.8. Optimal Trajectories for Bounded Heat Flux Control, Inlet Temperature = 30°C.

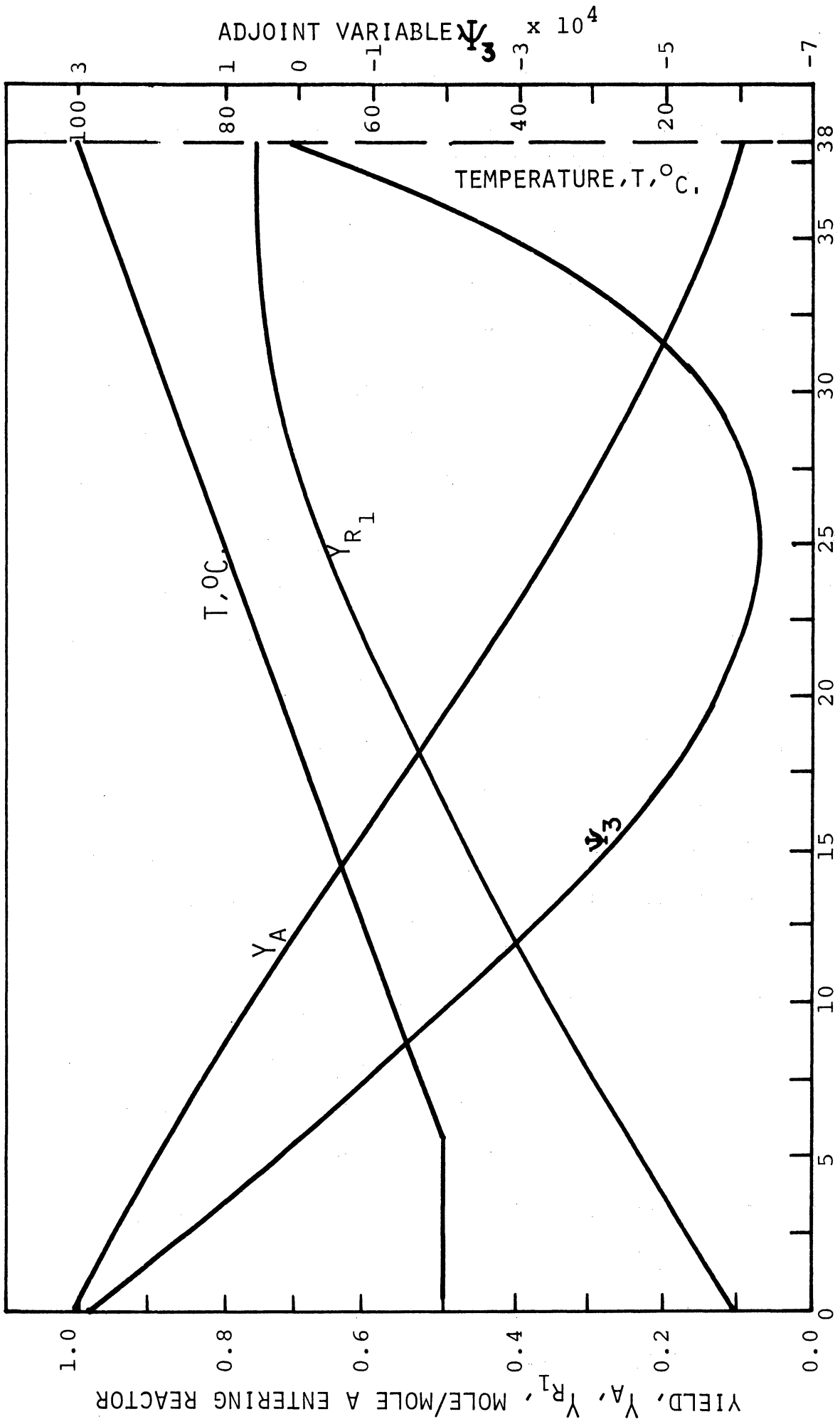

Figure 3.9. Optimal Trajectories for Bounded Heat Flux Control Inlet Temperature = 50°C.

This causes the Y_2 trajectory to reach a peak at $t=t_f$, but the value of $Y_2(t_f)$ is slightly less than for the case of $T(0) = T_{opt}$, shown in Figure 3.6. The differences in these two values of $Y_2(t_f)$ are very slight for this reaction system because the activation energies of the two reactions are quite similar. The greater the difference in activation energies, the greater will be the sensitivity of the optimal conversion to inlet temperature. Also, the higher the inlet temperature, the longer will be the period of adiabatic operation.

The optimal control of Figure 3.9 is analogous to that for the optimal temperature problem of Figure 3.6. It should also be apparent that if there is to be a period of high temperature followed by a period of low temperature, the low should precede the high temperature so that most of the required middle product forms in the latter part of the reactor and hence does not have as long a time to decompose.

A comment should be made on the lack of difference between the optimal trajectories for first and second order systems. In both cases, the isothermal maximum value of the middle product is a function only of the ratio of the first and second reaction rate constants. If this ratio is insensitive to temperature (E_1 and E_2 not too different), then the peak in middle product concentration may be shifted in time raising or lowering the reaction temperature with little effect on the value of the peak concentration. This is certainly the case for the system discussed here as shown in Figure 3.10, a plot of middle product concentration profiles for various temperatures.

A comparison of the exit concentrations for the various optimal trajectories is shown in Table 3.2.

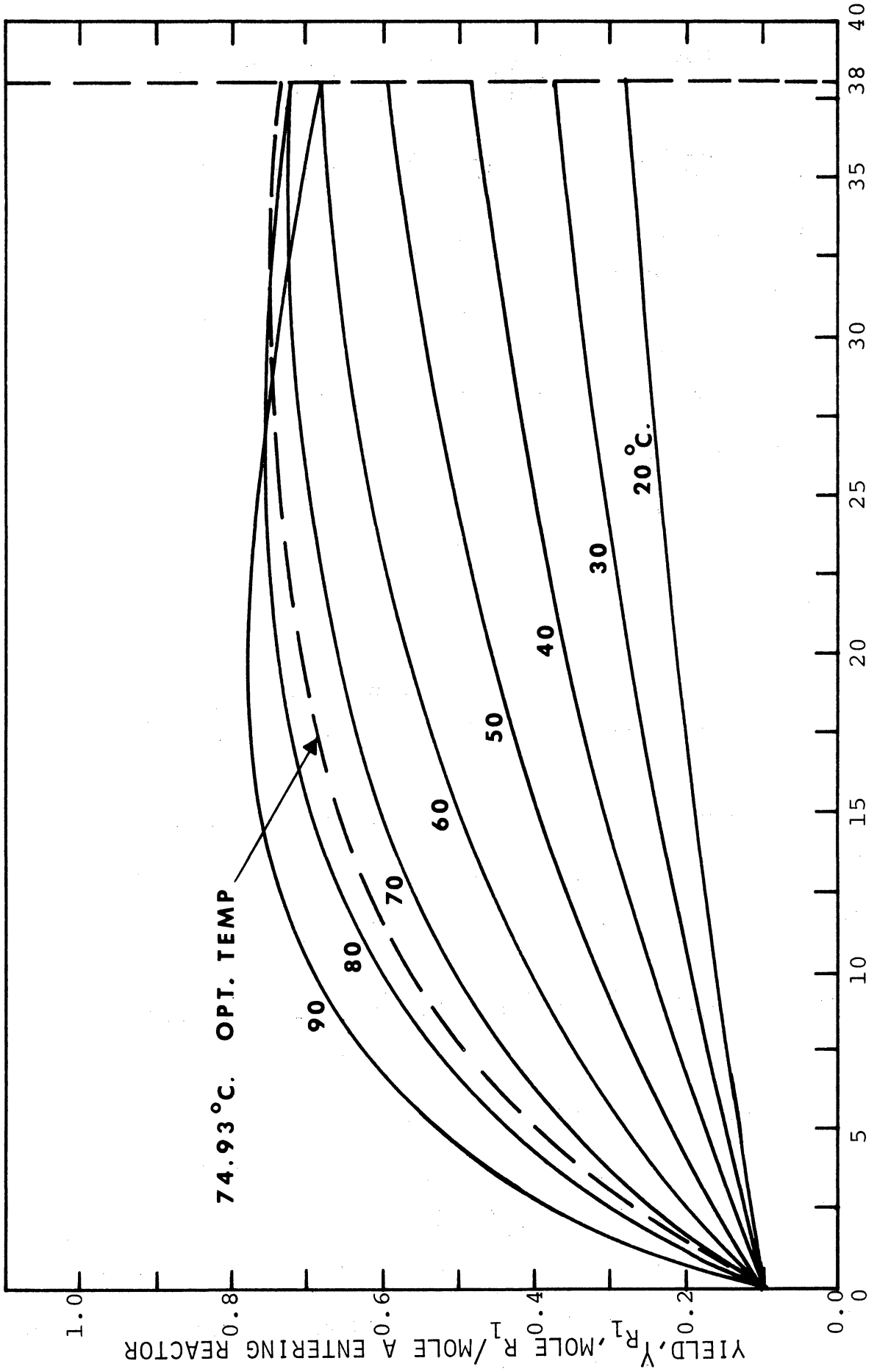

Figure 3.10. Middle Product Profiles for Isothermal Operation at Various Temperatures.

TABLE 3.2

COMPARISON OF EXIT CONCENTRATIONS FOR VARIOUS OPTIMAL TRAJECTORIES*

	Y_1	Y_2	Y_{R_2}	Y_B
Optimal Temp. Profile Figure 3.6	0.126	0.757	0.217	1.909
Optimal Heat Flux $T(0) = T(0)_{opt} = 41.43°C$	0.101	0.755	0.244	1.858
Optimal Heat Flux $T(0) = 50°C > T(0)_{opt}$	0.082	0.753	0.265	1.858
Optimal Heat Flux $T(0) = 30°C < T(0)_{opt}$	0.215	0.725	0.160	2.055
Optimal Isothermal Operation $T = 74.93°C$	0.105	0.733	0.262	1.843

* All concentrations at $t = t_f = 38$ seconds.

The more general form of the Maximum Principle as originally stated by Pontryagin is now illustrated by treating a problem in which the criteria for optimization is somewhat different.

H. Optimal Wall Heat Flux to Minimize Total Heating for a Fixed Conversion

Referring to the second order consecutive reaction system of Section F whose state equations are given by Equation (3.55) through (3.57) and (3.73), suppose the inlet compositions and temperature are fixed and that an exit composition $Y_2(t_f) = Y_{2f}$ is required. How should the wall heat flux profile be chosen such that this exit composition is indeed produced and at the same time, the "total amount of heating" (to be quantitatively defined) is minimized? Specifically, given $Y_1(0) = 1$,

$Y_2(0) = Y_{2i}$, $Y_3(0) = T_i$, how should $q(t)$, the wall heat flux be chosen such that $Y_2(t_f) = Y_{2f}$ and

$$J = \int_0^{t_f} q_f^2 \, dt \tag{3.89}$$

is minimized. Following Theorem 1, define Y_0 such that:

$$Y_0(t) = \int_0^t q_f^2 \, dt \tag{3.90}$$

The "zeroth" state equation may then be written

$$\frac{dY_0}{dt} = q_f^2 \quad , \quad Y_0(0) = 0 \tag{3.91}$$

and the problem becomes one of minimizing $Y_0(t_f)$.

The Hamiltonian has the form:

$$H = \vec{\psi} \cdot \vec{f} = C_B \left\{ k_1 Y_1 (-\psi_1 + \psi_2 + a_1 \psi_3) + k_2 Y_2 (-\psi_2 + a_2 \psi_3) \right\}$$

$$+ a_3 \psi_3 q_f + \psi_0 q_f^2 \tag{3.92}$$

The adjoint equations are:

$$\frac{d\psi_1}{dt} = C_B k_1 (\psi_1 - \psi_2 - a_1 \psi_3) - \frac{2}{C_B} (H - a_3 \psi_3 q_f - \psi_0 q_f^2) \tag{3.93}$$

$$\frac{d\psi_2}{dt} = C_B k_2 (\psi_2 - a_2 \psi_3) - (H - a_3 \psi_3 q_f - \psi_0 q_f^2)/C_B \tag{3.94}$$

$$\frac{d\psi_3}{dt} = \frac{C_B}{R Y_3^2} \left\{ k_1 E_1 Y_1 (\psi_1 - \psi_2 - a_1 \psi_3) + k_2 E_2 Y_2 (\psi_2 - a_2 \psi_3) \right\} \tag{3.95}$$

$$\frac{d\psi_0}{dt} = 0 \tag{3.96}$$

From Theorem 1, Equation (3.11),

$$\psi_o(t_f) \leq 0 \tag{3.11}$$

so that

$$\psi_o = \text{constant} \quad \leq 0 \tag{3.97}$$

Final conditions on the adjoint variables may be determined from the transversality condition (3.14):

$$\psi_1(t_f) = 0$$

$$\psi_3(t_f) = 0 \tag{3.98}$$

$\gamma_2(t_f)$ is given so that $\psi_2(t_f)$ is not fixed. Therefore we are faced with the possibility of $\psi_o = 0$ or $\psi_o < 0$. Both are possible because $\psi_2(t_f)$ is not necessarily zero. This is the reason for not using Rozonoer's form of the Maximum Principle, which only allows for the possibility $\psi_o < 0$.

First consider the case $\psi_o < 0$. Since the adjoint equations are homogeneous in $\vec{\psi}$, ψ_o can be chosen as any negative number. This will "scale" the adjoint variables. For convenience, as is usually done, set

$$\psi_o = -1 \tag{3.99}$$

The Hamiltonian then becomes:

$$H = C_B \left\{ k_1 \gamma_1 (-\psi_1 + \psi_2 + a_1 \psi_3) + k_2 \gamma_2 (-\psi_2 + a_2 \psi_3) \right\}$$
$$+ a_3 \psi_3 q - q^2 \tag{3.100}$$

Since $\gamma_0(t_f)$ is to be minimized, choose q in the interval $0 \leq q \leq q^2$ to maximize H at each instant of time.

The first and second derivatives of H with respect to the control variable q are:

$$\frac{\partial H}{\partial q} = a_3 \psi_3 - 2q \tag{3.101}$$

$$\frac{\partial^2 H}{\partial q^2} = -2 \tag{3.102}$$

Setting $\frac{\partial H}{\partial q} = 0$ requires that:

$$q = q_{\text{extremal}} = \frac{a_3 \psi_3}{2} \tag{3.103}$$

This is indeed a maximum point because $\frac{\partial^2 H}{\partial q^2} < 0$. The optimal control may now be stated. Compute q_{extremal} from Equation (3.103).

$$\begin{aligned} &\text{If} \quad 0 \leq q_{\text{extremal}} \leq q^* \text{ , Let } q = q_{\text{extremal}} \\ &\text{If} \quad q_{\text{extremal}} < 0 \text{ , Let } q = 0 \\ &\text{If} \quad q_{\text{extremal}} > q^2 \text{ , Let } q = q^* \end{aligned} \tag{3.104}$$

Solution of the two point boundary value problem to relate the optimal control to time or to the state variables requires somewhat different strategy than for the previous problems. Guesses must be made on $\gamma_1(t_f)$, $\gamma_3(t_f)$ and $\psi_2(t_f)$ with $\gamma_2(t_f) = \gamma_{2f}$ and other final conditions given by Equation (3.98). The set of six state and adjoint equations must then be integrated backwards to match the known initial conditions on the state variables. The difficulty is that a guess must be made on $\psi_2(t_f)$. This will directly affect the trajectory on ψ_3 and thus q_{extremal} . A poor guess will then produce very poor convergence,

or even worse, no convergence at all. To avoid this difficulty, trajectories were first determined for $\psi_2(t_f)$ varying over many orders of magnitude. Preliminary calculations indicated that for this particular system $\psi_2(t_f)$ was of the order of 10^6. Note also that $\psi_3(t_f) = 0$ so that the optimal control ends with adiabatic operation. Finally, if there is to be any heating at all, then q will be interior to the allowable control region at least until $q = q^*$, since $q_{extremal}$ is a continuous function of ψ_3 in the region $0 < q_{ext} < q^*$.

The optimal trajectories for $\psi_0 = -1$ are shown in Figure 3.11. Notice that convergence on the initial conditions was not nearly as good as in the previous problems. This difficulty has also been encountered by others when the optimal control is a continuous control.[101] The actual values obtained by the direct search method are compared with the required initial conditions in Table 3.3.

TABLE 3.3

COMPARISON OF REQUIRED INITIAL CONDITIONS AND THOSE OBTAINED BY DIRECT SEARCH

	Required	Obtained
$Y_1(0)$	1.0	0.99643
$Y_2(0)$	0.1	0.0686
$Y_3(0)$	30.0	29.286

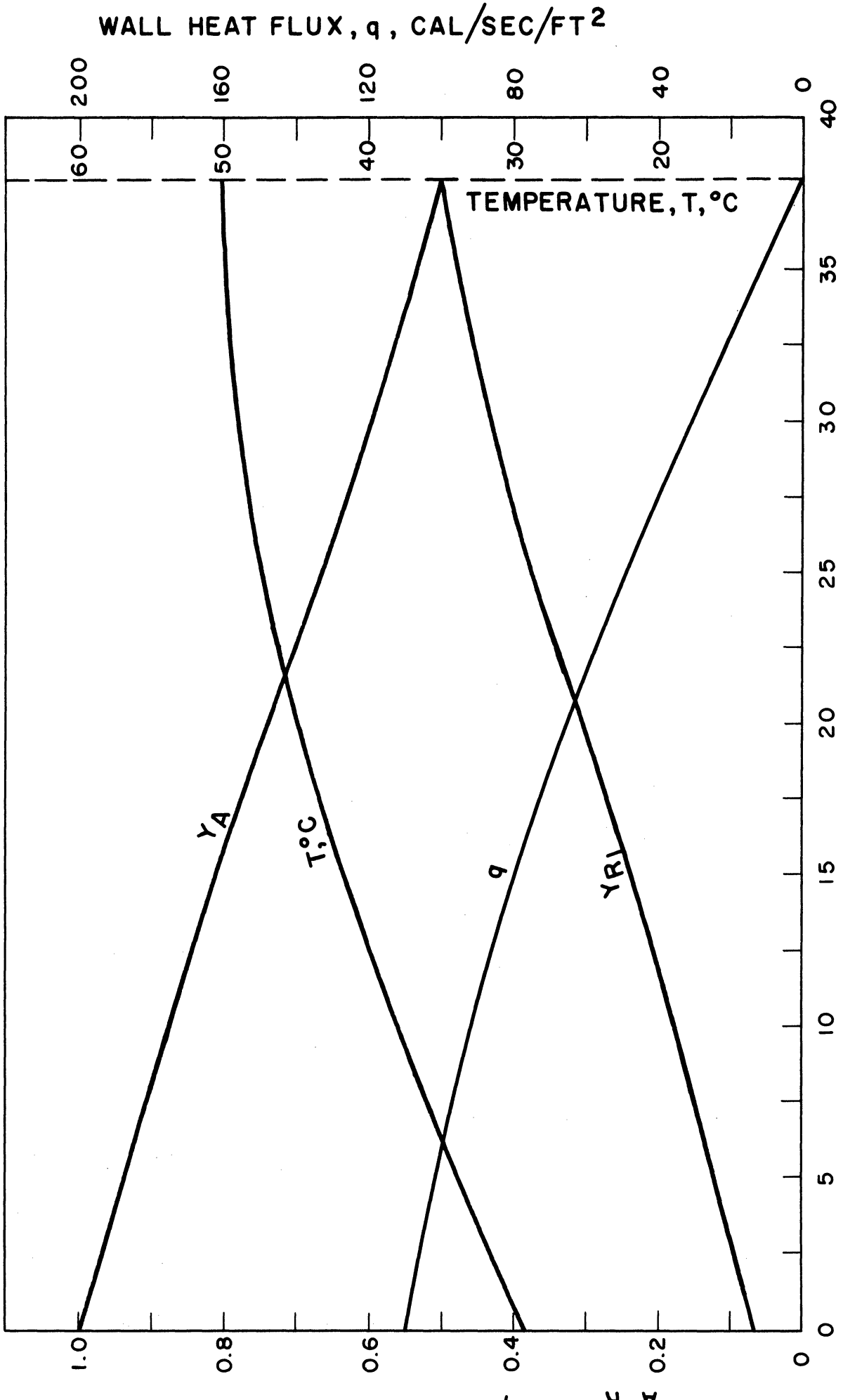

Figure 3.11. Optimal Trajectories to Produce a Specified Conversion and Minimize Total Heating.

This control is only a possibility for the optimal control. The consequences of setting $\psi_0 = 0$ must now be considered. The Hamiltonian then becomes:

$$H = C_B \left\{ k_1 Y_1 \left(-\psi_1 + \psi_2 + a_1 \psi_3 \right) + k_2 Y_2 \left(-\psi_2 + a_2 \psi_3 \right) \right\}$$

$$+ \psi_3 a_3 q \qquad (3.105)$$

This is exactly the same expression as the Hamiltonian for the problem of maximizing $Y_2(t_f)$ (3.74). However the Hamiltonian must now be maximized rather than minimized as in the previous problem, and furthermore, the final condition on ψ_2 will in most cases be quite different. The optimal control is apparent.

$$\begin{aligned}
&\text{If } \psi_3 > 0 \quad \text{, Let } q = q^* \\
&\text{If } \psi_3 < 0 \quad \text{, Let } q = 0 \\
&\text{If } \psi_3 = 0 \text{ and } \dot{\psi}_3 > 0 \text{ , Let } q = 0 \\
&\text{If } \psi_3 = 0 \text{ and } \dot{\psi}_3 < 0 \text{ , Let } q = q^*
\end{aligned} \qquad (3.106)$$

There is also the possibility that $\psi_3 = \dot{\psi}_3 = 0$ over a finite period of time. Then the Hamiltonian will become independent of the control q, and the singular control to keep $\psi_3 = 0$ must be calculated following the method of Section G. To find a reasonable starting point for the search to match the fixed initial conditions, optimal trajectories were obtained for various final values of $Y_1(t_f)$, $\psi_2(t_f)$, $Y_3(t_f)$. $\psi_2(t_f)$ was allowed to vary over the range -10^8 to $+10^8$. The results were quite surprising. There were no trajectories for which the value of ψ_3 changed sign. Furthermore changing the magnitude of

$\psi_2(t_f)$ only changed the magnitude of the $\psi_3(t)$ trajectory, but did not affect its shape. From Equation (3.106), the optimal control over the entire trajectory was either $q_f = 0$ or $q_f = q_f^*$. The required initial conditions were then assumed, and trajectories were obtained by forward integration for both full heating and adiabatic operation. If either of these trajectories were to be optimal, then $Y_2(t_f) = 0$ as given in the problem statement. For adiabatic operation $Y_2(t_f) = 0.374$ while for full heating $Y_2(t_f) = 0.722$. Thus the case of $\psi_0 = 0$ does not produce any possible solutions. The required optimal solution is therefore obtained for $\psi_0 = -1$, as shown in Figure 3.11.

I. Optimal Wall Heat Flux for a More General Profit Function

To include the cost of reactor operation the following profit function might be considered:

$$J = Y_2(t_f) - a_0 \int_0^{t_f} q_f^2 \, dt \tag{3.107}$$

where a_0 is the ratio of the unit heating cost to the unit product value. If a new variable Y_0 is defined according to:

$$\frac{dY_0}{dt} = q_f^2 \quad , \quad Y_0(0) = 0 \tag{3.108}$$

then Rozonoer's modification of the Maximum Principle may be used and the objective function will be:

$$J = \sum_{i=0}^{3} c_i Y_i(t_f) = Y_2 - a_0 Y_0 \Big|_{t_f} \tag{3.109}$$

The Hamiltonian and adjoint equations are the same as for the problem of Section H and are given by Equations (3.92) through (3.96). Final conditions on the adjoint variables are:

$$\psi_0(t_f) = a_0 \,, \quad \psi_1(t_f) = \psi_3(t_f) = 0 \,, \quad \psi_2(t_f) = -1 \tag{3.110}$$

Since $\psi_0(t) = a_0 =$ constant, the Hamiltonian becomes:

$$H = c_B \left\{ k_1 \gamma_1 \left(-\psi_1 + \psi_2 + a_1 \psi_3 \right) + k_2 \gamma_2 \left(-\psi_2 + a_2 \psi_3 \right) \right\} + \psi_3 a_3 q_f + a_0 q_f^2 \tag{3.111}$$

Differentiating Equation (3.111) twice

$$\frac{\partial H}{\partial q_f} = a_3 \psi_3 + 2 a_0 q_f \tag{3.112}$$

$$\frac{\partial^2 H}{\partial q_f^2} = 2 a_0$$

Setting $\frac{\partial H}{\partial q_f} = 0$,

$$q_f = q_{f\,\text{extremal}} = - \frac{a_3 \psi_3}{2 a_0} \tag{3.113}$$

Since $\frac{\partial^2 H}{\partial q_f^2} > 0$, $q_{f\,\text{extremal}}$ does produce the required minimum in H . The possibility of singular control may immediately be disposed of since the last term in H , $a_0 q_f^2$ cannot be made independent of q_f . The optimal control then is:

$$\begin{aligned} &\text{If} \quad 0 \leq q_{f\,\text{extremal}} \leq q_f^* \,, && \text{Let} \quad q_f = q_{f\,\text{extremal}} \\ &\text{If} \quad q_{f\,\text{extremal}} < 0 \,, && \text{Let} \quad q_f = 0 \\ &\text{If} \quad q_{f\,\text{extremal}} > q_f^* \,, && \text{Let} \quad q_f = q_f^* \end{aligned} \tag{3.114}$$

It is surprising that this most general problem of all those considered should have the simplist control law.

Optimal trajectories are shown in Figure 3.12 through 3.14 for a_0 equal to 3×10^{-6} , 3×10^{-7} , and 3×10^{-8} . These cases cover the range of high, medium and low heating costs compared with product

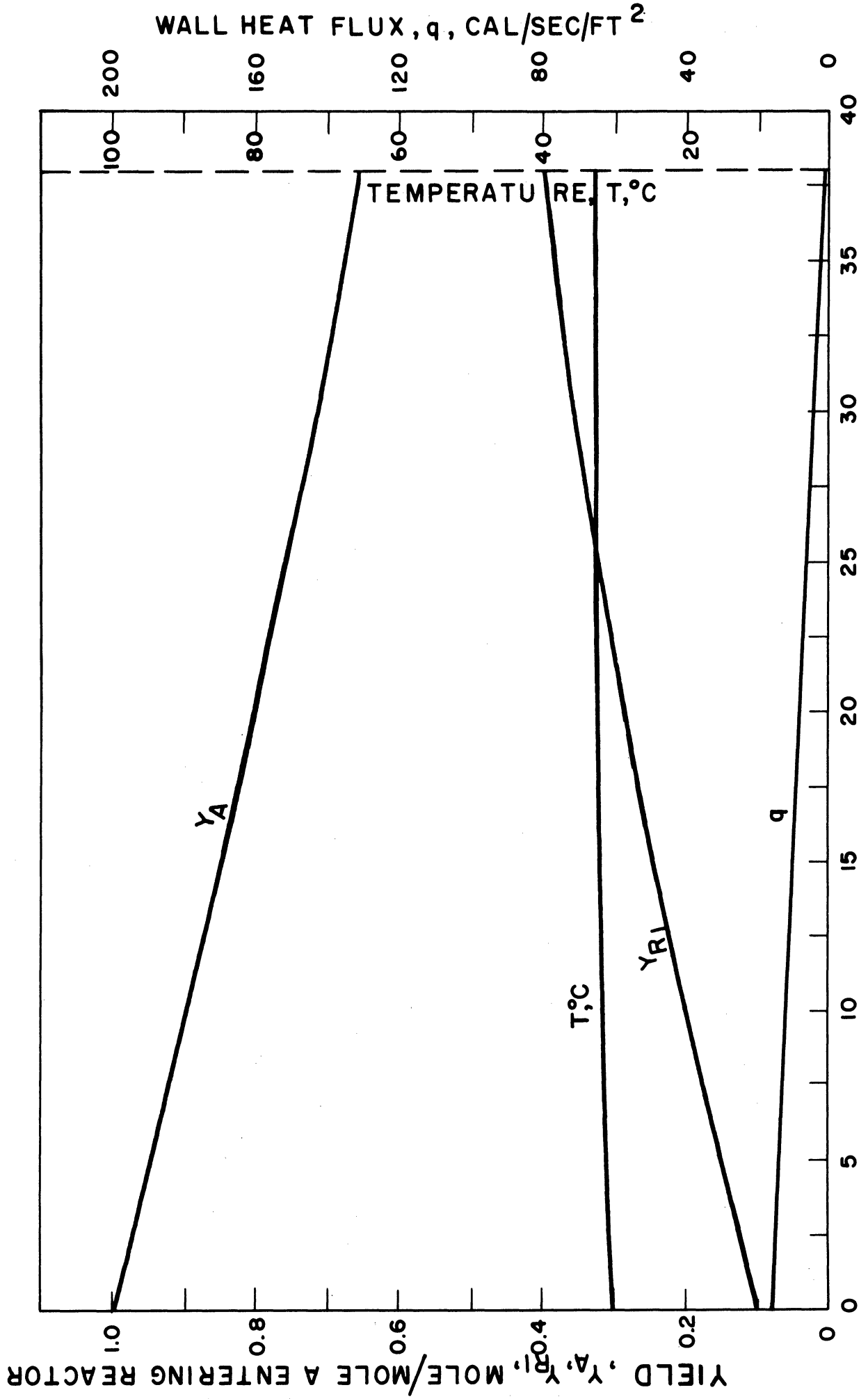

Figure 3.12. Optimal Trajectories for General Profit Function - $A_o = 3 \times 10^{-6}$.

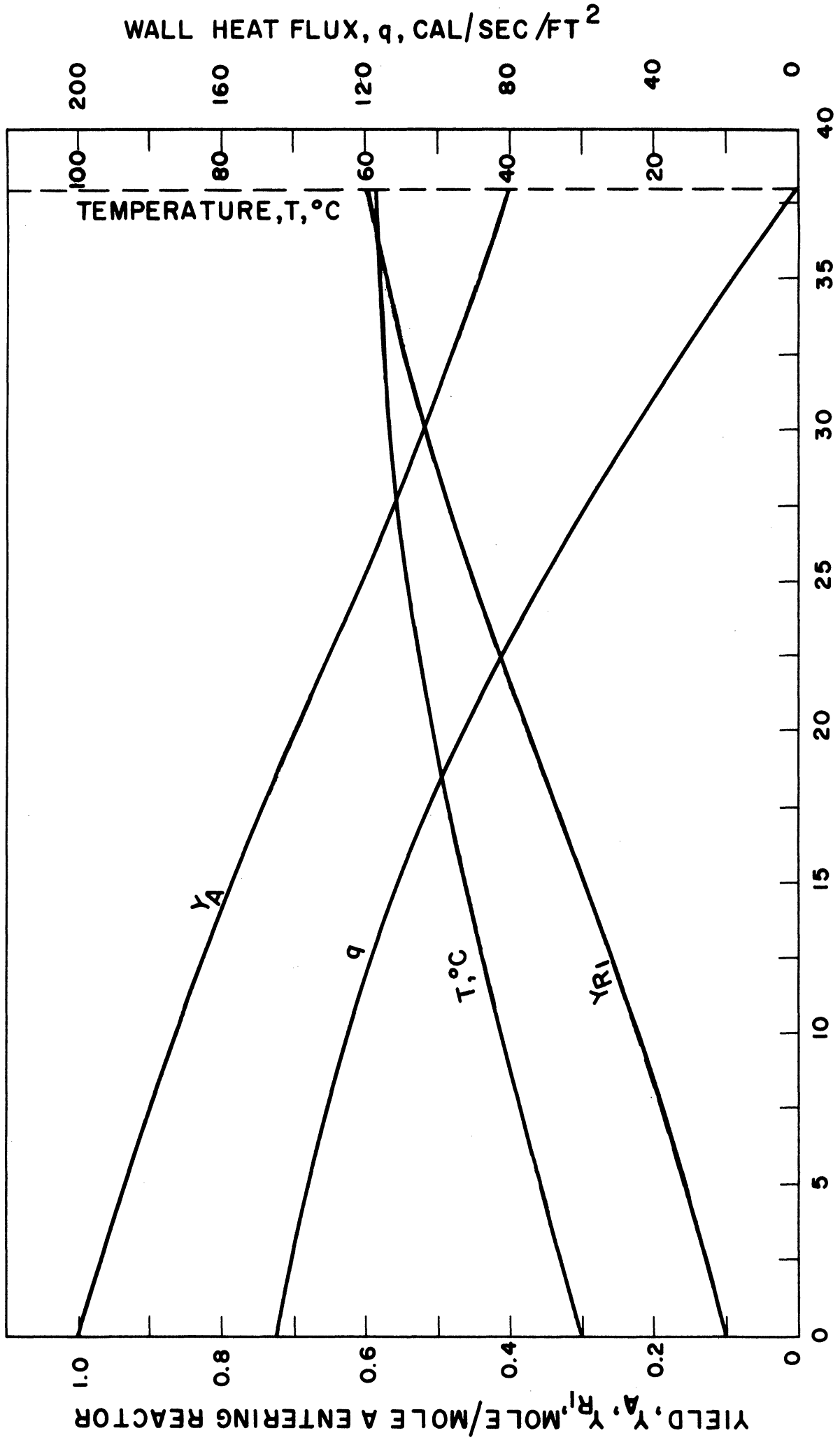

Figure 3.13. Optimal Trajectories for General Profit Function $A_o = 3 \times 10^{-7}$.

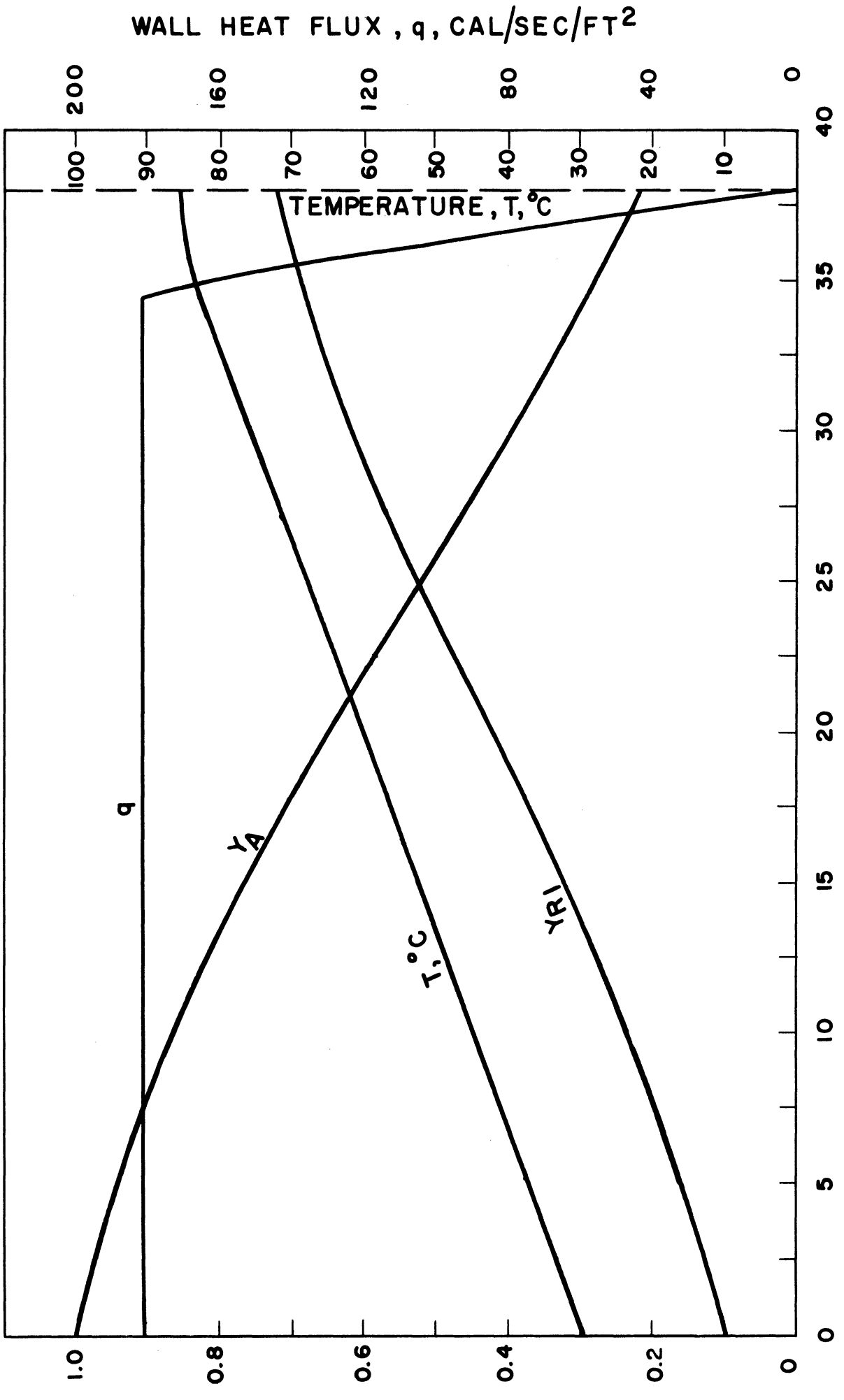

Figure 3.14. Optimal Trajectories for General Profit Function - $A_o = 3 \times 10^{-8}$.

value. In all cases, the optimal trajectory ends with adiabatic operation. For the case of high heating cost ($a_o = 3 \times 10^{-6}$), heat flux is held at a low level throughout. Consequently, temperature and conversion remain low. As the cost of heating decreases ($a_o = 3 \times 10^{-7}$) higher heat flux more than pays for itself with higher conversion. Finally for very inexpensive heating ($a_o = 3 \times 10^{-8}$), the heat flux should be held at the highest possible value for most of the reactor length. For even lower values of a_o, the final section of intermediate heating would become smaller. In the limit as $a_o \to 0$, the optimal trajectory approaches that of Section G, and full heating is required along the entire length. Table 3.4 summarizes the components of the profit function (3.107) as well as the degree of convergence obtained on the given initial conditions.

TABLE 3.4

COMPARISON OF OPTIMAL FINAL AND INITIAL CONDITIONS FOR SEVERAL RATIOS OF HEATING COST TO PRODUCT VALUE

Ratio of Unit Heating Cost to Product Value, a_o	$Y_2(t_f)$	$\int_o^{t_f} q^2 dt$	J^{**}	Convergence on Initial Conditions*		
				$Y_1(0)$	$Y_2(0)$	$Y_3(0)$
3.0×10^{-6}	0.4010	3.113×10^3	0.3979	1.000001	0.099999	30.355
3.0×10^{-7}	0.5984	3.649×10^5	0.5619	0.999976	0.100006	29.999
3.0×10^{-8}	0.7212	1.175×10^6	0.7095	1.000006	0.099989	29.383

* The required initial conditions were $Y_1(0) = 1.0$, $Y_2(0) = 0.10$, $Y_3(0) = 30.0°C$. IBM 7090 computing time to achieve this convergence averaged four minutes per run.

** See Equation (3.107).

From the comparison above, it is apparent that as the ratio of unit heating cost to product value decreases, it becomes more profitable to expend more heat to produce a higher temperature and produce a higher conversion to middle product.

From the solution of the problem of Section H, an initial guess was obtained to start the search to match the fixed initial conditions. For the first run a_0 was set at 3.0×10^{-6}. Convergence was obtained to within 10^{-4} percent on $y_1(0)$ and $y_2(0)$ but only to within two percent on $y_3(0)$, the inlet temperature. Computing time amounted to approximately four minutes. Most of this time was used in the final convergence in the vicinity of the given initial conditions. Reducing the required step size to end the search did not give any better convergence on the inlet temperature, mainly because of the propagation of computer roundoff error, and the finite step approximation of the continuously varying optimal heat flux.

For the next case considered, $a_0 = 3 \times 10^{-7}$, convergence to within 0.002 percent on all variables was obtained in less than two minutes. Such good convergence on the inlet temperature was probably due to the order of magnitude of the optimal heat flux. Roundoff error was insignificant in the computed temperature change at each step of integration. For the final case, $a_0 = 3 \times 10^{-8}$, the optimal heat flux remained at its upper bound except for the last ten percent of reactor length. Convergence was within 10^{-3} percent on $y_1(0)$, 0.02 percent on $y_2(0)$ but only within two percent on $y_3(0)$. As in Section G, precise location of the point at which q reaches its upper bound might improve convergence on the inlet temperature. To obtain the

degree of convergence shown in Table 3.4, almost five minutes of computing time was required from a starting point within ten percent of all three unknown final conditions. Slow convergence toward the end of the search has been characteristic of the problems considered in this section. The gradient method was found to be very fast in reaching the region of the "optimum", but was inferior to the direct search in the degree of final convergence. Possibly another search technique such as that of Powell,[95] Fletcher and Reeves,[46] or Rosenbrock[100,101] might converge more quickly. The first two take advantage or possible quadratic convergence, while the last rotates the search coordinate system such that one coordinate is aligned with the direction of the rising "ridge." A multivariable Newton-Raphson method[126] might also be more successful in precisely matching the known initial conditions.

4. DESIGN OF THE TUBULAR REACTOR SYSTEM

The Pontryagin Maximum Principle has provided an upper bound on yield of middle product in real reactors. Even operating optimally, one cannot expect to match these predictions, for heat flux cannot be varied continuously at will. "Best" operation depends upon the specific reactor design chosen, such as steam or hot water jacketing, co-current or counter-current heating, recycle of heating water or product, etc. In this chapter, a detailed description is given of the tubular reactor system built for this study.

A. The Chosen Reaction

In doing a carefully controlled experiment, it is best to choose a reaction system whose operating conditions are not so severe as to make normal measuring techniques impossible. Costs of reactants and reactor materials were also major factors in influencing the choice. It was hoped that a reaction would be found which was represented by a series of second order steps and whose rate law had been determined over a wide range of temperatures. Even after a thorough survey of the literature, this last requirement could not be satisfied. For the reaction chosen, saponification of diethyl adipate with sodium hydroxide, the rate constants had been determined only at 20°C and 25°C, and at very dilute concentrations where the reaction rate was extremely slow. Therefore, the reaction rate law was determined over the range of temperatures 29°C to 85°C as the initial part of this research. The overall saponification reaction may be represented by two consecutive second order steps. The reaction is of the form:

$$A + B \xrightarrow{k_1} R_1 + EtOH \qquad (4.1)$$

$$R_1 + B \xrightarrow{k_2} R_2 + EtOH$$

where

$$k_i = k_{i_o} \exp\{-E_i/RT\} \qquad (4.2)$$

and $E_1 > E_2$

A = diethyl adipate B = hydroxyl ion

R_1 = monoethyl adipate EtOH = ethanal

The details of this phase of the research are discussed in Chapter 5. The dependence of reaction rate constants on temperature is shown in Figure 5.2.

B. Reactor Design

The dimensions of the tubular reactor were governed by several factors. Sufficient reactor length was necessary to provide adequate residence time. The Reynolds number for the reactant stream was to be greater than 5,000 to assure turbulent flow. Finally the tube cross sectional area had to be such that with the above two conditions satisfied, the tube flow rate did not exceed approximately 25 gallons per hour. The solubility limit of diethyl adipate in water placed the upper bound on ester concentration at about 0.02 mole/l. Furthermore, to keep the reaction mixture at the required 0.018 mole/l. ester, and 0.05 mole/l. sodium hydroxide, the following nominal flow rates and concentrations were required:

Diethyl Adipate Solution

1.44 liter/minute 0.04 eq/l

Nominal Analysis: 90.7% diethyl adipate

9% monoethyl adipic acid (1 ester group, 1 free acid group)

0.3% adipic acid

Sodium Hydroxide Solution

55 cc/minute, 1.46 Normal

The reactor length was approximately 150 feet, divided into ten, 15 foot lengths. (Exact dimensions are shown in Figure 4.2) The tube outer diameter was 0.25 inches by 0.025 inch wall thickness. This was concentric with another tube of outer diameter 0.625 inches by 0.040 inch wall thickness, both tubes being of hard drawn copper. Yellow brass spacers as shown in Figure 4.1 were soldered to the inner tube at three foot intervals to keep the tubes concentric.

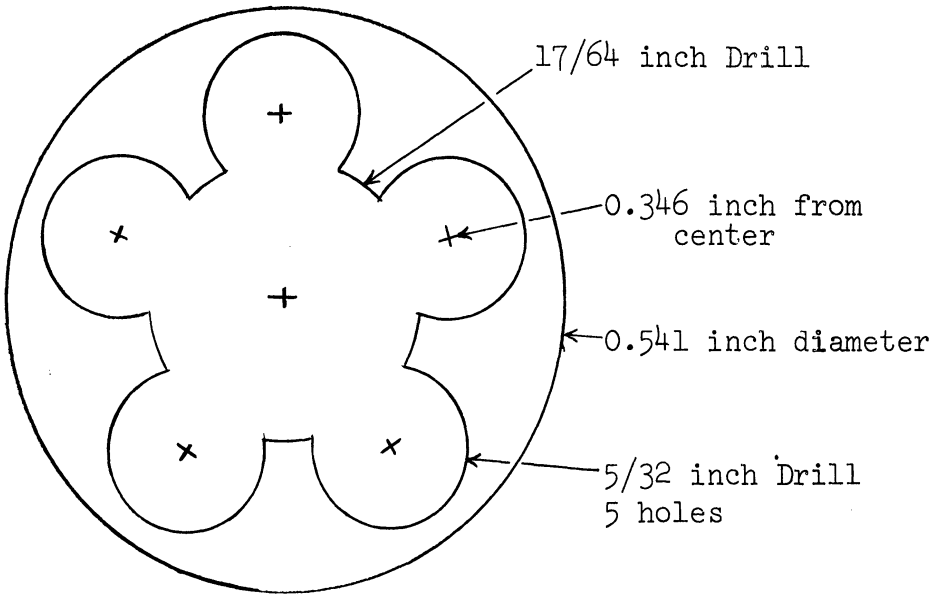

Figure 4.1. Reactor Tube Spacer.

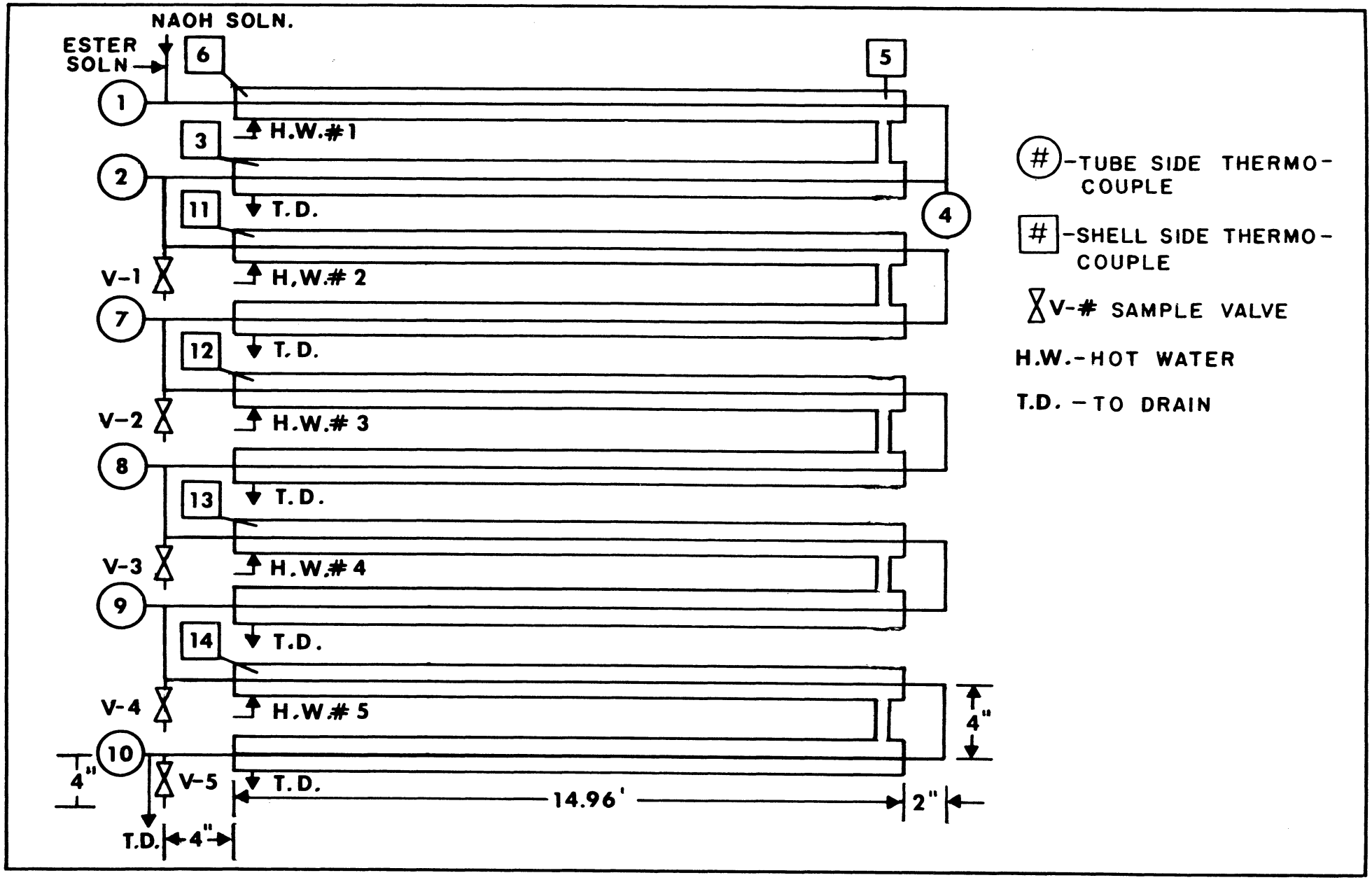

Figure 4.2. Schematic Drawing of Tubular Reactor.

As shown in Figure 4.2, all tube passes were connected while every two shell passes were connected. The end fittings were made with standard 1/2 inch brass pipe tees, nipples, unions and Hoke Gyrolock tube to male NPT fittings, as shown in Figure 4.3. In order to facilitate removal of the tubes if necessary, 1/4 inch polystyrene ferrules from Imperial "Polyflo" tube fittings were used in place of the standard brass ferrules. Polystyrene tubing (Imperial Impolene, 4 inch by 1/4 inch O.D.) was used to connect tube passes. The entire reactor was insulated with 1/2 inch fiberglass pipe insulation.

Hot water was fed co-currently with the tube flow into every second shell section, from which it passed to the adjoining shell pass and then to the drain. In this manner, separate control could be exercised over the heating rate in each of the five shell sections.

Capillary tubing, 0.036 inch I.D. leading to 1/4 inch Imperial brass needle valves was placed every 30 feet to allow sampling of the tube flow. Thus, tube fluid samples flowed from the reactor to a quenching flask containing hydrochloric acid in less than 0.2 seconds at a sampling rate of 150cc/minute. A sketch of a typical capillary sampling tube and its connection to the reactor is shown in Figure 4.4.

C. Ester Control System

In this and the following sections, we refer to Figure 4.5, a schematic drawing of the complete reactor system, and Table 4.1, the accompanying legend. The ester solution was made by filling a 55 gallon polyethylene lined steel drum with 39 gallons of distilled water. 612 grams of diethyl adipate were then added while stirring the batch with

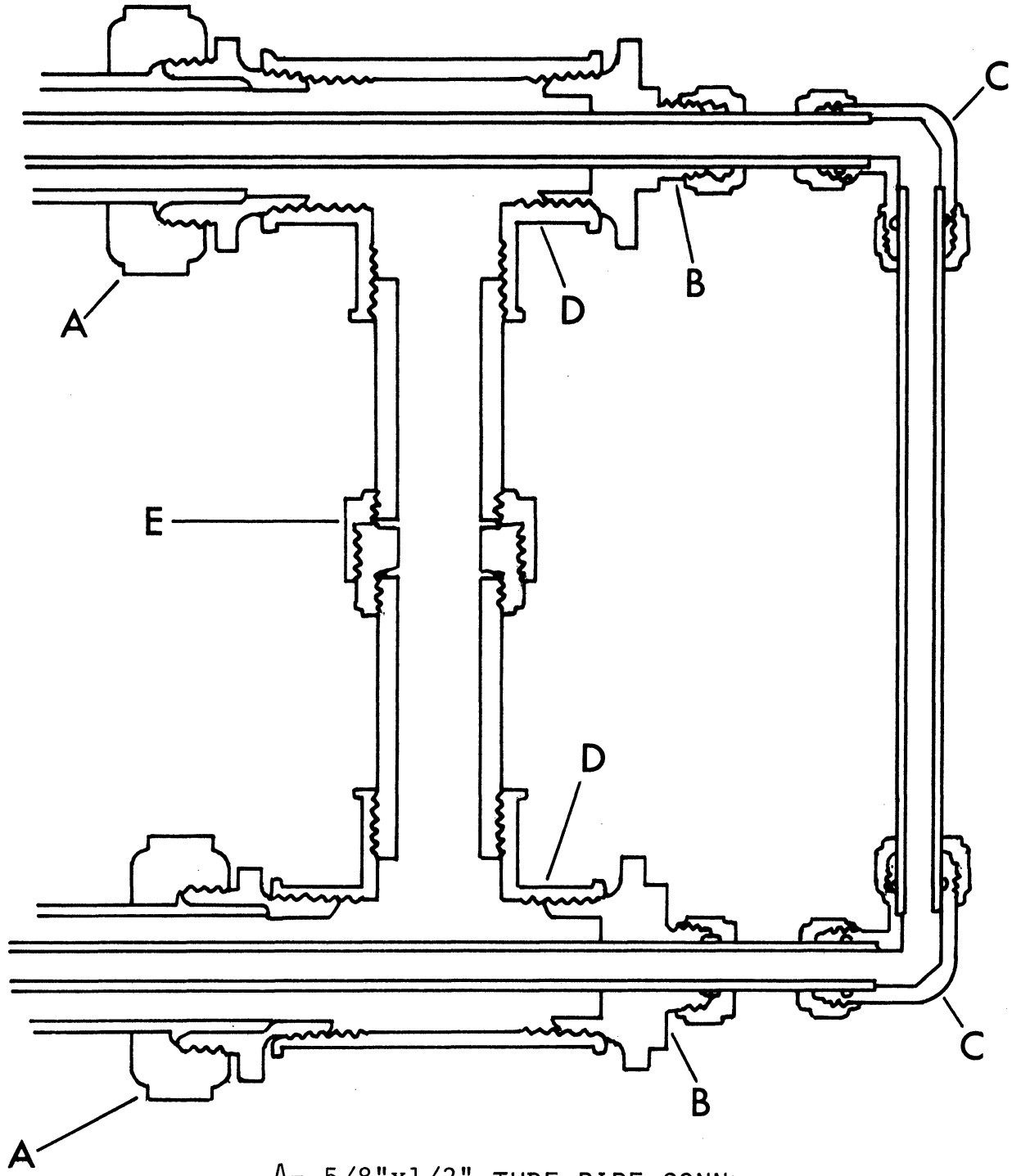

A- 5/8"x1/2" TUBE-PIPE CONN.
B- 1/4"x1/2" TUBE-PIPE CONN.
C- 1/4"x1/4" TUBE ELBOW
D- 1/2" PIPE TEE
E- 1/2" PIPE UNION

Figure 4.3. Detailed Design of Reactor End Fittings.

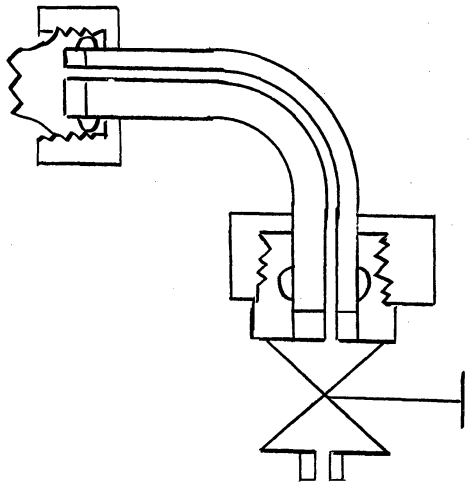

Figure 4.4. Reactor Capillary Sampling Tube.

a stainless steel, barrel mounted 1/4 horsepower mixer. Generally, solution of the ester was complete in one half hour. The feed drum, manufactured by the Rheem Manufacturing Company of Linden, New Jersey, cost only $15 complete with 2-1/2 inch NPT polyethylene fittings. When polyethylene is adequate, this type of drum should find many applications as a very inexpensive substitute for stainless steel.

From the feed drums, ester solution was pumped by an Oberdorfer bronze gear pump to a "reserve" heat exchanger. This heat exchanger was used to compensate for large changes in the temperature of the entering ester solution, caused by fluctuation of the ambient temperature from winter to summer (20°F). Depending on ambient conditions, either cold or hot water was fed to the shell side countercurrent to the tube flow. In very hot weather (90°F), this heat exchanger was not adequate and a cooling coil was placed in the ester feed drum to reduce the batch temperature.

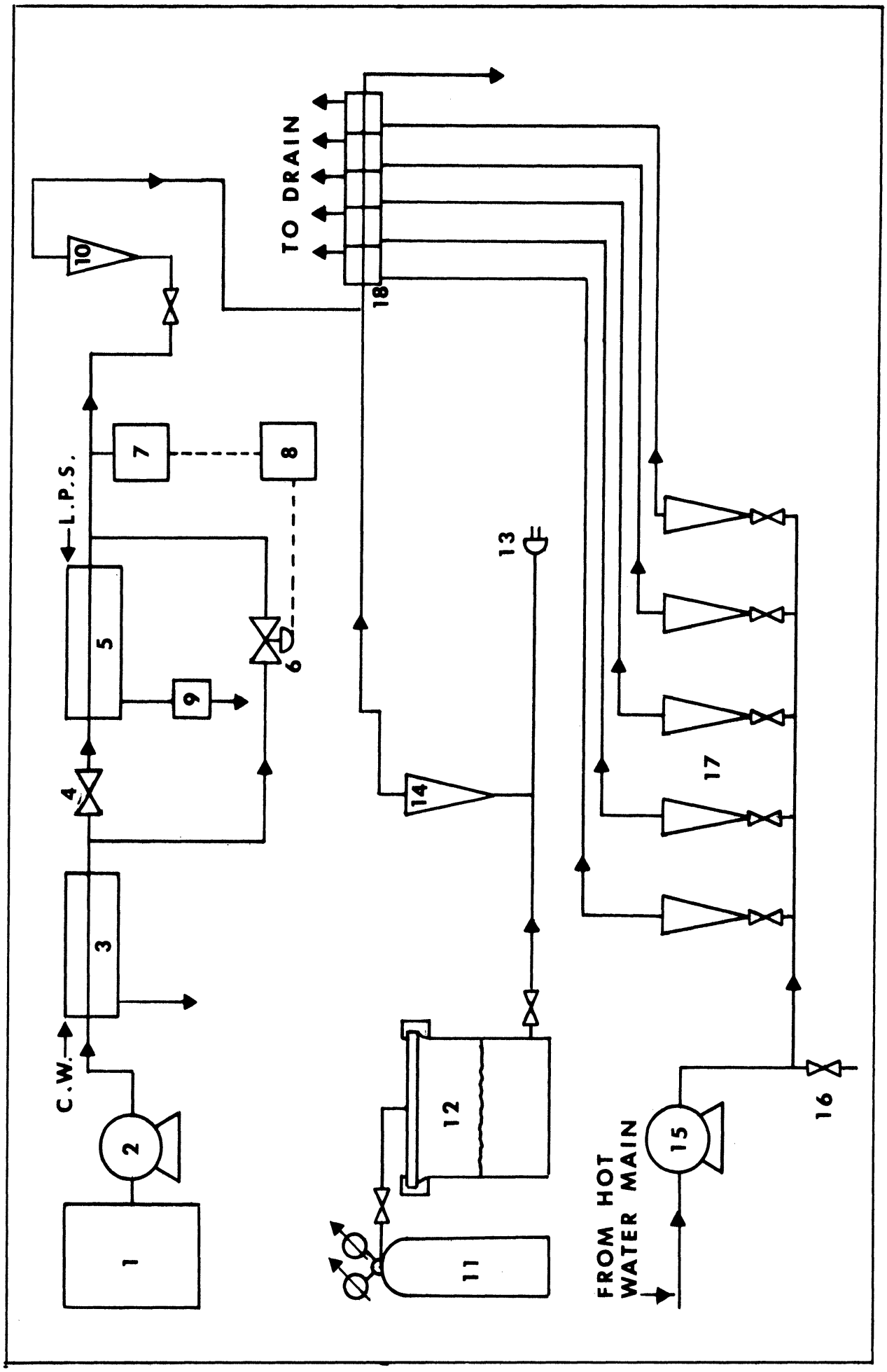

Figure 4.5. Schematic Drawing of Reactor System.

TABLE 4.1

LEGEND FOR FIGURE 4.5--REACTOR SYSTEM

1. Ester Feed Drum--55 gallon polyethylene lined steel
2. Ester Feed Pump--Oberdorfer Bronze Gear Pump-Model 1000, 1.5 l/minute at 80 psig, 800 rpm.
3. Ester Pre-cooling Heat Exchanger
4. Pressure Equalizing 1/8 inch Needle Valve
5. Ester temperature Control Heat Exchanger--Steam
6. Bypass Control Valve--Annin
7. Pneumatic Temperature Transducer--Taylor
8. Two Mode Recorder, Controller--Foxboro
9. Steam Trap--Yarway
10. Ester Rotameter--Brooks
11. Nitrogen Gas Cylinder
12. Sodium Hydroxide Feed Tank--Polyethylene lined Steel
13. Sodium Hydroxide Thermocouple
14. Sodium Hydroxide Rotameter--Brooks
15. Hot Water Pump--Oberdorfer Bronze Gear Pump Model 4000
16. Hot Water Bypass Valve
17. Hot Water Rotameters--Brooks
18. Tubular Reactor

The solution then entered the temperature control system, consisting of a steam jacketed heat exchanger in parallel with an Annin pneumatic control valve. For a given setting of this valve, a fraction of the fluid passed through the exchanger, the rest being bypassed. After mixing, the fluid temperature was monitored by a Taylor pneumatic temperature transducer. The 3-15 psi signal from the transducer was fed to a Foxboro two mode pneumatic controller (proportioned plus reset), which in turn adjusted the valve position to maintain the required ester temperature. After initial difficulties due to instabilities in the heat transfer coefficient of the steam heat exchanger, the temperature control system maintained the inlet temperature within 0.2°F during any given run (about one hour operation). The instability in heat transfer coefficient resulted from operation in the laminar-turbulent transition region (Re = 3000).

The fluid then passed through a Brooks rotameter containing a needle valve on the inlet (flow control valve), then to the reactor entrance where it mixed with the sodium hydroxide stream in a 1/4 inch Imperial brass tube tee.

D. Sodium Hydroxide System

The required flow conditions for the caustic stream, steady flow of 55cc/minute at 80 psig, made selection of a pump very difficult. The flow rate was only five percent of the capacity of the smallest gear pump available, and the pressure was too high for centrifugal or impeller pumps. The system therefore employed a different method, nitrogen pressure to displace the sodium hydroxide.

Sodium hydroxide, 1.46 N., was made up and stored in a 24 liter polyethylene jug. For use it was transferred to a 13 liter steel tank containing a polyethylene liner. This tank was fabricated from schedule 40, 8 inch pipe with 3/4 inch welded steel bottom and 3/8 inch steel upper flange and cover, as shown in Figure 4.5. The cover was fastened with 16-3/8 inch "x" 1 inch bolts. Under pressure of nitrogen entering through a 1/4 inch MPT fitting in the cover, sodium hydroxide was pumped out through a valve near the bottom.

Initially no physical separation was provided between the nitrogen and caustic solution. Nitrogen was absorbed by the caustic solution at 95 psig. Upon passing through a needle valve, the pressure decreased by 10 psig. Nitrogen gas was evolved causing two phase flow in the sodium hydroxide rotameter. This occurrence was avoided by placing a polyethylene diaphragm between the solution and nitrogen gas. The diaphragm was sealed between the tank cover and upper flange with two 1/8 inch rubber gaskets. An acceptable diaphragm was found to be a common polyethylene laundry bag available in most coin laundramats for 25 cents.

From the steel tank, the solution passed through a Hoke Milli-Mite Needle valve and was metered in a Brooks rotameter. The rotameter calibration was found to be very sensitive to temperature. Therefore, a thermocouple was installed in the entrance fitting to monitor this temperature. The rotameter was calibrated as a function of temperature. The sensitivity was attributed to viscosity variation.

Except for occasional drifts which were immediately corrected, sodium hydroxide flow rate remained constant within one percent. Drift

was minimized by maintaining the sodium hydroxide tank at a high pressure compared with the reactor inlet (95 psig versus 65 psig) and taking a large pressure drop across a needle valve. However, even with the smallest available needle valve having a ten turn stem, the flow was sensitive to valve position. An additional valve was placed in series with the needle valve so that most of the pressure drop was taken by this fixed position valve. The needle valve was used to "trim" the flow setting. This proved to be the most satisfactory arrangement. However, a flow controller to maintain the caustic flow rate would have required much less attention.

E. Hot Water System

From the laboratory main, hot water was pumped by an Oberdorfer bronze gear pump to a manifold from which it flowed through valves to each of five Brooks rotameters. It then flowed to the reactor jackets. The water temperature remained constant within 1°C after approximately 30 minutes. However, even with a relief bypass valve on the pump, surges in the line pressure caused fluctuations in the flow. These fluctuations were corrected immediately. Jacket flows were generally held within ± 1 percent.

Consideration was given to allowing hot water to flow into a feed drum open to the atmosphere, and pumping from this drum to the hot water manifold. However, under normal 40 psig line pressure, the hot water flow from the main would have been insufficient. The problem might be alleviated in the future by using two pumps. The first would pump from the main to an insulated feed drum, vented to the atmosphere. The

second would pump from this feed drum to the hot water manifold. The feed drum would be kept full and slightly overflowing to maintain a constant head for the second pump. Although this system would entail additional time lags, it would probably be satisfactory in the opinion of the author. The time delay could be minimized by diverting the hot water from the feed drum until operating temperature was reached.

F. General Operating Procedure

In addition to the design of each component of the reactor system, it is of value to describe the general operating procedure and discuss in some detail those phases which otherwise would not be apparent.

Before starting the ester and caustic flows, hot and cold water were turned on and allowed to come to steady state temperature. This also preheated the reactor jackets and minimized the startup period after reactant flows began. Next, steam flow to the ester temperature control heat exchanger was initiated. Steam was throttled by a 1/4 inch needle valve followed by a 1/8 inch needle valve to maintain 0 psig in the shell of the control heat exchanger. The steam trap in the shell exit then remained open. Attempts to operate at a higher steam pressure produced severe temperature fluctuations when the steam trap opened to discharge condensate. These fluctuations were damped by the temperature control system, but could not be eliminated, except by operation at 0 psig.

When the steam trap began to discharge steam, the ester pump was started, and the flow was adjusted with the needle valve on the rotameter. A relief valve between outlet and inlet of the ester gear pump

allowed the flow rate to be adjusted with a valve, even though the pump was of the positive displacement type. This arrangement proved very satisfactory.

Under manual control, the ester temperature was set, and the controller switched to automatic control. The sodium hydroxide needle valve was then opened to set the caustic flow, the ester flow again being adjusted. The reactor was then allowed to reach steady state operation. (10 minutes was adequate).

While at steady state, all temperature measurements were made. Stainless steel sheathed, iron-constantan thermocouples, 1/16 inch O.D. manufactured by the Claud S. Gordon Company of Cleveland were used to measure all temperatures with the following two exceptions. Ambient temperature was read from a mercury in glass thermometer, and the hot water manifold temperature was recorded on a direct reading digital thermometer accepting a thermistor input. This unit was manufactured by United Systems Incorporated, and was found to be accurate to 0.2°F when checked against the thermocouples. All thermocouple voltages compared with an ice junction were measured with a Honeywell Model-2733 Potentiometer. Measurements were easily made to 0.003 millivolts equivalent to 0.1°F.

After measuring all temperatures, the appropriate sample valve was opened. Even with capillary sampling tubes, the pressure distribution changed enough to cause both ester and caustic flows to fluctuate. They were reset and at least two reactor residence times were allowed before collecting a sample of reactant solution for chemical analysis. After sampling at a given position, the valve was closed and the sampling procedure repeated at the next position.

Approximately 25 ml. of reactant solution per sample were collected in a 50 ml. Erlenmeyer flask containing 10 ml. of 0.15 N. hydrochloric acid. The acid instantaneously reacted with excess hydroxyl ion and effectively quenched the saponification reaction. Chemical analysis of this solution is discussed in Chapter 6, the detailed procedure being given in Appendix C.

5. REACTOR SYSTEM CHARACTERISTICS

It was necessary to investigate several factors before reactor performance could be predicted. In this chapter, experiments and results are described concerning the determination of system reaction rate constants, heat transfer coefficients, and effective axial diffusivity. Comparisons are made with literature values where available. Finally, some corrosion tests are described.

A. Reaction Rate Constants for the Saponfication of Diethyl Adipate with Sodium Hydroxide

The saponification of diethyl adipate may be represented by the following stoichiometric relations:

$$A + B \xrightarrow{k_1} R_1 + EtOH$$

$$R_1 + B \xrightarrow{k_2} R_2 + EtOH \qquad (5.1)$$

where A = diethyl adipate

B = hydroxyl ion

R_1 = sodium monoethyl adipate

R_2 = sodium adipate

EtOH = ethyl alcohol

The course of these reactions has been found to be well represented by second order rate laws. The reaction rates (mole/time/volume) are therefore:

$$r_A = -k_1 C_A C_B$$

$$r_{R_1} = C_B (k_1 C_A - k_2 C_{R_1})$$

$$r_B = -C_B (k_1 C_A + k_2 C_{R_1})$$

$$r_{R_2} = k_2 C_{R_1} C_B$$

$$r_{EtOH} = C_B (k_1 C_A + k_2 C_{R_1}) \qquad (5.2)$$

The reactions are irreversible in alkaline solution due to the stabilizing effect caused by resonance of the carboxyl ion.[51] In a batch isothermal system, material balances yield the following differential equations:

$$\frac{dC_A}{dt} = -k_1 C_A C_B$$

$$\frac{dC_{R_1}}{dt} = (k_1 C_A - k_2 C_{R_1}) C_B \qquad (5.3)$$

Differential equations may also be written for C_B, C_{R_2} and C_{EtOH} but they are more easily obtained by overall material balances:

$$C_B = C_{Bi} - 2(C_{Ai} - C_A) + (C_{R_1} - C_{R_{1i}})$$

$$C_{R_2} = C_{R_{2i}} + (C_{Ai} - C_A) - (C_{R_1} - C_{R_{1i}})$$

$$C_{EtOH} = C_{EtOH} + (C_{R_1} - C_{R_{1i}}) + (C_{R_2} - C_{R_{2i}}) \qquad (5.4)$$

Because of the non-linear character of the differential equations, no analytic solution is available for concentration-time profiles. Before the advent of high speed computers, workers in this area concentrated on graphical and numerical methods which minimized computation, but at

the expense of accuracy. Having a high speed computer at hand, we may now view the problem of determining the reaction rate constants k_1 and k_2 as one in non-linear regression. That is, given a set of concentration-time data, we may find the values of k_1 and k_2 which best fit this data by repeatedly solving Equations (5.3) and employing a numerical search method to minimize:

$$\sum_{i=1}^{n} \left(C_i(t)_{EXP.} - C_i(t)_{CALC.} \right)^2 \quad .$$

In saponification reactions, hydroxyl ion concentration may be determined directly by titration, whereas other species must be found in more complicated ways.

In order to obtain measures of k_1 and k_2 over the complete temperature range, 29°C to 85°C, batch tests were made in 50 ml. Erlenmeyer flasks immersed in a constant temperature bath. The saponification reaction was initiated by pipetting the required volume of sodium hydroxide solution into the ester solution. After the required time, a known volume of hydrochloric acid was added to quench the reaction. Hydroxyl ion concentration was then determined by back titration with standard sodium hydroxide solution. This procedure was repeated for various time periods to obtain complete concentration time profiles.

A glass stirrer was provided in the reaction flask to assure uniform concentrations throughout. The constrictions at the bottom of the pipettes used to deliver NaOH and HCl were removed to allow delivery in approximately one second and the pipettes were recalibrated. Finally NaOH and ester solutions were both stored in the constant temperature bath prior to use.

Eight sets of batch runs were made between 29°C and 85°C. The maximum variations in temperature were ± 0.1°C. A typical concentration-time profile is shown in Figure 5.1. All sets of data are listed in Appendix D. Figure 5.2 shows the values of reaction rate constants and the range of probable errors in computed rate constants due to small errors in all measurements. The solid lines on Figure 5.2 represent the equations:

$$k_i = k_{io} \exp(-E_i/RT) \quad i = 1,2$$

$$k_{i_o} = 4.868 \times 10^6 \text{ l./mole/sec.} \quad E_1 = 10{,}079 \text{ cal./g.mole}$$

$$k_{2_o} = 3.487 \times 10^6 \text{ l./mole/sec.} \quad E_2 = 5964.6 \text{ cal./g.mole} \tag{5.5}$$

The numerical values in Equation (5.5) are those which best fit the sodium hydroxide and monoethyl adipate data on tubular reactor run number 3. The "best" fit was taken as the one which minimized the function:

$$\sum_{i=1}^{n} \left\{ \left(\frac{C_{B_{CALC}} - C_{B_{EXP}}}{C_{B_{EXP}}} \right)^2 + \left(\frac{C_{R_{1_{CALC}}} - C_{R_{1_{EXP}}}}{C_{R_{1_{EXP}}}} \right)^2 \right\} \tag{5.6}$$

Normalization was necessary because C_B ranged from 0.035 to 0.054 whereas C_{R_1} ranged from 0.0018 to 0.01.

To understand the apparent discrepancy between batch and flow data and how it was resolved, it is best to describe the experiments in the order that they were performed, and what motivated each succeeding one.

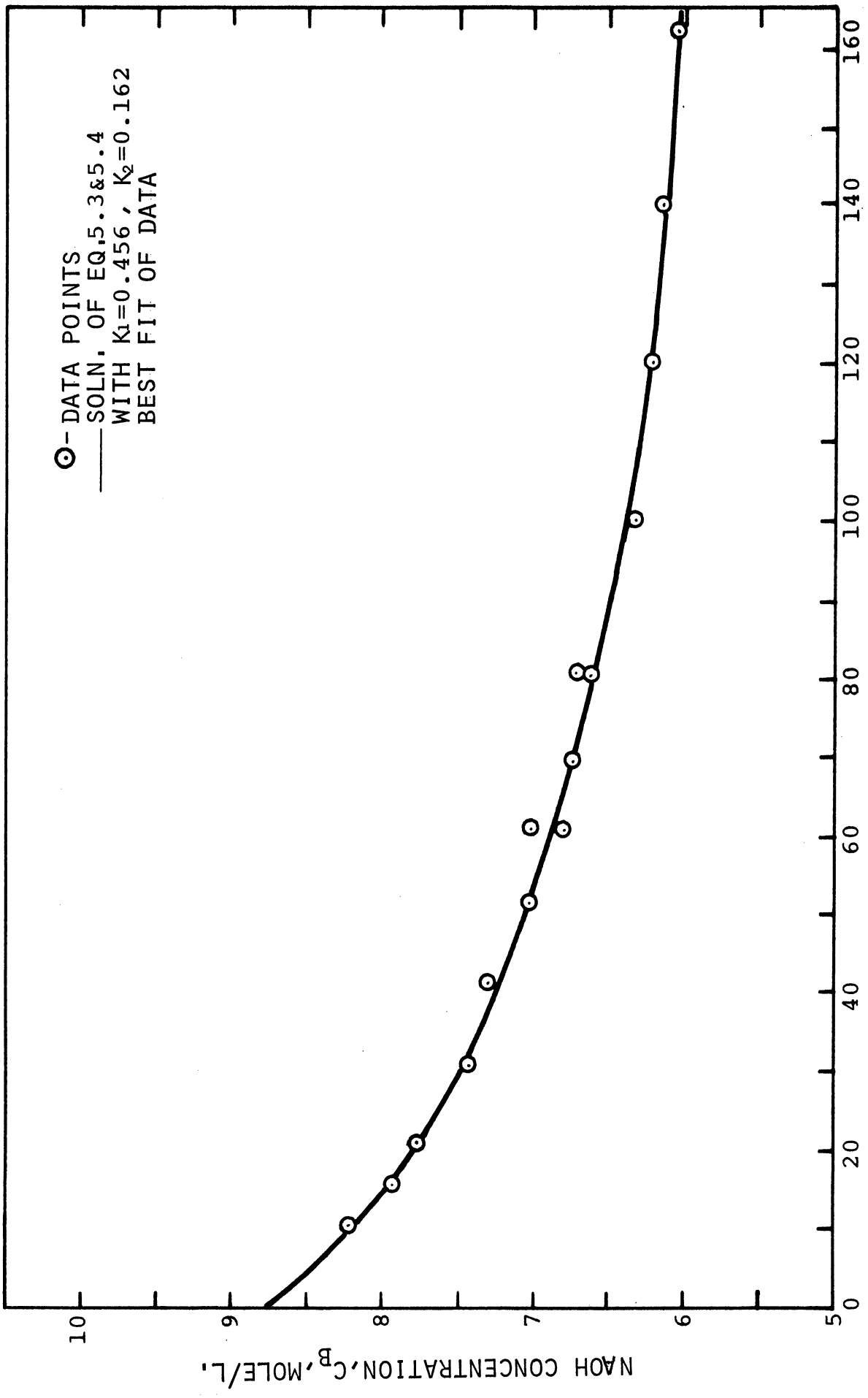

Figure 5.1. Sodium Hydroxide Concentration Profile for Batch Saponification at 46.1°C. Run No. 5.

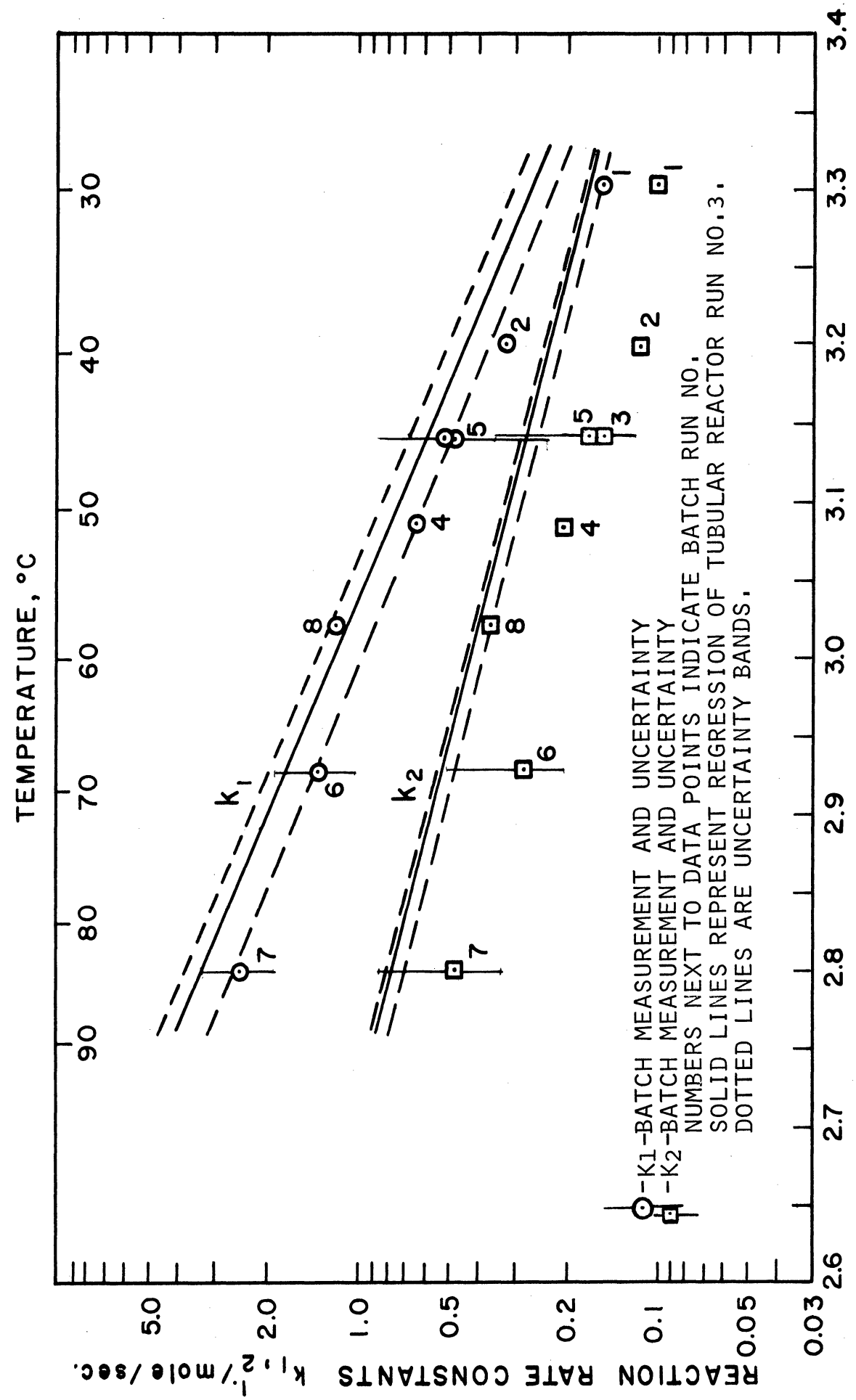

Figure 5.2. Reaction Rate Constants for Saponification of Diethyl Adipate with Sodium Hydroxide.

Diethyl adipate was obtained from the Eastern Chemical Company of Pequanock, New Jersey, where it was made from chemically pure adipic acid and ethanol. To check its purity, weighed samples of ester were saponified with sodium hydroxide. The excess sodium hydroxide was titrated with standard hydrochloric acid to a bromthymol blue endpoint. The saponification equivalent obtained, agreed within 0.4 percent with that calculated from the sample weight. Since the error was within estimated experimental error, the ester was taken as pure diethyl adipate, and kinetic runs 1 through 4 were carried out. Each run consisted of between 17 and 27 batch saponifications to obtain hydroxyl ion concentration profiles at 29.2, 39.8, 46.1, and 51.6°C. These data were analyzed using gradient and direct search methods to find the values of k_1 and k_2 which gave the "best" fit.

Rather than continue with kinetic experiments, it was decided to first obtain a procedure for analysis of monoethyl adipate in the reaction mixture so that preliminary tubular reactor runs could be made. An important result of this work was that although the diethyl adipate used in the previous kinetic experiments gave the proper saponification equivalent, it did not consist of pure diester. Approximately ten percent was hydrolyzed to monoethyl adipic acid and a small amount to adipic acid. Analysis of all kinetic data was then repeated with corrected estimates of initial conditions, and an investigation was made of the effect of changes in these initial conditions on the calculated values of k_1 and k_2. The results were quite surprising. An error in acidity of the ester solution of 0.001 mole/l. which reduced the initial hydroxide concentration in the reaction mixture by one percent, produced

a ten percent error in the regressed values of k_1 and k_2. Furthermore, the effects on k_1 and k_2 were in opposite directions. This situation is depicted in Figure 5.3. Also shown is the residual sum of squares of the errors between the data and calculated values of C_B. The most probable set of k_1 and k_2 was that which minimized this residual sum. However, the plot of residual sum versus assumed acidity in quite flat, indicating very wide confidence limits. For example, the bounds of the 95 percent confidence region are at values of the residual sum of squares equal to 30×10^{-6} compared with 6.5×10^{-6}, the largest value shown.

To confirm this analysis, another set of batch runs (run no. 5) was made at 46.1°C, this time measuring initial acidity and initial middle product concentration. The values of k_1 and k_2 are shown in Figure 5.4. This figure combines the k_1 and k_2 plots of Figure 5.3 with acidity as a parameter. The value of k_1 from run number 5 is seen to be within 6.5 percent of that which minimized the residual sum of squares in Figure 5.3, while k_2 agrees within 0.8 percent.

As the next phase in this study, an acceptable tubular reactor operating procedure was developed in preliminary reactor runs 1 and 2. These preliminary runs were followed by reactor runs 3, 5, 6, and 7. In all tubular reactor runs, reaction rates appeared to be 20 to 30 percent higher than those predicted by a plug flow model containing reaction rate constants obtained from the batch experiments. Other models were developed to account for the effect of reaction and diffusion in the laminar boundary layer, but corrections to the plug flow concentration profiles were insignificant.*

---

* The details of the mathematical models and a discussion of experimental results for the tubular reactor runs are given in Chapters 7 and 8.

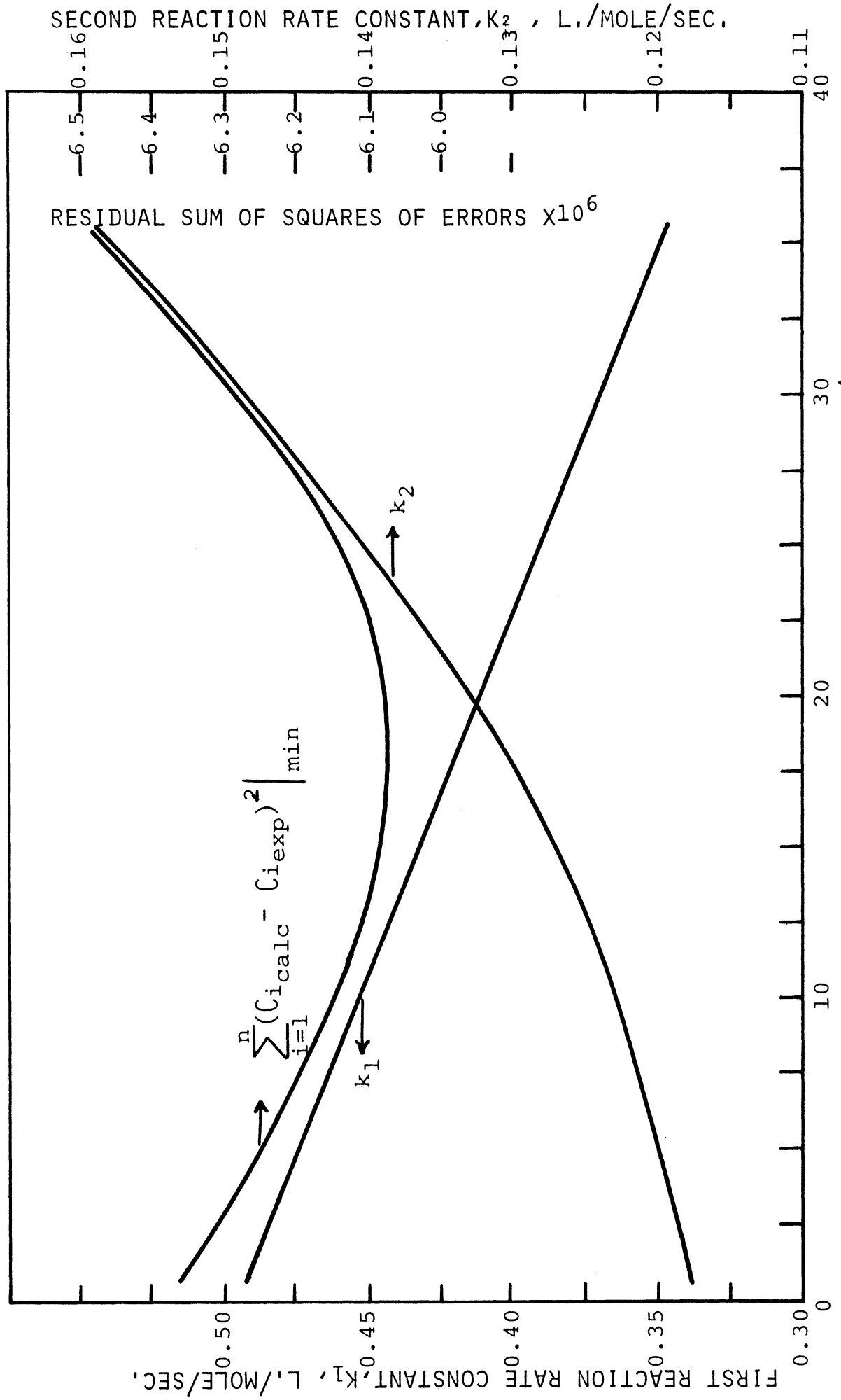

Figure 5.3. Variation of Computed Rate Constants with Assumed Acidity of Ester Solution.

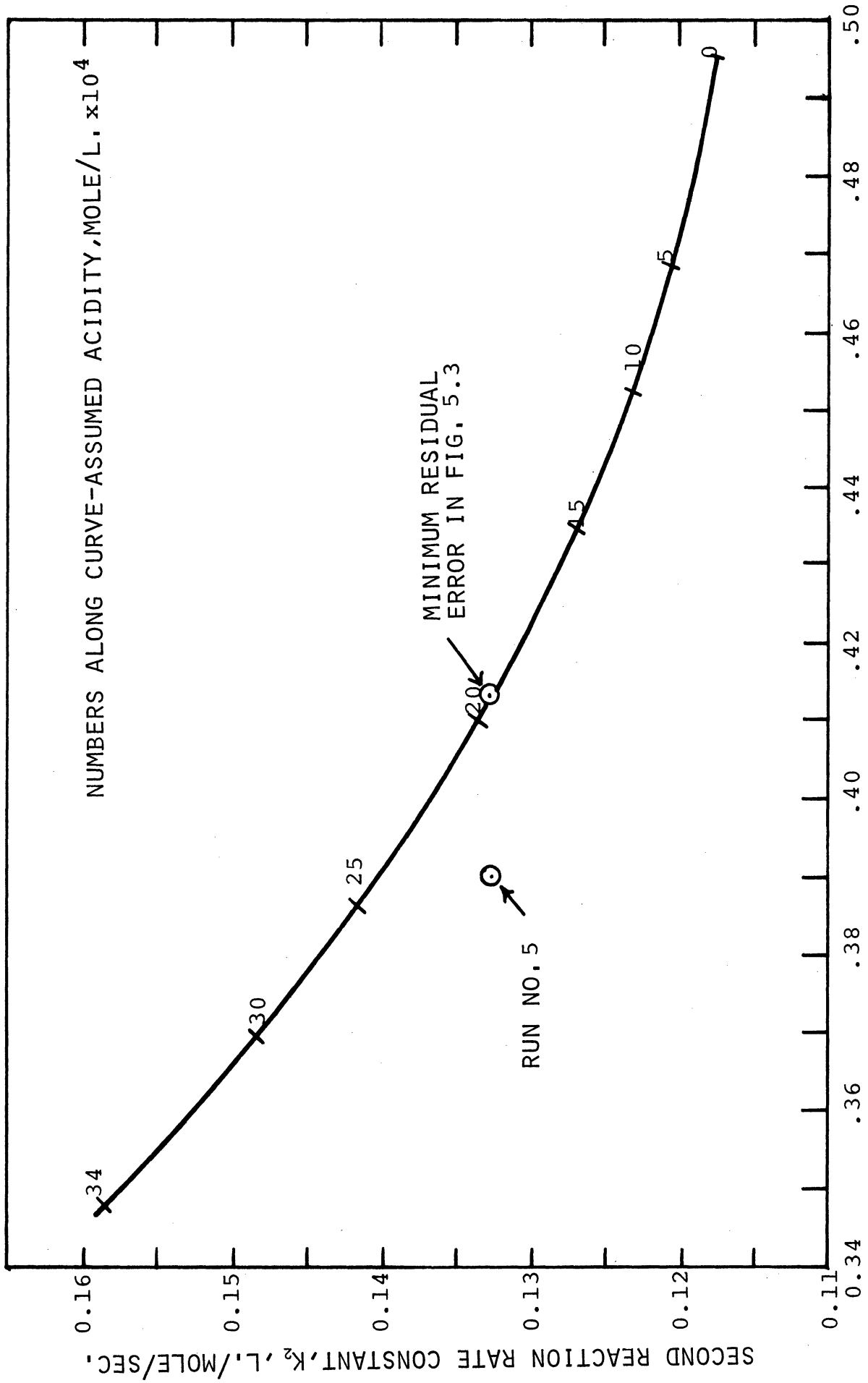

Figure 5.4. Variation of Computed Rate Constants with Assumed Acidity of Ester Solution - Parametric Plot.

At this point the following question was raised: Could a plug flow model give an acceptable fit of the data, if the parameters in the Arrhenius law were properly chosen? Using a four variable gradient search k_{1_0} , k_{2_0} , E_1 and E_2 were chosen in the Arrhenius law (5.5) such that the plug flow model gave the "best fit" for data of tubular reactor run number 3. (See Equation (5.6) for the "best fit" criteria). The numerical values of the four constants are given in Equation (5.5). Using these values, the plug flow model was found to fit all other tubular reactor data within experimental uncertainty.

It remained to explain why the batch kinetic data did not produce an acceptable model for the tubular reactor runs. The discrepancy was due in part to neglecting carbonate present in hydroxide solutions, and in part to propagation of errors through the data analysis.

Carbon dioxide is absorbed by alkaline solutions. It reacts with water to form carbonic acid which is immediately neutralized to form the carbonate. Carbon dioxide is not always excluded in the manufacture of sodium hydroxide, and consequently sodium carbonate represents the chief impurity. For example, the sodium hydroxide flakes used to prepare caustic solutions for the tubular reactor runs were found to contain 0.0303 equivalents carbonate per mole hydroxide. Total carbonate may be determined by titrating hydroxide solutions with hydrochloric acid using phenolphthalein followed by methyl orange indicators. The phenolphthalein endpoint (colorless) corresponds to neutralization of the hydroxide only, whereas the methyl orange color change from yellow to orange corresponds to neutralization of hydroxide plus carbonate. Carbonate, if unaccounted for can introduce two different errors. In

dilute solutions it hydrolyzes significantly as hydroxyl ion is consumed, and acts as a buffering agent. The derivation of the correct differential equations governing saponification in the presence of carbonate is given in Appendix E.

The effects on computed reaction rate constants, of including a correction for carbonate in the differential equations were investigated for batch kinetic run number 8 (See Appendix D for data). In run number 8, hydroxyl ion concentration was at the lowest level of all batch kinetic runs, and consequently the buffering effect of carbonate was greatest. The maximum correction to hydroxyl ion concentration was 7×10^{-5} mole/liter, only 1.4 percent of the minimum hydroxyl ion concentration (0.005 mole/liter). The corresponding changes in computed reaction rate constants were only 0.02 percent, neglible compared with other uncertainties.

A more serious error introduced by the presence of carbonate was its consumption of H^+ in acid solution. It may be explained as follows. When sodium hydroxide was added to ester solution, saponification proceeded with carbonate acting essentially as an inert. When hydrochloric acid was added to quench the reaction, carbonate was transformed to carbonic acid which in turn dissociated to carbon dioxide and water, thus consuming acid. The solubility of carbon dioxide at room temperature and normal atmospheric conditions is only 5×10^{-5} mole/liter, so that most of the carbon dioxide which formed, was evolved as gas. After back titration with sodium hydroxide (also containing carbonate which evolved carbon dioxide and consumed more acid), the calculated hydroxide concentration was too high, since both OH^- and carbonate

were actually determined. The error was systematic and occurred in all runs. Without measurements of monoester concentration, there was no reason to doubt the calculated OH^- concentration profiles.

Hydroxyl ion concentration data for all previous batch runs were recalculated taking into account the loss of acid due to evolution of carbon dioxide. New estimates of reaction rate constants were obtained as before by regression. A new set of batch runs was then made (run no. 8, 57.8°C), but this time monoester as well as hydroxyl ion concentration was measured. The procedure used was similar to that described in Appendix C for analysis of tubular reactor run data. The results, shown in Figure 5.2, agreed with the flow kinetic curves within six percent for k_1 and ten percent for k_2. This agreement suggested that error propagation in the hydroxyl ion concentration profile was far too serious to allow precise estimation of the rate constants.

Confirmation of the possibility of large errors was given by an error analysis of batch kinetic runs in which precise measurements of initial conditions were made (batch runs 5, 6, and 7). Small perturbations were made in all volumes and normalities measured in these runs. The directions of these changes were chosen first to raise the measured OH^- concentration profile, then to lower it. The perturbed data was then regressed to obtain the uncertainties in predicted rate constants depicted by vertical lines through data points in Figure 5.2.

A similar analysis was made on the data of tubular reactor run 3 to determine the range of uncertainty of the kinetic curves (solid lines) shown in Figure 5.2. In all cases, the regions of uncertainty are seen to overlap. The details of these error analyses are listed in Appendix F.

Only three investigators have reported measured values of the rate constants for the saponification of diethyl adipate with sodium hydroxide. Temperatures were restricted to 20°C and 25°C. Conconcentration levels were much lower than those of this study. In all cases, only hydroxyl ion concentration profiles were measured. The results of these investigations are shown in Table 5.1.

TABLE 5.1

SUMMARY OF DETERMINATIONS OF RATE CONSTANTS FOR SAPONIFICATION OF DIETHYL ADIPATE WITH SODIUM HYDROXIDE

Investigator	Initial Conditions			Temp°C	Rate Const.		Ref.No.
	diester	NaOH	NaCl		k_1	k_2	
Ingold	0.002	0.002	--	20.0	3.52	0.704	62
Frost and Schwemer*	0.01	0.01	0.2	25.0	5.20	1.83	50
Westheimer et al.	0.005-0.011	0.005-0.011	0.006-0.07	20.0	5.7-6.1	--	125
Westheimer et al.	0.01**	0.01-0.02	0.02-0.3	20.0	--	1.7-2.2	125
This study (extrapolated)	0.02	0.05	--	20.0	9.3	7.7	

* Solvent was one part dioxane, three parts water.

** Sodium monoethyl adipate.

For comparison, extrapolated values at 20°C from this study are also given. Note that the extrapolated constants of this study are considerably higher than other values reported.

The original data of Frost and Schwemer were reanalyzed using the search techniques described above. The values of rate constants obtained were in precise agreement (0.1 percent) with their estimates. This agreement verifies their method of data analysis, but does not imply anything about the uncertainty of their calculated reaction rate constants.

Using Equation (5.5) to represent the rate constants for the saponification, the temperature-time profile for the saponification reaction in a Dewar flask was measured. This data was used to estimate the two heats of reaction simultaneously. The method used was non-linear regression similar to that for estimating reaction rate constants. That is, the heats of reaction $-\Delta H_1$ and $-\Delta H_2$ were chosen by direct search to best fit the measured temperature profiles. The results are shown in Table 5.2. The original data is given in Appendix D. The values obtained for $-\Delta H_1$ and $-\Delta H_2$ were then used in the tubular reactor simulation as parameters in the heat balance equation. The heats of reaction actually had very little effect except for adiabatic operation since they caused only a 1°F. temperature rise for complete reaction in the tubular reactor.

TABLE 5.2

MEASURED HEATS OF REACTION

Run Number	$-\Delta H_1$ kcal./g. mole	$-\Delta H_2$ kcal./g.mole
1	10.08	17.34
2	11.48	15.21
Average	10.78	16.27

B. Reactor Heat Transfer Characteristics

In this section an experiment is described for determining the overall heat transfer coefficient for transfer between shell and tube. The results are compared with those obtained using the correlation for tube heat transfer coefficients given by Bird et al.[17,110] This experiment was done for two reasons. Precision of the correlation in predicting reactor temperature profiles was important because of the sensitivity of the reaction rate constants to temperature. Performing reactor heat balances also provided a check on all temperature measuring apparatus. In fact, poor agreement of preliminary heat balances helped to detect an error in the wiring of a 20-position thermocouple switch.

These experiments were performed with water in both shell and tube. Prior to making temperature measurements, the reactor was filled with a mixture of diethyl adipate and sodium hydroxide, so that the surface layer of copper adipate described in Section D of this chapter would form, and the reactor would be "conditioned." Hot water was pumped through the first reactor shell, cocurrent with cold water in the tube. Temperature measurements were made at the inlet, at 15 feet and at 30 feet from the inlet. Shell and tube flow rates were varied over the range of values used in the reaction experiments. Table 5.3 illustrates the closure of heat balances between the inlet and 15 foot position. This section was also used to compute overall heat transfer coefficients. The average heat transferred for tube and shell was employed in the calculation. At 30 feet, shell and tube temperature were too close to allow an accurate determination of the overall heat transfer coefficient. As shown, closure was generally within one to three percent.

TABLE 5.3

ILLUSTRATION OF HEAT BALANCE CLOSURE BETWEEN INLET AND FIFTEEN FEET FROM REACTOR INLET

Run Number	Tube Flow lb./hr.	Shell Flow lb./hr.	Q Tube BTU/hr.	Q shell BTU/hr.	Overall Heat Transfer Coeff. BTU/hr./ft.^{2}/°F
1	203.1	144.0	8,469	- 8,251	210.7
2	203.1	252.0	11,170	-11,415	321.0
3	203.1	345.7	13,425	-13,586	404.3
4	203.1	345.7	13,242	-13,378	389.0
5	203.1	539.0	15,557	-15,469	498.2
6	203.1	771.5	17,263	-17,204	621.9
7	203.1	1013.0	17,995	-18,132	675.8
8	180.9	345.7	11,632	-11,615	357.6
9	220.0	345.7	13,068	-13,067	381.0
10	246.6	345.7	13,686	-14,070	403.4
11	246.6	345.7	13,735	-14,035	395.7

The Reactor Heat Balance

To develop the mathematical model needed to predict tube temperatures, consider the schematic drawing in Figure 5.5. Differential heat balances on tube and shell yield:

$$\frac{dT_T}{dz} = \frac{U_o \pi D_o}{W_T C_T} (T_S - T_T) \qquad (5.7)$$

$$\frac{dT_S}{dz} \qquad \frac{U_o \pi D_o}{W_S C_S} (T_T - T_S) \qquad (5.8)$$

with known initial conditions.

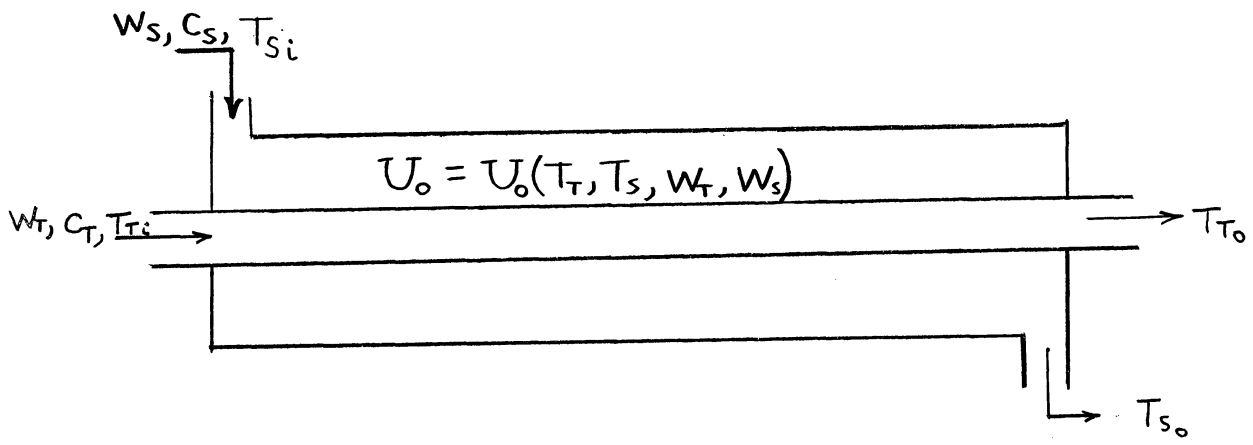

Figure 5.5. Schematic Drawing of Reactor Section.

When U_o , the overall heat transfer coefficient, is constant, these equations may be integrated exactly to yield the familiar expression:

$$Q = U_o A_o \frac{(T_{Ti} - T_{Si}) - (T_{To} - T_{To})}{\ln\left[\frac{T_{Ti} - T_{Si}}{T_{To} - T_{So}}\right]} \tag{5.9}$$

The overall heat transfer coefficient is given by:

$$U_o = \left\{ \frac{1}{h_o} + \frac{R_o \ln\left(\frac{R_i}{R_o}\right)}{k_w} + \frac{R_o/R_i}{h_i} \right\}^{-1} \tag{5.10}$$

The individual heat transfer coefficients for tube and shell, h_i and h_o may be estimated from the correlation of Sieder and Tate[110] as:

$$h = \frac{k}{D} [Re] [Pr]^{1/3} \left[\frac{\mu_b}{\mu_w}\right]^{0.14} \cdot f(Re)^* \tag{5.11}$$

$f(Re)$ is a function of the Reynolds number and is usually given in graphical form. Over the range of temperatures considered, (80 to 180°F)

---

* D represents D_i or D_o .

the viscosity of water varies from 1cp. to 0.33cp.[92] Density varies only by three percent, so that $[Re]$, $[Pr]$, and consequently h will vary. It is true that changes in h_i and h_o along the reactor are somewhat compensating since tube temperature increases while shell temperature decreases. In spite of this, it would be extremely fortuitous if U_o remained constant. Consequently, the differential equations (5.7), (5.8) were integrated numerically on a digital computer using the Runge-Kutta Fourth order method.[88] Point values of $f(Re)$ for $10^3 \leqslant Re \leqslant 10^5$ from the Sieder Tate correlation[17,110] were read in as a data table for the computer program. Lagrange interpolation on this table was then employed to obtain values of $f(Re)$. Physical properties of both tube and shell fluids, and the heat transfer coefficients (5.10 to 5.11) were calculated along the integration each time the derivatives were evaluated (four times per step). Comparisons between predicted and measured temperatures and heat transfer coefficients are given in Tables 5.4 and 5.5.

From Table 5.4, it is seen that except for run number one, made at very low shell flow, measured and predicted temperatures generally agree within 1°F. This deviation was equivalent to an uncertainty in reaction rate constants of approximately two percent due to uncertainty in temperature. This uncertainty is much smaller than the uncertainty of the measured rate constants. Figure 5.6 shows a comparison between temperature profiles for heat transfer run number 10 obtained by integration of Equations (5.7) through (5.8), using the predicted variation of U_o along the reactor, and using U_o as constant and equal to the experimentally determined value. The maximum deviation between the two

TABLE 5.4

COMPARISON BETWEEN PREDICTED AND MEASURED TEMPERATURES
FOR HEAT TRANSFER STUDY

Run No.	Tube Temperature, °F			Shell Temperatures, °F		
	Inlet	15 ft.*	30 ft.**	Inlet	15 ft.*	30 ft.**
1 meas.	73.2	115.0	120.0	182.3	125.0	120.3
pred.	"	108.2	114.9	"	133.1	123.7
2 meas.	74.3	129.3	133.0	181.6	136.3	133.3
pred.	"	128.9	133.2	"	137.6	134.1
3 meas.	73.2	139.3	142.3	184.0	144.7	142.4
pred.	"	139.7	142.8	"	144.9	143.1
4 meas.	73.1	138.3	141.6	183.0	144.3	142.1
pred.	"	139.1	142.2	"	144.3	142.4
5 meas.	73.4	150.0	153.3	183.0	154.3	153.1
pred.	"	151.0	153.0	"	153.8	153.0
6 meas.	73.6	158.6	160.7	183.6	161.3	160.8
pred.	"	159.4	160.7	"	161.0	160.7
7 meas.	73.7	162.3	164.3	182.6	164.7	164.4
pred.	"	163.5	164.4	"	164.6	164.4
8 meas.	73.2	137.5	141.0	176.9	143.3	141.2
pred.	"	138.3	141.1	"	142.8	141.3
9 meas.	73.7	133.1	136.5	177.8	140.0	137.0
pred.	"	133.8	137.1	"	139.6	137.5
10 meas.	73.4	128.9	133.4	176.7	136.0	133.8
pred.	"	129.7	133.4	"	136.5	133.9
11 meas.	73.2	129.8	133.2	177.0	136.4	133.6
pred.	"	129.8	133.5	"	136.6	134.0

* Precisely 15.78 feet.

** Precisely 31.23 feet.

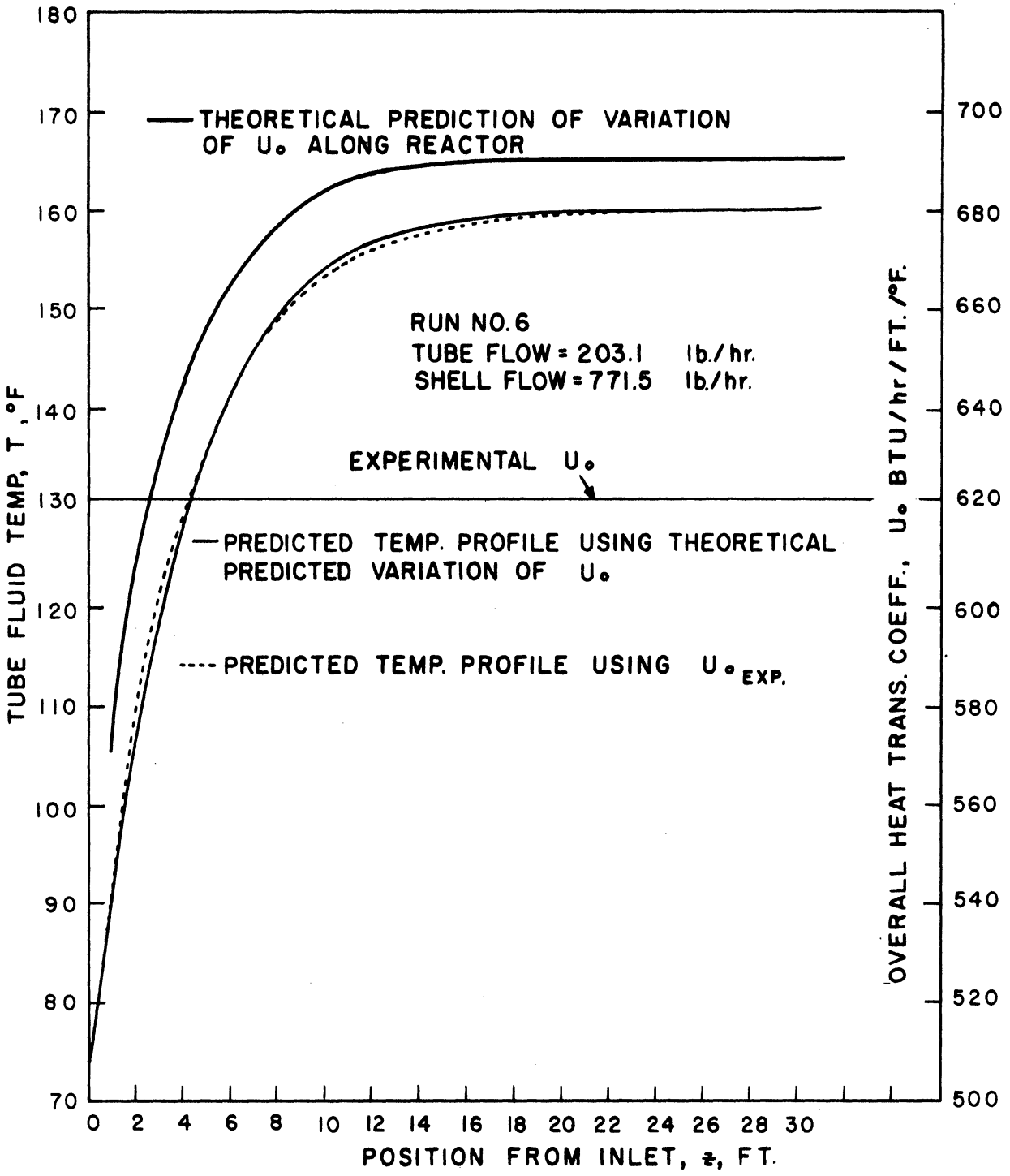

Figure 5.6. Run No. 6 - Predicted Reactor Temperature Profile and Overall Heat Transfer Coefficient.

profiles occurs in the reactor entrance section where the temperature gradient is steepest. However, in no case is this difference more than 1.5°F. It is less than 0.5°F for most positions. Profiles for other runs yielded similar agreement.

TABLE 5.5

COMPARISON BETWEEN PREDICTED AND MEASURED OVERALL HEAT TRANSFER COEFFICIENTS

Run No.	Measured Overall Heat Trans. Coeff. From 0-15 FT. BTU/hr. $ft.^2$°F	Variations of Predicted Heat Trans. Coeff. From 0-15-30 ft. BTU/hr.
1	210.7	107-102-84
2	321.0	304-264-256
3	404.3	387-380-378
4	389.0	385-379-376
5	498.2	458-535-537
6	621.9	523-664-667
7	675.8	568-762-763
8	357.6	346-366-363
9	381.0	377-385-371
10	403.4	396-376-370
11	395.7	396-376-370

C. Determination of Effective Axial Dispersion Coefficient

To determine whether back mixing was significant for the flows considered here, a method for determining the effective axial dispersion

coefficient was developed. Most previous studies have used concentration pulses and the method of moments to determine the axial Peclet number. Aris has shown that a pulse of arbitrary shape may be used if it is measured at two positions along the reactor.(7)

Measured axial dispersion is the result of two occurrences, axial diffusion and also the combination of a radial velocity gradient and radial diffusion. G. I. Taylor showed that the residence time distribution produced in the latter case could be duplicated by a model considering a uniform velocity across the tube and an effective axial dispersion obeying Ficks Law.(114) It is therefore termed Taylor diffusion.

Under the turbulent flow conditions found in the reactor considered here, the mechanisms for heat and mass transfer are identical, eddy diffusion. Molecular diffusion may be neglected, since measured eddy diffusion coefficients are found to be several orders of magnitude greater than those for molecular diffusion.

Due to the ease of obtaining continuous reactor temperature measurements, compared with concentration measurements, it was decided to use the dispersion of heat rather than mass to characterize effective axial dispersion. Although this procedure was far simpler experimentally, there was an added theoretical complication, that of the reactor wall heat capacity. This may be illustrated by referring to the schematic drawing of the reactor as modified for dispersion measurements.

A three way quick action ball valve was connected to the reactor inlet, so that either hot or cold water would flow through the reactor depending on the valve position. The valve was set in the "cold" position

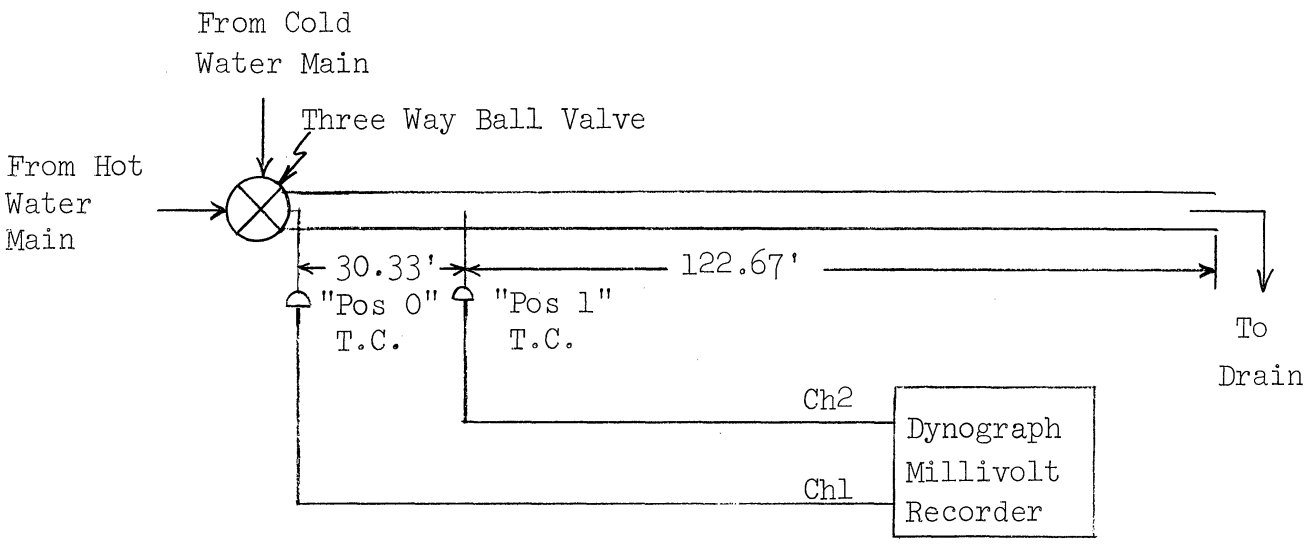

Figure 5.7. Schematic Drawing of Reactor Modified for Dispersion Measurements.

and the reactor allowed to come to steady state. The valve was then momentarily switched to "hot", then back to "cold" so that a pulse of hot water was injected at the reactor inlet. The water flow rate was monitored in the ester rotameter. Except at the instant of switching hot and cold water flows were regulated to the same constant value with a needle valve. The reactor shell was evacuated to three inches of mercury absolute pressure, to help reduce the heat leak between the tube wall and shell. Even then, only approximately 90 percent of the energy of the pulse at point "0" could be detected at point "1". This was due to heat leak through the end fitting 15 feet down the reactor.

Now we may explain the complication mentioned above. Consider pulses of mass and heat. In the absence of axial mixing, a pulse of mass would remain unchanged as it moved along the reactor. This is not

the case for a pulse of heat. The hot pulse comes in contact with a cold tube wall and gives up some of its energy to the wall. Cold water follows the hot pulse and comes in contact with the warmed wall. Heat is then transferred back to the water. Consequently, even in the absence of axial mixing, a pulse of heat will spread as it moves along the reactor. To obtain a measure of axial mixing this "wall effect" had to be separated from other mixing effects. The required results are stated below. The derivation appears in Appendix B.

As shown above, suppose a pulse of hot water is injected into a stream of cold water, and the fluid temperature is monitored continuously at two positions, "0" and "1". Define the n-th moment of temperature at position z by:

$$\mathcal{M}_n(z) = \int_0^\infty \tau(\bar{z},\theta)\,\theta^n\,d\theta \tag{5.12}$$

where: $\tau = T - T_{w_i}$

$\theta = vt/L$ = dimensionless time

$\bar{z} = z/L$ = dimensionless position

Also define

$$\mu' = \left\{ \mathcal{M}_1(1) - \mathcal{M}_1(0) \right\} / \mathcal{M}_0 \tag{5.13}$$

and the n-th central moment at $\bar{z}$ by:

$$\mathcal{M}_n^c(\bar{z}) = \int_0^\infty \tau(\bar{z},\theta)\cdot(\theta-\mu')^n\,d\theta \tag{5.14}$$

Then the axial Peclet number is given by:

$$\frac{\mathcal{M}_2^c(1)}{\mathcal{M}_0} - \frac{\mathcal{M}_2^c(0)}{\mathcal{M}_0} = \frac{2(\mu'-1)}{b_2} + \frac{2\mu'^2}{[Pe]} \tag{5.15}$$

where :

$$[Pe] = \frac{v L}{D_e} \quad , \quad b_2 = \frac{4 h D_i}{\rho_w C_w (D_o^2 - D_i^2)} \cdot \left(\frac{L}{v}\right)$$

and D_e is the effective axial dispersion coefficient. $\mathcal{M}_o$ need not have a position associated with it since it is theoretically independent of the measuring point.

Typical temperature response curves are shown in Figure 5.8. Points along the curves were read into a computer program which used second order interpolation and the Runge-Kutta method to numerically obtain the required moments. Notice that the input pulse at position "0" is actually a multiple pulse. This was required to minimize the effect of the "tail" section on the value of the second moment. Points in the "tail" section were most difficult to read from the curves. For a single pulse the tail could easily contribute 50 percent of the second moment, $\mathcal{M}_2^c(1)$. Using the multiple pulses, the main section of the pulse was expanded, and the influence of the "tail" on the second moment was reduced to only 10 percent. The introduction of similar errors due to uncertainties in measurements in the "tail" sections for pulses of mass, has also been reported by Curl and McMillan.[34]

Three such tests were made. The results and conditions of the tests are given in Table 5.6.

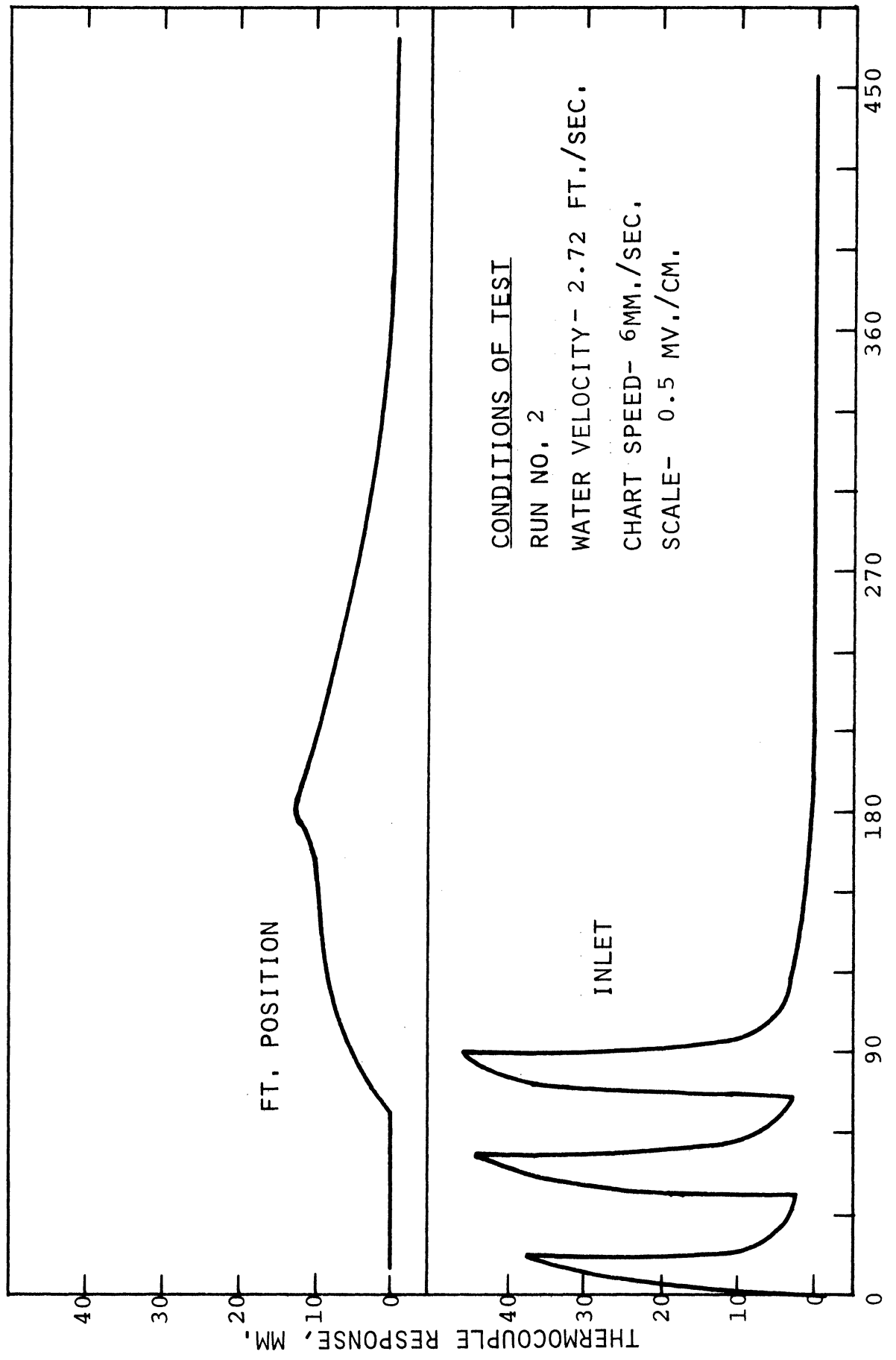

Figure 5.8. Response Curves at Inlet and 30 Feet for Hot Water Pulse.

TABLE 5.6

RESULTS OF AXIAL DISPERSION DETERMINATION
BY PULSE TESTING

Run Number	μ' *	Fractional Heat Loss**	$Pe^{-1} = \frac{D_e}{vL}$
1	18.6	0.145	0.0294
2	21.4	0.104	0.0623
3	20.8	0.109	0.0466
Average	20.3 sec.	0.119	0.046

$$Pe^{-1}_{\text{average}} = 0.046$$

Standard deviation = 0.016 = 35.2 percent

Conditions of tests

$\frac{L}{v}$ = 11.1 sec.

v = 2.72 ft/sec.

h = 500 BTU/hr. ft^2

= 0.25 in.

= 0.20 in.

ρ_w = 556 lb/ft^3

C_w = 0.0935 BTU/lb./°F

ρ = 62.4 lb./ft^3

C_t = 1 BTU/lb./°F

* $\mu' = \frac{m_1(1)}{m_0(1)} - \frac{m_1(0)}{m_0(0)}$

** $\frac{m_0(1) - m_0(0)}{m_0(0)}$

To determine the effect of dispersion on reactor performance, the average dispersion number (reciprocal Peclet Number) should first be determined for the entire reactor length. Assuming a constant effective axial dispersion coefficient along the reactor, this is simply:

$$\text{Dispersion Number} = \left[\frac{D_e}{vL}\right] = \left[Pe^{-1}\right]_{\substack{\text{TEST}\\\text{SECTION}}} \cdot \frac{L_{\text{TEST SECT.}}}{L_{\text{REACTOR}}}$$

The reactor dispersion number was then 0.0092. Tichacek[115] has considered the effect of dispersion on maximum yield of middle product for second order consecutive reactions. He concluded that the fractional decrease in peak yield to middle product due to axial dispersion is roughly equal to the dispersion number. (Yield = mole middle product per mole of pure reactant in feed.) Thus, axial dispersion in this reactor will reduce yield by less than one percent. Since this decrease is well within the uncertainty of experimental concentration profiles, neglecting axial diffusion is a valid simplification in the mathematical model.

No pulse testing procedure is complete without an estimate of magnitude and direction of probable errors. Two obvious sources of error are evident from Table 5.6:

1. The discrepancy between measured and calculated values of μ'
2. Heat loss along the reactor.

The discrepancy between measured and calculated values of μ' was probably due to neglecting the thermal inertia of the tube end fitting sealing the tube from the shell pass at the 15 foot position. This fitting weighed 1.8 pounds compared with only 20 pounds for the

entire 30 feet of copper tubing. An effective thermal inertia may be determined from Equation (B.13) by inserting the experimental value of μ' and the calculated value of b_1. This allows calculating an effective b_2 which could then be used with the experimental value of μ' to calculate a correct Peclet number. Such an analysis increases effective wall thermal inertia ($\rho_w C_w$) by 43.4 percent, and yields an effective value of b_2 equal to 7.13 compared with a calculated value of 12.6. The average value of the dispersion number (Pe^{-1}) is then reduced by 25 percent. Consequently, this analysis provides added evidence that axial dispersion is negligible in this reactor.

The effect of the heat loss on calculated dispersion number is more difficult to evaluate quantitatively. Referring to Figure 5.8 and Table 5.6, there are several possible effects on $\frac{m_2^c(1)}{m_0(1)}$ if the response curve at position "1" were raised to equate $m_0(1)$ with $m_0(0)$. If the heat loss occurred about the centroid of the pulse, then this correction would decrease $\frac{m_2^c(1)}{m_0(1)}$ and hence decrease the calculated dispersion number in Equation (5.15). If the heat loss correction were made uniformly along the curve by multiplying the entire curve by a constant factor, then there would be no effect on $\frac{m_2^c(1)}{m_0(1)}$. Raising the response curve in the tail section would tend to increase $\frac{m_2^c(1)}{m_0(1)}$ and would therefore increase the calculated dispersion number.

Levenspiel[82] presents a summary of the available experimental data on axial dispersion in straight pipes. Using his plot, an estimate of the dispersion number for the entire reactor (150 feet) would be 0.0011. Carter and Bir[27] obtained experimental dispersion numbers for a high pressure ethylene reactor containing twelve, eight foot sections

connected by sharp 180° return bends. They used a helium tracer technique and obtained dispersion numbers higher by a factor of three than those given by Levenspiel. Even these results are only one half of the corrected values found in this work. Therefore all indications are that axial dispersion may be neglected in the mathematical model.

D. Experiences with Corrosion

As a matter of record two occurrences relating to corrosion are described in this section. The first relates to the formation of copper adipate on the inner surface of the reactor.

It is well known that copper is a satisfactory reactor material for caustic solutions. Before building the reactor, pieces of copper tubing were immersed in diethyl adipate and sodium hydroxide solutions. Except for a mild cleansing action (removal of scale), no affect was noticed for up to two weeks of immersion. The reactor was then built but before operation, some copper tubing was immersed in reaction mixture (initially 0.02M. diethyl adipate, 0.05M. NaOH). The results were surprising. After one day, the surface of the copper darkened. After two days, the entire surface was coated with a black material which would not wash off in water but was easily removed by nitric acid. This coating is thought to have been copper adipate. The coating action seemed to cease after two days. No further change in the surface was noticed. It was presumed that in the presence of a high concentration of adipate ion (final reaction product), the solubility product of copper adipate was exceeded at the copper surface. Copper adipate then precipatated on the copper surface protecting it from further attack. The

reactor was run periodically for five months. Reactor runs lasted a maximum of 90 minutes. Maximum reactor pressure was 65 psig, and maximum temperature was 185°F. No failures occurred in any copper tubing during this period.

The second noteworthy experience relates to failure of brass fittings in contact with reaction mixture and ester solution. Thermocouple glands, made from 316 stainless steel were threaded into brass tubing fittings to connect them to the reactor. During the course of operation, failure in the brass occurred at the point of contact with stainless steel. This was not unexpected because sodium hydroxide will attack the zinc in brass. However, similar failures occurred in the brass end fittings of the ester rotameter. Failure was by cracking in both cases. The rotameter end fittings contained chrome plated 1/8 inch female pipe threads. Stainless steel (316) tube to pipe fittings were connected to both rotameter end fittings. The lower brass end fitting failed by cracking along the threads after two months of operation. One month later, the upper brass end fitting failed in the same fashion. Both cracks were at the point of contact between brass and stainless steel, and were thought to be due to stress corrosion cracking and galvanic action due to a dissimilar metal junction. Stainless steel rotameter end fittings were inserted as replacements and no further failures resulted. It is interesting to note that 20 brass tubing fittings were used to make up reactor end fittings connecting copper to polystyrene tubing. No failures resulted in any of these fittings.

6. CHEMICAL ANALYSIS OF REACTION PRODUCTS

The ideal product analyzer is one through which a material flows and out of which comes a continuous composition analysis. Such analyzers have been developed for complex hydrocarbon systems using chromatography. For single liquid phase reactions, continuous electrical conductivity measurements sometimes provide the required information.[111] Such was not the case for the consecutive saponification reactions studied in this work. No on-line instrumental method of analysis was found. Analysis was possible only after separating monoester from diester using benzene extraction. The general procedure and the work involved in its development are described in this chapter. A detailed step by step procedure is given in Appendix C.

The first problem was one of stopping the reaction very quickly. This was accomplished by allowing reactor effluent to flow into weighed flasks containing known quantities of hydrochloric acid. This effectively removed hydroxyl ion and quenched the saponification reaction. Subsequent reweighing and a previous density determination allowed direct calculation of sample volumes. The original hydroxyl ion concentration was also easily determined by back titration with standard soidum hydroxide. The end point was calculated to occur near pH-7.3. Following the work of Frost and Schwemer[50] bromthymol blue indicator having a color change from yellow to blue between pH 6.8 and 7.5 was used. Experimental titration curves using a pH meter verified the applicability of this indicator. Typical curves are shown in Figure 6.1.

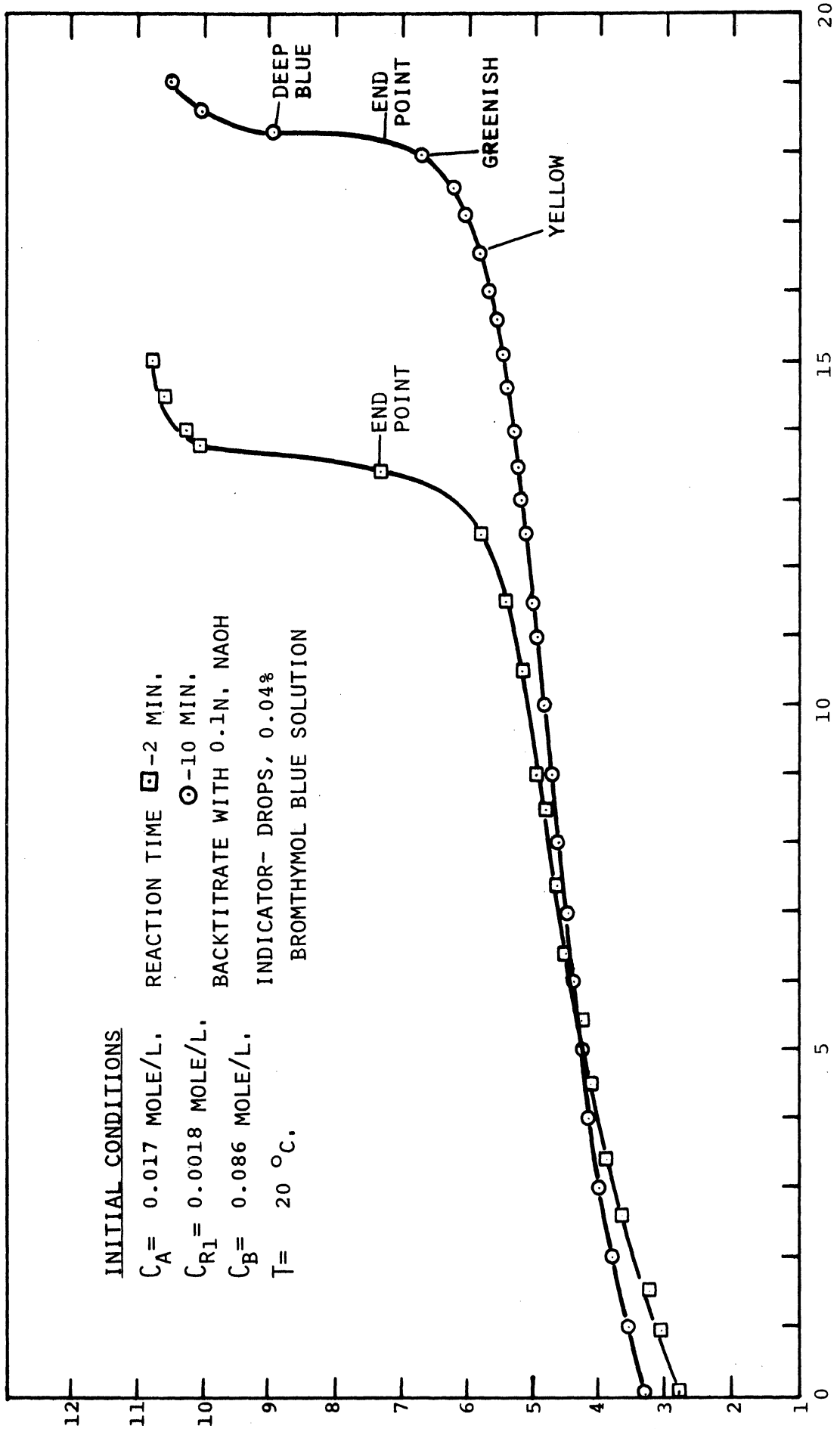

Figure 6.1. Experimental Titration Curves.

Ingold[62] employed benzene and pentane to extract all unreacted ester from a mixture of diethyl adipate, monoethyl adipate and adipate ion. His purpose was to produce a monoester, free of diester so that the second reaction rate constant could be determined independently. His work showed that benzene extracts all the diester and a small fraction of monoester from aqueous solution. To make this technique useful for analysis of monoethyl adipate concentration in the original reactor sample, it was necessary to know the equilibrium distribution of monoethyl adipate between benzene and water. This information was obtained by the following experiments. A solution of diethyl adipate was saponified with sodium hydroxide in the ratio of one mole NaOH per mole ester. Since the limiting component was OH^-, the final product distribution was high in monoester with diester and disodium adipate present in lower concentrations. The reaction mixture was then washed twice with benzene (one volume benzene per volume solution) to remove unreacted diester. The aqueous phase was centrifuged to remove entrained benzene, and the benzene phase was discarded. An aliquot of the aqueous phase was saponified to completion to determine the monoester concentration. The remainder was used to prepare 25 ml. volumes of various dilutions ranging from full strength to 1/5 strength. These solutions were shaken in separatory funnels with benzene ranging in volume from 100 to 400 ml. The aqueous phases were then centrifuged to remove entrained benzene, and a portion of each was saponified to completion with an excess of standard NaOH. Back titration to neutral with standard HCl allowed determination of the final monoester concentration in each case. Monoester concentrations in the benzene phases were then calculated from losses in the aqueous phases.

The resulting concentration distribution data are shown in Figure 6.2. The least square line passing through the origin is given by the following equation:

$$(C_{R_1})_{\text{benzene phase}} = 0.0033\ (C_{R_1})_{\text{aqueous phase}} \qquad (6.1)$$

Large volumes of benzene were used for the extraction in an attempt to minimize the effect of experimental error. Nevertheless, the difference between data points at $C_{R_1\ \text{aq.}} = 0.01147$ and 0.01152 was due to a difference of 0.03 ml. (3.92 versus 3.95 ml.) in the back titration for duplicate samples. This difference was the limit of experimental precision. Using Equation (6.1), the correction for monoester lost in the benzene wash is readily calculated. For a solution washed with "n" consecutive volumes of benzene having a distribution coefficient, k', the initial concentration is given by:

$$C_{\text{in.}} = (1 + k')^{n}\ C_{\text{meas.}} \qquad (6.2)$$

Substituting $k' = 0.0033$ and $n = 2$:

$$C_{\text{in.}} = 1.0066\ C_{\text{meas.}} \qquad (6.3)$$

Consequently, the correction term is only 0.66 percent and of the order of experimental error in determining $C_{R_1\ \text{meas.}}$. No further precision in measuring the extraction coefficient was warranted.

After extraction of diester, the monoester concentration was determined by total saponification with excess NaOH followed by back-titration with standard HCl. After determining both hydroxyl ion and monoester concentrations, all other compositions were calculated using

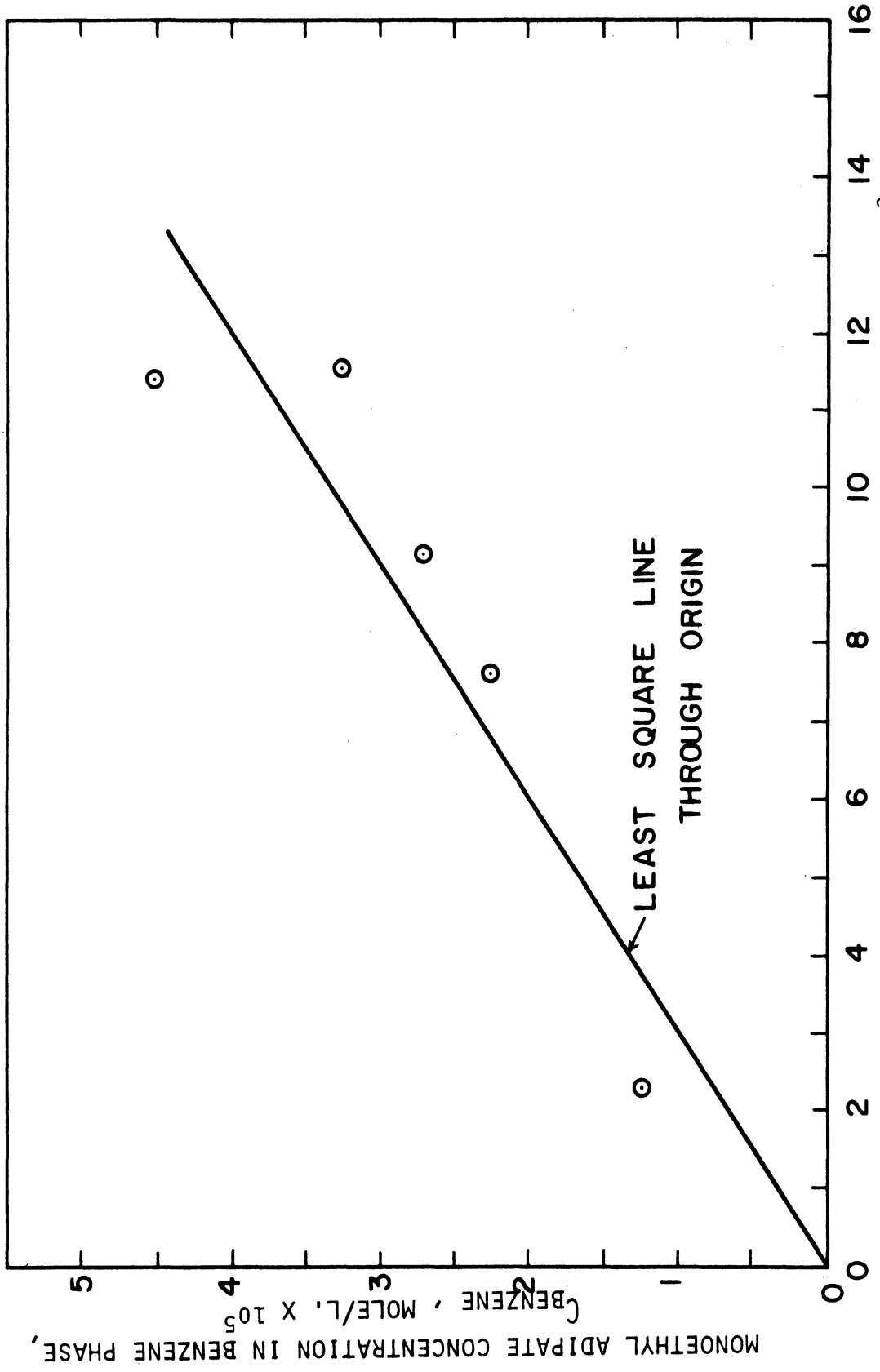

Figure 6.2. Equilibrium Distribution of Monoethyl Adipate between Benzene and Water at 25°C.

an overall material balance. This was valid for batch and plug flow reactors. The equations for this calculation are given in Appendix C.

7. REACTOR SIMULATION AND EXPERIMENTAL VERIFICATION OF THE MATHEMATICAL MODEL

Mathematical modeling of tubular reactors is discussed in most texts on chemical engineering kinetics, such as those of Levenspiel[82] and Denbigh.[38] Jacketed reactors are usually only briefly mentioned. For a real reactor such as that described in Chapter 4 of this work, conditions are not uniform along the entire length, so that proper equations must be written to describe mass and heat transfer, and chemical reaction in each section. The studies described in Chapter 5 indicated that axial mixing should have had a negligible effect. Therefore, the first model developed was based on plug flow assumptions. Section A of this chapter describes in detail the plug flow model. In Section B, comparisons of predicted concentration profiles with experimental data show that the plug flow model satisfactorily predicts performance for adiabatic as well as non-adiabatic operation. However, several models may provide agreement with a set of experimental data. With this in mind, a modification of the plug flow model is described in Section C. This modification takes into account the effect of reaction and diffusion in the boundary layer. Section D provides evidence to support the use of the plug flow model under different conditions and in larger size reactors.

A. Simulation of a Jacketed Chemical Reactor--Plug Flow Model

The equations governing the operation of the experimental reactor described in Chapter 4 are developed here. Consider a cross section of the reactor at an arbitrary position, as shown in Figure 7.1.

Diester and sodium hydroxide solutions are considered to have mixed at the reactor entrance. Initial concentrations and temperatures are known.

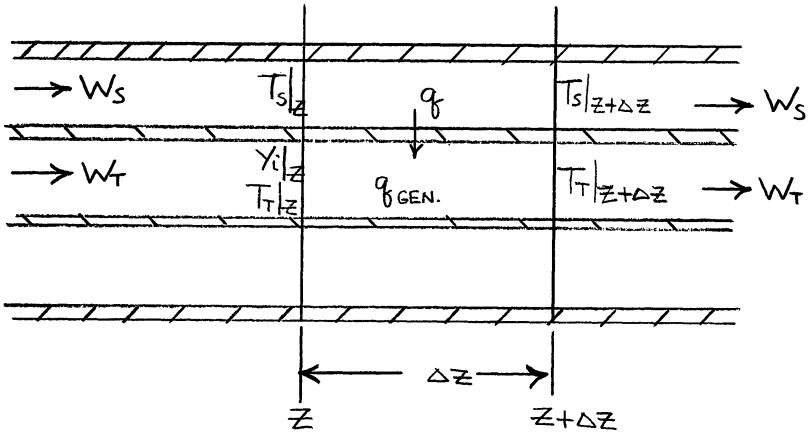

Figure 7.1. Reactor Mass and Heat Fluxes.

A differential steady state material balance on component A (diester) is:

$$G_{A_o}\left[Y_A\Big|_z - Y_A\Big|_{z+\Delta z}\right] + r_A \cdot S_T \Delta z = 0 \qquad (7.1)$$

where G_{A_o} = molar feed rate of ester entering reactor

Y_i = moles of component "i" per mole of A entering reactor

r_i = rate of generation of component "i" per unit volume

S_T = tube cross sectional area

Division by Δz and taking the limit as $\Delta z \rightarrow 0$ yields:

$$\frac{dY_A}{dz} = \frac{S_T}{G_{A_o}} \cdot r_A \qquad (7.2)$$

In this material balance, the following assumptions were made:

1. Axial diffusion may be neglected.

2. Conversion Y_i, temperature, and velocity are independent of radial position.

3. Overall density is a function of temperature only. This is reasonable for dilute solutions.

Similar balances for monoester (R_1) and hydroxyl ion (B) yield:

$$\frac{dY_{R_1}}{dz} = \frac{S_T}{G_{A_0}} r_{R_1} \tag{7.3}$$

$$\frac{dY_B}{dz} = \frac{S_T}{G_{A_0}} r_B \tag{7.4}$$

The stoichiometric equations and rates of generation of each component are given in Equations (5.1) through (5.2). For clarity, the generation terms are repeated:

$$r_A = -k_1 C_A C_B$$

$$r_{R_1} = k_1 C_A C_B - k_2 C_{R_1} C_B$$

$$r_B = -k_1 C_A C_B - C_{R_1} C_B \tag{5.2}$$

where the reaction rate constants are given by the Arrhenius law:

$$k_i = k_{i_0} \exp\{-E_i/RT\} \quad , i = 1,2 \tag{7.5}$$

The activation energies and frequency factors are given in Equation (5.5).

Finally, concentration, C_i and conversion, Y_i for component "i" are related by:

$$C_i = C_{A_{in}} Y_i (\rho/\rho_{in}) \tag{7.6}$$

The factor $\rho/\rho_{in.}$, the ratio of solution density to that at the reactor inlet is required because bulk density is temperature dependent. Combining Equations (7.6) with (5.2) and (7.2) through (7.4) the results are:

$$\frac{dY_A}{dZ} = -\alpha \rho^2 k_1 Y_A Y_B \tag{7.7a}$$

$$\frac{dY_{R_1}}{dZ} = \alpha \rho^2 Y_B \left(k_1 Y_A - k_2 Y_{R_1} \right) \tag{7.7b}$$

$$\frac{dY_B}{dZ} = -\alpha \rho^2 Y_B \left(k_1 Y_A + k_2 Y_{R_1} \right) \tag{7.7c}$$

where

$$\alpha = \left\{ \frac{S_T}{G_{A_o}} \left(\frac{C_{A_{in}}}{\rho_{in}} \right)^2 \right\} \tag{7.8}$$

Equations (7.7a) through (7.7c) are not independent. By combining (7.7a) through (7.7c):

$$2 \frac{dY_A}{dZ} + \frac{dY_{R_1}}{dZ} = \frac{dY_B}{dZ} \tag{7.9}$$

Therefore:

$$2 Y_A + Y_{R_1} - Y_B = \text{constant} = 2 + Y_{R_{1i}} - Y_{B_i} \tag{7.10}$$

Solving for Y_B :

$$Y_B = Y_{Bi} + \left(Y_{R_1} - Y_{R_{1i}} \right) - 2 \left(1 - Y_A \right) \tag{7.11}$$

Equation (7.11) replaces Equation (7.7c) and only two differential equations are required.* Similar analysis or an overall material balance on adipate ion (R_2) yields the equation:

$$Y_{R_2} = Y_{R_{2i}} + (1 - Y_A) - (Y_{R_1} - Y_{R_{1i}}) \qquad (7.12)$$

Since Y_{R_2} does not occur on the right side of Equations (7.7), it need not be computed.

Differential heat balances are required because the reaction rate constants (as well as density to a lesser extent) are temperature dependent. Again referring to Figure 7.1, heat is transferred into the differential tube and shell element of width ΔZ by bulk flow and by transfer through the tube wall. Heat is also generated by chemical reaction in the tube fluid. Following the same reasoning as for the previous mass balances, heat balances for tube and shell fluids yield:

$$\frac{dT_T}{dZ} = \left(\frac{1}{W_T C_T}\right)\left\{\pi D_{T_o} U_o (T_S - T_T) + \alpha G_{A_o} Y_B \rho^2 \cdot \left[(-\Delta H_1) k_1 Y_A + (-\Delta H_2) k_2 Y_{R_1}\right]\right\} \qquad (7.13)$$

$$\frac{dT_S}{dZ} = \left(\frac{\pi D_{T_o} U_o}{W_S C_S}\right)(T_T - T_S) \qquad (7.14)$$

where: T_T, T_S = tube and shell fluid temperatures

U_o = Overall heat transfer coefficient based on tube outside area

D_{T_o} = tube outside diameter

C_T, C_S = tube and shell fluid heat capacities

$(-\Delta H_1), (-\Delta H_2)$ = molar heats of reaction for first and second saponification reactions (Equation (5.1)).

---

* A very systematic method for eliminating dependent equations from complex sets is given by Ames.(5)

Dispersion effects in the shell need not be considered since these effects are lumped into the "empirical" shell side heat transfer coefficient.

To solve the above set of mass and heat balances, expressions are needed for U_o and ρ. These expressions are obtained from the following seven calculations.

1. Calculate Shell Fluid and Tube Fluid Densities

Since reactant density occurs in Equations (7.7) through (7.4) as the ratio ρ/ρ_{in}, and solutions were dilute, it was assumed that the ratio ρ/ρ_{in} was the same function of temperature as the corresponding ratio for water. Over the range of temperature 20° to 90°C (68° to 194°F) the density of water varies by 3 percent and is adequately represented by a linear expression:*

$$\rho(t/ml) = -2.494 \times 10^{-4}\, T(°F) + 1.016 \qquad (7.15)$$

2. Calculate Viscosity of Tube and Shell Fluids

The viscosity of water, μ was used for both fluids: It is adequately represented by the Bingham Equation:(92)

$$\mu = 100 \Big/ \left\{ 2.1482 \left[(T - 8.435) + \sqrt{8078.4 + (T - 8.435)^2} \right] - 120 \right\} \qquad (7.16)$$

over the temperature range 0 to 100°C. The units of T and μ are degrees C and centipoise, respectively. Over the temperature range of this study, 29 to 85°C, the viscosity varied from 0.82 to 0.33 centipoise.

---

* Least square line through data of Chemical Engineers' Handbook.(92)

3. Calculate Thermal Conductivity of Tube and Shell Fluids

The thermal conductivity of both fluids were taken as those of water at the same temperature, which is adequately represented by the linear equation:*

$$k = 2.975 \times 10^{-4} T + 0.333 \qquad (7.17)$$

over the temperature range 0 to 93°C. The units of k and T are BTU/hr./ft./°F and °F respectively. Over the temperature range of the study k, varied from 0.35 to 0.39 BTU/hr./ft./°F.

4. Calculate Reynolds Numbers for Tube and Shell Fluids

$$Re = \left[\frac{DW}{\mu S}\right] \qquad (7.18)$$

D = tube diameter or shell hydraulic diameter ($D_{i\,shell} - D_{o\,tube}$) feet

W = total flow rate in tube or shell, pound/hour

S = cross sectional area of tube or shell, ft.^{2}

μ = viscosity pound/foot, hour

Due to viscosity variation over the temperature range of this study, the tube Reynolds number varied at constant tube flow rate (197 pound/hour) from 7,800 to 18,500. Shell Reynolds number varied from 0 to 14,000 corresponding to temperature variation and to shell flow variation (0 to 600 pound/hour).

5. Calculate Prandtl Number for Tube and Shell Fluids

$$Pr = \frac{c\mu}{k} \qquad (7.19)$$

---

* Least square line through data of Chemical Engineers' Handbook.(92)

Tube and shell fluid specific heats were taken constant at 1 BTU/lb./°F. The error incurred with this assumption was less than 0.8 percent over the temperature range 15 to 90°C. In this study, tube and shell fluid Prandtl numbers varied from 2.1 to 5.4 and from 2.0 to 4.0 respectively.

6. Calculate Heat Transfer Coefficients for Tube and Shell

The correlation of Sieder and Tate[110] as given by Bird et al.[17] was used to calculate both tube and shell coefficients.

$$h = \frac{k}{D} [Re][Pr]^{1/3} [\mu_b/\mu_w]^{0.14} \cdot f(Re)^{*} \qquad (7.20)$$

$f(Re)$ is given in graphical form. Points from this graph in the range $10^3 \leq Re \leq 10^5$ were stored in the computer program and second order Lagrangian interpolation was employed to obtain $f(Re)$.

7. Calculate Overall Heat Transfer Coefficient Between Tube and Shell, U_o

The overall heat transfer coefficient U_o based on the tube outside area is given by:[17]

$$U_o = \left\{ \frac{1}{h_s} + \underbrace{\left(\frac{D_{To} \ln\left(\frac{D_{To}}{D_{Ti}}\right)}{2 k_w} \right)}_{C_3} + \frac{D_{To}/D_{Ti}}{h_T} \right\} \qquad (7.21)$$

The factor C_3 was constant and had the value 1.066×10^{-5} BTU/hr./ft.^{2}/°F In this study, the overall heat transfer coefficient varied over the range 390 to 630 BTU/hr./ft.^{2}

The use of the above Equations (7.5) and (7.7) through (7.20) may be understood by referring to Figure 7.2, a schematic drawing of the first reactor pass.

* D represents D_i or D_o.

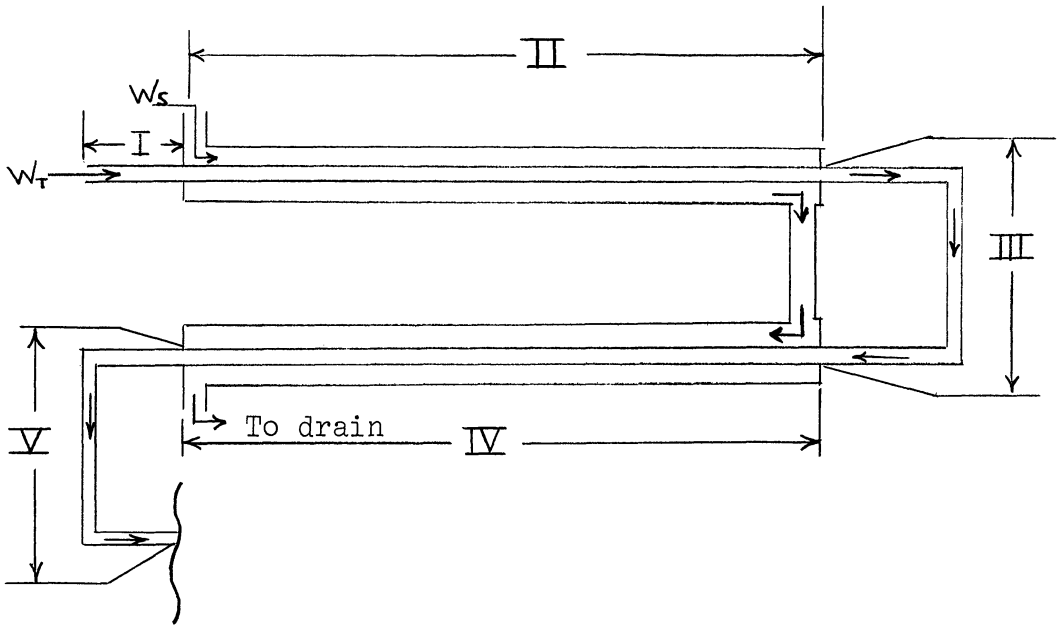

I - Entrance Section (0.333 feet)
II, IV - Heating Section (14.61 feet)
III, V - Adiabatic Return Bends (0.833 feet)
VI - Adiabatic Exit Section (Not Shown)(0.633 feet)

Figure 7.2. Schematic Drawing of First Reactor Pass.

Using known initial compositions Y_i , temperatures and flow rates, integration of the four differential Equations (7.7a,b), (7.13), and (7.14) and the accompanying algebraic Equations (7.5), (7.11) and (7.12) was performed initially over the entrance section (I). A single integration step was used. Here tube and shell flows were isolated so that U_o was set equal to zero in Equations (7.13) and (7.14). (Actually the shell flow did not begin until the start of Section II.)

In Section II, U_o was calculated from Equations (7.15) through (7.20) each time derivatives were computed in the Runge-Kutta integration routine. Reaction rate constants were similarly calculated in all sections. At the start of Section II, W_S , the shell flow rate was set to the proper value for that reactor pass. The total length of Section II was divided into five steps for the numerical integration. In Section

III, U_o was again set equal to zero since shell and tube bends were separately insulated. The total length of III was covered in a single step. Sections IV and V were identical to II and III respectively. The simulation then proceeded into the second heating section where W_s was set equal to the shell flow for the second pass, and shell temperature was set to its inlet value. This section was identical to Section II and integration proceeded in cycles II-III-IV-V. Five such sections made up the entire reactor. The adiabatic exit section from the fifth heating section was only 0.633 feet compared with 0.833 feet for the other bends.

Modification for No Shell Flow

To minimize transients during startup, shell passes in which there was to be no flow, were blown out with compressed air. At first, U_o was set equal to zero to simulate adiabatic operation in such passes. However, there was a measurable heat leak through the shell wall which changed the tube fluid temperature. This heat leak was found experimentally to correspond to an effective overall heat transfer coefficient of 1.76 BTU/hr./ft.^{2}/°F. between tube fluid and surrounding air (based on tube outside area).

$$U_L = 1.76 \text{ BTU/hr./ft.}^2/^\circ\text{F} \qquad (7.22)$$

The term $U_L (T_{SURR} - T_T)$ was included in Equation (7.13) only when shell flow was set equal to zero and the jacket blown out. During operation with heating water in the jacket, heat lost to surroundings was negligible compared with heat transferred to the tube fluid.

B. Use of the Plug Flow Model to Predict Reactor Performance

Two types of errors may cause discrepancy between results of experiment and simulation. The first is due to faults in the form of the mathematical model (e.g.--plug flow assumptions when back-mixing is significant), while the second is due to incorrect numerical estimates for the model parameters. Initially, simulations were attempted using estimates of activation energies and frequency factors obtained from preliminary batch studies. (Preliminary values are given in Table 3.1). Agreement with tubular reactor data was poor. Reaction rates were found to be 20 to 30 percent higher than predicted. This led to the investigation of boundary layer effects (Section C, this chapter) but these effects were found to be negligible. Further work uncovered large errors in the preliminary estimates of reaction rate constants due to two factors. Carbonate absorbed by sodium hydroxide solutions was neglected in analysis of the data. This was found to produce calculated reaction rate constants which were approximately 20 to 30 percent low. Secondly, propagation of small errors through the calculations caused very large uncertainties to be present in the estimates of reaction rate constants. The major difficulty was that only hydroxyl ion profiles were measured in the preliminary batch studies. (A Later batch experiment in which both hydroxyl ion and monoethyl adipate concentrations were measured gave agreement with tubular reactor data within experimental uncertainty). These tests are described in detail in Chapter 5.

In order to obtain more accurate estimates of the reaction rate constants, the plug flow model described above and experimental concentration profile data for tubular reactor run number 3 were employed.

Activation energies and frequency factors were chosen such that the plug flow model gave the "best fit" of the experimental data. The "best fit" was the set of trajectories which minimized Equations (5.6). The trial and error method was mechanized using both gradient and direct search algorithms on an IBM 7090 digital computer. Computing time amounted to two minutes for 51 function evaluations. (A single function evaluation consisted of integration of the four differential equations along the entire reactor length and calculation of the object function (5.6)). The fit of reactor run number 3 is shown in Figure 7.3. The activation energies and frequency factors which produced the "best fit" are given in Equation (5.5). Reaction rate constants calculated using these estimates are shown as solid lines in Figure 5.2. The broken lines of Figure 5.2 show the results of an error analysis of the "best fit" data from run number 3. All volumes and normalities used to calculate the experimental concentration profiles were perturbed by small amounts, and the profiles recalculated. Perturbations were in such directions to first raise the OH^- profile and lower the R_1 profile, and then the reverse. These perturbed profiles were then fit as before by choosing both activation energies and frequency factors in the plug flow model. The resulting activation energies and frequency factors yielded the reaction rate constants denoted by the broken lines of Figure 5.2. The details of this error analysis are given in Appendix F.

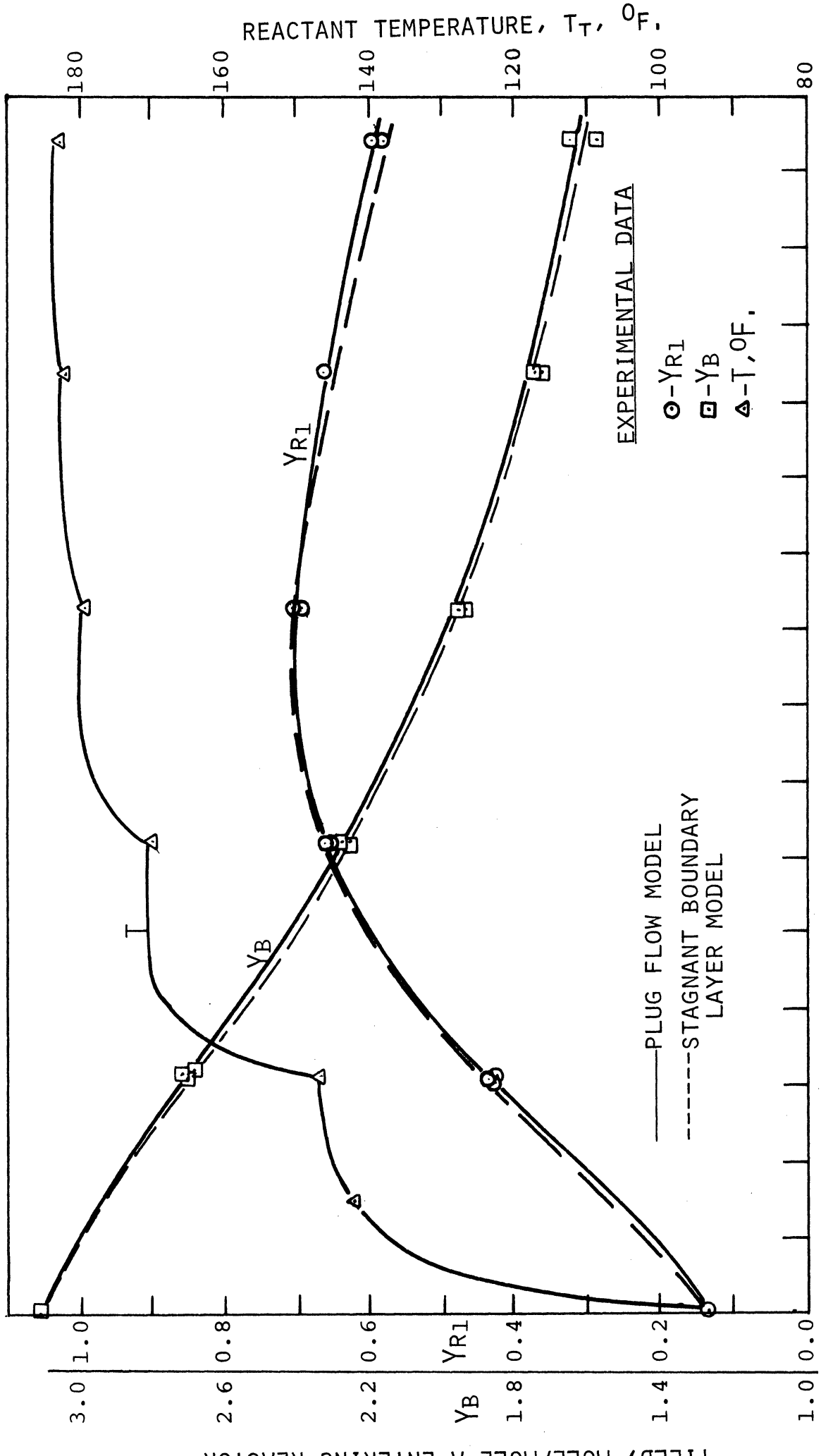

Figure 7.3. Run No. 3 Reactor Concentration and Temperature Profiles.

Predicted changes in reaction rate constants are seen in Figure 5.2 to be +15 percent, -17 percent for k_1 and +0, -11 percent for k_2 . Calculated perturbations in the concentration-time data which produced these changes in reaction rate constants are given in Appendix F, Table F.3. The maximum calculated perturbations in measured mole ratios are in the range 4.5-10.5 percent for hydroxyl ion and 5.5 - 9.8 percent for monoethyl aidpate.

Using the "best fit" kinetics (solid line Figure 5.2) in the plug flow model, other tubular reactor runs were simulated on the digital computer. Figures (7.4)-(7.7) illustrate experimental data and simulated concentration and temperature profiles for reactor runs 5 - 8. Initial conditions and shell flows for all reactor runs are shown in Table 7.1. The maximum percent error in the fit for hydroxyl ion mole ratio occurred in run number 5 at the 150 foot sampling position. Here the simulation exceeded the experimental data by four percent. The maximum error for monoethyl adipate occurred in run number 8 where the simulation was 6.3 percent lower than experimental data. This deviation also occurred at the reactor exit.

If these discrepancies are assigned completely to experimental measurements, then comparison with Table F.3 shows that these errors are within the range of calculated experimental error. On the other hand, the discrepancy may be assigned completely to uncertainty in values of reaction rate constants. The broken curves in Figure 7.7 for run

TABLE 7.1

SUMMARY OF INITIAL CONDITIONS FOR REACTOR RUNS

Run No.	3	5	6	7	8	9	10
C_A, mole/liter x 100	1.678	1.902	1.737	1.796	1.786	1.718	1.811
Y_{R_1}	0.1310	0.1073	0.1023	0.1036	0.1113	0.111	0.1021
Y_{R_2}	0.00933	0.00438	0.00440	0.00455	0.00320	0.00100	0.00402
Y_B	3.108	2.975	3.098	3.045	2.953	2.960	2.798
T_{T_i}, °F	81.8	83.0	83.7	84.6	143.8	86.5	86.4
T_{S_i}, °F	184.3	186.5	184.7	186.6	---	179.6	183.6
Tube Flow lb./hr.	198	198	197	197	194	197	197
			Shell Flows, pound/hour				
No. 1	346	0	538	0	0	0	0
No. 2	346	0	0	0	0	392	0
No. 3	346	346	0	0	0	597	436
No. 4	346	346	0	0	0	597	600
No. 5	346	346	0	538	0	597	600

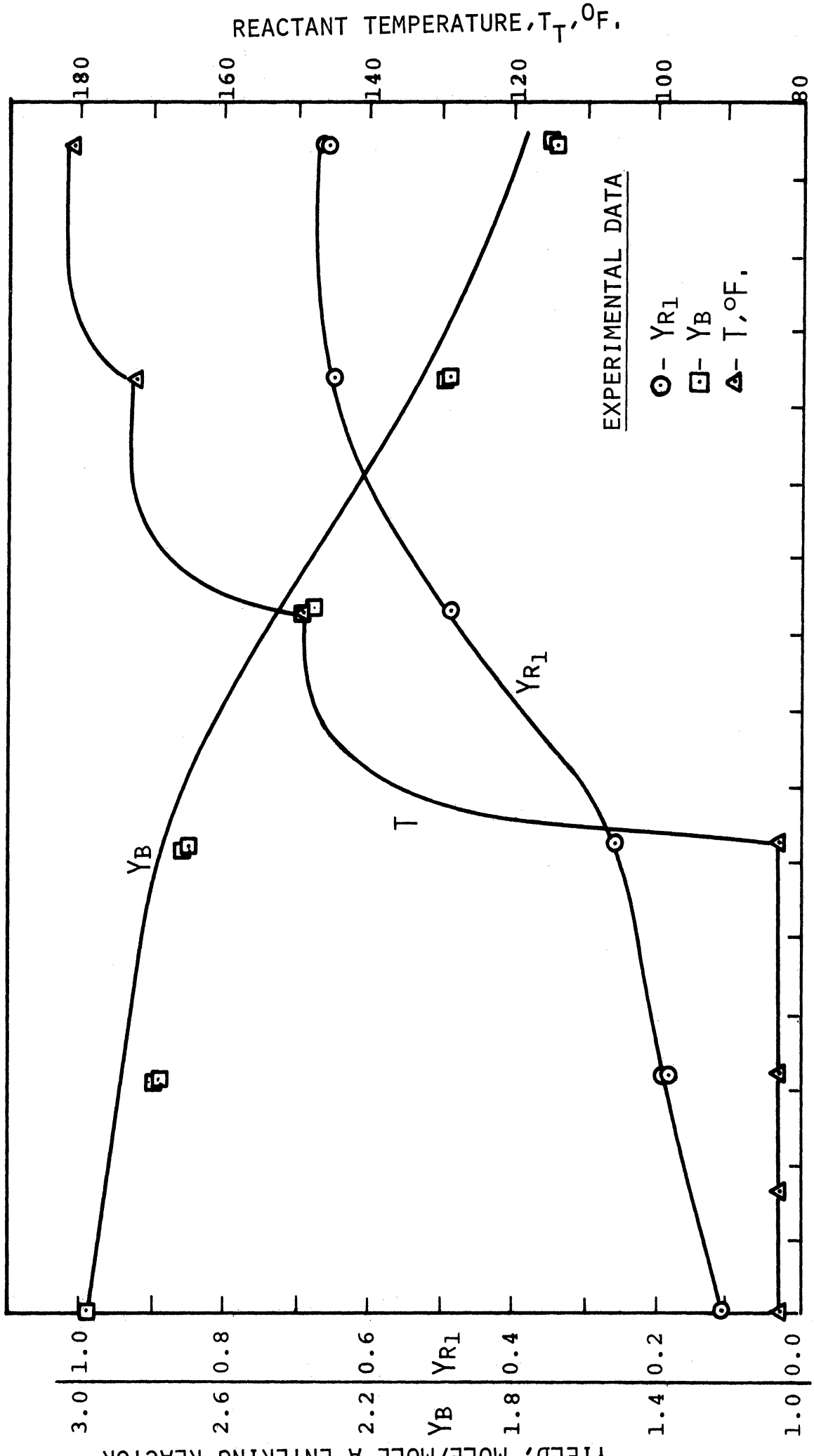

Figure 7.4 Run No. 5 Reactor Concentration and Temperature Profiles.

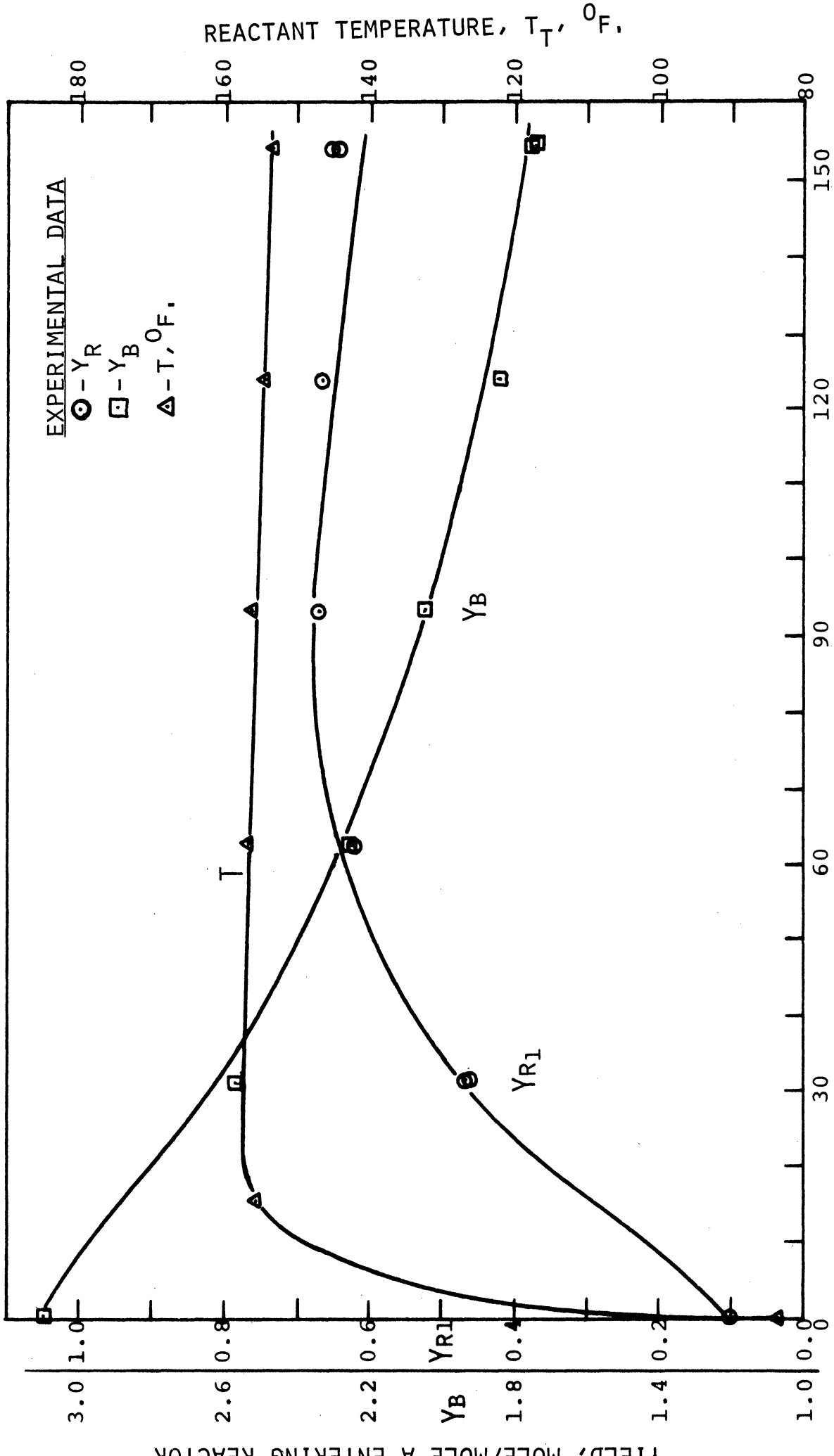

Figure 7.5. Run No. 6 Reactor Concentration and Temperature Profile.

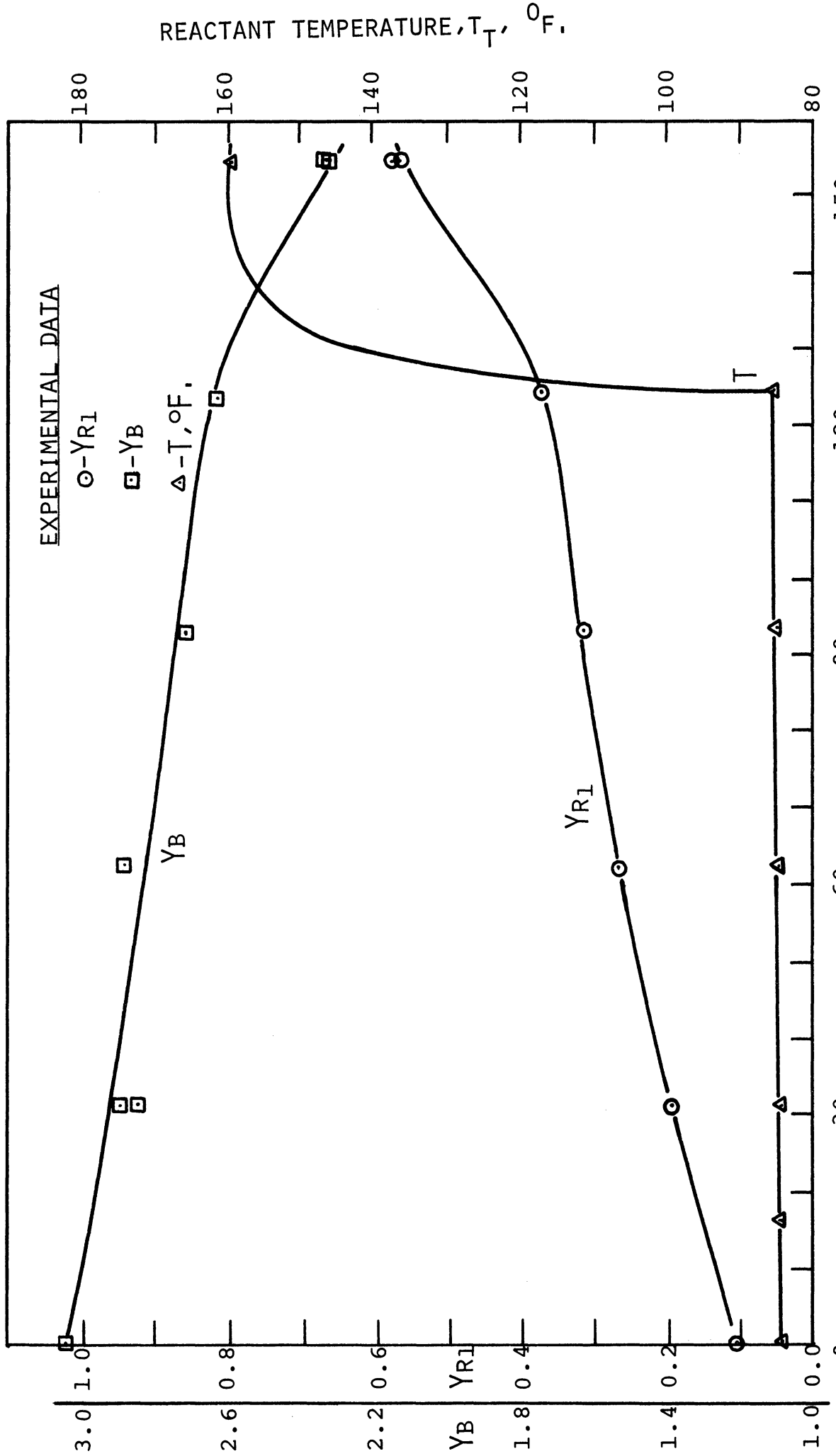

Figure 7.6. Run No. 7 Reactor Concentration and Temperature Profiles.

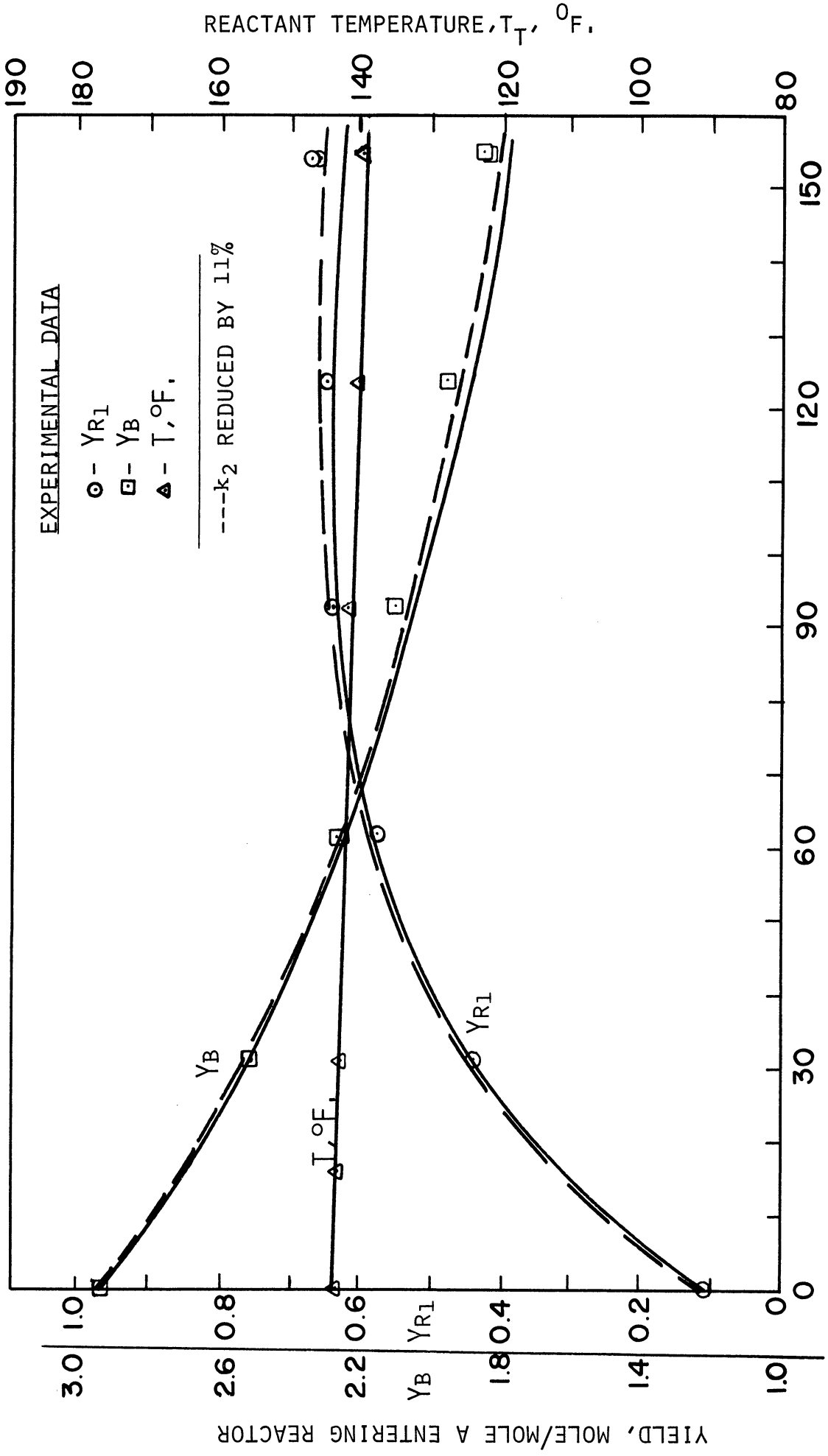

Figure 7.7. Run No. 8 Reactor Concentration and Temperature Profiles.

number 8 is a plug flow simulation with k_2 taken at its lower limit, (11 percent decrease in k_2 - see lower broken line of Figure 5.2). The discrepancy between measured and predicted monoester conversion is seen to have been reduced from 6.3 percent to 1.5 percent. The error between predicted and measured hydroxyl ion conversion was also reduced from 3.8 percent to 2.8 percent.

The maximum discrepancy between predicted and measured temperature profiles occurred in run number 5. At the reactor exit, the predicted temperature was 1°F higher than the measured value, and at 120 feet, it was 0.8°F higher. At all other measuring points, measured and predicted temperatures agreed within 0.1°F. The discrepancy over the last 60 feet caused the calculated reaction rates to differ by 2.3 percent for k_1 and 1.3 percent for k_2 from those calculated at the measured temperatures.

In view of the general agreement between measured and predicted conversions and temperatures the plug flow model presented here does give an accurate representation of performance of the reactor employed for this study. The major uncertainty is in the knowledge of the reaction rate constants. In more concentrated solutions or if heats of reaction were larger in magnitude, uncertainties in heats of reaction would also be a major source of error.

C. Stagnant Boundary Layer Model

In the previous section it was shown that the plug flow model gives an accurate representation of reactor performance for a non-isothermal jacketed tubular reactor. In Chapter 5, axial dispersion effects under isothermal operation were ruled out. However, there was no justification for generalization until the effects of diffusion and reaction in the boundary layer next to the hot wall were theoretically investigated. The effects were found to be small compared with experimental error, for the parameters of this system. This result adds confidence to use of the plug flow model in similar systems. For reactions having very large activation energies, boundary layer effects in wall heated reactors would not be negligible.

In this section, theoretical analysis of boundary layer effects is described, and predicted trajectories are compared with those of the plug flow model.

Since the tube side boundary layer made up a substantial part of the resistance to heat transfer, the boundary layer temperature in parts of the reactor was significantly higher than that of the bulk fluid. Since reaction rates increase exponentially with temperature, higher conversions should be achieved in the boundary layer than in the bulk fluid. The concentration difference between boundary layer and bulk fluid should then cause mass transfer by radial diffusion.

The model used to investigate this phenomena determined an upper bound on the change in conversion from plug flow operation. The boundary layer was taken as stagnant (no axial velocity) with material diffusing to and from the bulk fluid stream by molecular diffusion. Boundary layer temperature was taken uniform in the radial direction and equal to the wall temperature. To simplify the analysis, hydroxyl ion concentration was taken independent of radial position within the boundary layer. Curvature and axial diffusion in the boundary layer were also neglected. Referring to the sketch in Figure 7.8, mass balances for components A and R_1 yield:

$$\frac{d^2 C_A}{d R^2} - \alpha_1^2 C_A = 0 \qquad (7.23)$$

$$\frac{d^2 C_{R_1}}{d R^2} + \alpha_2^2 C_A - \alpha_3^2 C_{R_1} = 0 \qquad (7.24)$$

where:

$$\alpha_1^2 = \frac{k_{1w} \bar{C}_B}{D_A} \quad , \quad \alpha_2^2 = \frac{k_{1w} \bar{C}_B}{D_{R_1}} \quad , \quad \alpha_3^2 = \frac{k_{2w} \bar{C}_B}{D_{R_1}} \qquad (7.25)$$

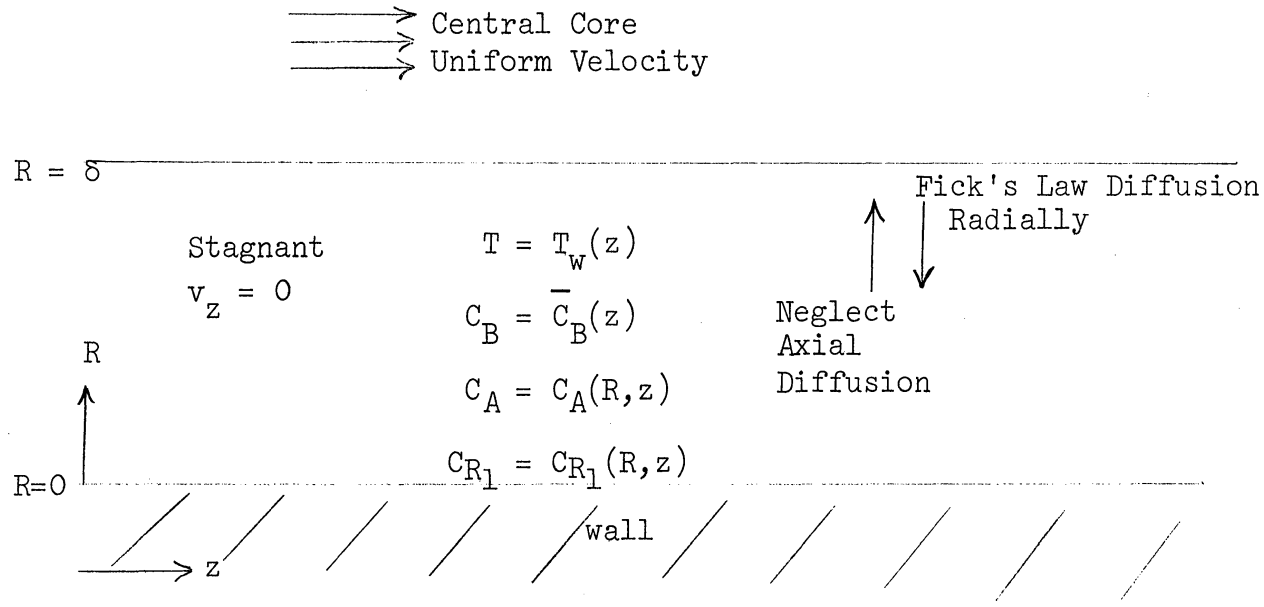

Figure 7.8 Simplified Boundary Layer

For each equation, the boundary conditions require no diffusion flux at the tube wall, and a match of concentrations at the interface between boundary layer and central core.

$$\left.\frac{dC_A}{dR}\right|_{R=0} = 0 \quad , \quad \left.\frac{dC_{R_1}}{dR}\right|_{R=0} = 0 \tag{7.26}$$

$$C_A(\delta, z) = C_{A_B}(z) \quad , \quad C_{R_1}(\delta, z) = C_{R_{1B}}(z) \tag{7.27}$$

C_{A_B} and $C_{R_{1B}}$ are bulk fluid concentrations in the turbulent central core. Equations (7.23)-(7.24) are linear and may be solved by standard

operator techniques. The results are:

$$C_A(R) = C_{A_B} \frac{\cosh(\alpha_1 R)}{\cosh(\alpha_1 \delta)} \tag{7.28}$$

$$C_{R_1}(R) = \left[\frac{\alpha_2^2 C_{A_B}}{\alpha_1^2 - \alpha_3^2}\right]\left[\frac{\cosh(\alpha_3 R)}{\cosh(\alpha_3 \delta)} - \frac{\cosh(\alpha_1 R)}{\cosh(\alpha_1 \delta)}\right] \tag{7.29}$$

$$+ C_{R_1 B} \frac{\cosh(\alpha_3 R)}{\cosh(\alpha_3 \delta)}$$

The flux of each component into the turbulent core is then given by:

$$N = - D \left.\frac{dC}{dR}\right|_{R=\delta} \tag{7.30}$$

Performing the indicated operations on Equations (7.28) and (7.29), the results are:

$$N_A = - D_A \alpha_1 C_{A_B} \cdot \tanh(\alpha_1 \delta) \tag{7.31}$$

$$N_{R_1} = \left[\frac{\alpha_2^2 C_{A_B} D_{R_1}}{\alpha_1^2 - \alpha_3^2}\right]\left[\alpha_1 \cdot \tanh(\alpha_1 \delta) - \alpha_3 \tanh(\alpha_3 \delta)\right] \tag{7.32}$$

$$- D_{R_1} \alpha_3 C_{R_1 B} \tanh(\alpha_3 \delta)$$

To evaluate N_A, and N_{R_1} values of $\bar{C}_B$, D_A, D_{R_1} and δ are needed in addition to reaction rate constants and bulk concentrations. Estimates of diffusivities were made following suggestions of Reid and Sherwood.(97)

$$D_A = 1.84 \times 10^{-8} T/\mu \tag{7.33a}$$

$$D_{R_1^-} = 2.94 \times 10^{-8} T/\mu \tag{7.33b}$$

The units of temperature, T, and viscosity, μ are °K and centipose respectively. Diffusivity, D is calculated in cm^2/sec.

To avoid a trial and error determination, $\bar{C}_B$ was taken equal to the hydroxyl ion concentration in the turbulent core. This assumption was later checked and found to be in error by only one percent.

Using film theory, the boundary layer thickness is given by:

$$\delta = D/k_m \tag{7.34}$$

where D is molecular diffusivity and k_m is the empirical mass transfer coefficient. Using the analogy between heat and mass transfer, k_m was calculated from Equation (7.20) substituting Schmidt number for Prandtl number and the Nusselt number for mass transfer for that of heat transfer. Bird(17) gives a thorough discussion of this analogy. Taking expression (7.33a) for D in (7.34) values of boundary layer thickness were obtained within 25 percent of those calculated from the universal velocity profile data of Deissler.(17) Boundary layer

thicknesses were of the order of one percent of the tube inner diameter. The differential equations describing conversions in the turbulent core are quite similar to those for plug flow. Differential mass balances yield:

$$\frac{dY_A}{dz} = \frac{C_c N_A}{G_{A_o}} + \frac{S_c}{G_{A_o}} r_A \qquad (7.35)$$

$$\frac{dY_{R_1}}{dz} = \frac{C_c N_{R_1}}{G_{A_o}} + \frac{S_c}{G_{A_o}} r_{R_1} \qquad (7.36)$$

where: C_c = circumference of turbulent core

S_c = cross sectional area of the turbulent core

N_A, N_{R_1}, r_A, and r_{R_1} are given by Equations (7.31), (7.32) and (5.2). The plug flow model computer program was modified by substituting Equations (7.35) - (7.36) for (7.7a) and (7.7b), and adding the required instructions to calculate boundary layer thickness, (7.34) and flux terms (7.31) - (7.32) each time derivatives were calculated.

The results of this simulation for the conditions of run number 3 are shown as broken curves in Figure 7.3. The maximum difference in conversions between this simulation and that of the plug flow model is 0.015 for R_1 and 0.023 for OH^-, both occurring at the reactor exit. This difference for OH^- is only 1/7 of the maximum calculated experimental error and for R_1 only 1/3. The changes in peak value of Y_{R_1} and the position of this peak are negligible. Consequently, the hot boundary layer plays an insignificant role in determining reactor performance in this system.

D. Scaleup

Volumetric reaction rates in the stagnant boundary layer of section C reached more than twice those in the central core due to the higher temperature. However, the volume of the boundary layer was only approximately two percent of the central core. Consequently, the net flux from the boundary layer was insufficient to cause a substantial difference in the computer trajectories compared with those for plug flow. For larger diameter reactors the effect of the boundary layer on reactor performance can be found by comparing the volume fraction of the boundary layer with that for this reactor. The volume fraction is given by:

$$\frac{Vol_{B.L.}}{Vol_{TOTAL}} = 2\left(\frac{\delta}{R}\right) - \left(\frac{\delta}{R}\right)^2 \qquad (7.37)$$

where R = tube inside radius.

The change in effective boundary layer thickness with tube diameter may be found from the film theory.

$$\delta = \frac{D}{k_m} = \frac{2R}{[Re]\cdot[Sc]^{1/3}\cdot[\mu_B/\mu_W]^{0.14}\cdot f(Re)} = \frac{2R}{g} \qquad (7.38)$$

where $$g = [Re][Sc]^{1/3}[\mu_B/\mu_W]^{0.14} f(Re) \qquad (7.39)$$

Combining (7.37) and (7.38)

$$\frac{Vol_{BL}}{Vol_{TOTAL}} = \frac{4(g-1)}{g^2} \qquad (7.40)$$

Hence for reactor operation at the same Reynolds and Schmidt numbers, the fractional tube volume occupied by the boundary layer is independent of tube diameter and the results of section C are directly applicable. For different Reynolds and Schmidt numbers, the change in fractional volume with the function g must be investigated. Differentiating (7.40) with respect to g :

$$\frac{d}{dg}\left(\frac{VOL_{BL}}{VOL_{TOTAL}}\right) = -\frac{4(g-2)}{g^3} \qquad (7.41)$$

For turbulent flow, under normal conditions the factors of g vary as follows:

$$\begin{aligned} 3000 \leq Re \leq 100{,}000 \\ 300 \leq Sc \leq 2{,}700 \\ 0.002 \leq f(Re) \leq 0.004 \end{aligned}$$

Then conceivably, g can vary between 40 and 5600. The expression in (7.40) is then always negative. The fractional volume occupied by the boundary layer therefore decreases with increasing Reynolds and Schmidt numbers.

In summary, this analysis coupled with that of section C indicates that for activation energies of the same order as those of this study, conversions in larger scale reactors may be predicted using the plug flow model. The boundary layer effect decreases with increasing Reynolds and Schmidt numbers. For higher activation energies than those of this study, the effect of reaction in the boundary layer may become significant.

8. OPTIMAL OPERATION

After a model is developed which fits measured reactor concentration and temperature data within experimental uncertainty, it is usually much more efficient to employ the model than the physical process for reactor optimization. If the fit of the model to experimental data has been verified over the complete range of control values, there is little reason to doubt that agreement will also be obtained at optimal conditions. Optimal operation was demonstrated in this study as a final verification of the applicability of the mathematical model.

Even in "steady state" processes, slow changes in operating conditions often call for control action to maintain peak efficiency. An analysis of the effects of small changes on process efficiency is therefore a logical adjunct to an optimization study. Such a sensitivity analysis was carried out both numerically and experimentally on the effects of changes in jacket flow rates about the optimal conditions. The effects of uncertainties in initial feed compositions is also discussed. This uncertainty was a very real problem caused by the lack of a precise estimate of reactor initial concentrations at the time the computer optimization was done.

Although the Maximum Principle was applied to a simplified model, its importance as a logical starting point for reactor optimization is established.

A. Problem Statement and Optimization Methods

The criteria for optimization are strongly dependent on local operating conditions. Physical parameters enter the problem in the mathematical model, but economic factors usually enter in the objective function. To demonstrate optimal operation of a tubular reactor, this study was limited to a single set of controls and a single objective function. The problem posed was: How should the shell flows in each of the five jacket sections be set such that the steady state conversion of diethyl adipate to monoethyl adipate is maximized at the reactor exit? Inlet jacket hot water temperature, reactant temperature and concentrations were taken as constants in the optimization problem. Limitations of the hot water supply system required that no single flow rate exceed 600 pounds/hour. The above statements completely define the problem and were grouped in an "internal function" in the MAD language called MARCH which did the following:

1. Given the following fixed parameters:
   a. initial concentrations
   b. initial temperatures
   c. reaction rate law constants
   d. heats of reaction
2. Given values of shell water flow rates in the range:

$$0 \leq W_{s_i} \leq 600, \quad i = 1, \ldots 5$$

3. Utilize the plug flow model (described in Chapter 7) to perform numerical integration of heat and mass balances.

4. Return the value of exit conversion of monoethyl adipate, Y_{R_1} to the calling program.

This "internal function" was combined with either a gradient search or a direct search optimization scheme written as an "external function". Both methods were named OPT., had the same argument lists, and could be used interchangeably. These optimization programs performed the following operations:

Step 1. Given the following arguments:

a. Number of independent variables, N

b. An initial set of values for these independent variables

$x_1, \ldots x_N$

c. Upper and lower bounds on independent variables

$XL_1, \ldots XL_N$, $XU_1, \ldots XU_N$

d. Allowable deviation from actual optimum in each coordinate direction

e. Number of additional inequality constraints, M (There were none for this problem).

f. Name of array (G_1 ... G_M) in which numerical values characterizing these inequality constraints were stored. (i.e. If $G_i < 0$ then the ith constraint is violated.)

g. The name of a linear array of statment labels (BAD_1 ... BAD_4) to which OPT. could return for the following reasons:

BAD_1 - maximum number of steps exceeded
BAD_2 - lost in constraints
BAD_3 - indeterminate constraints
BAD_4 - constrained maximum

h. F. - the name of an internal function in the main program (in this case MARCH), which first checked for violated constraints. If violations were found it returned control to the calling program. If no constraints were violated, calculation of the object function proceeded.

i. the required frequency of printing of intermediate values of $x_1, \ldots x_N$, and J, the object function by OPT.

j. Maximum allowable number of steps by OPT. before terminating execution.

Step 2. Vary the independent variables $x_1, \ldots x_N$ within allowable regions, and call on F. to calculate J, until no increase in J is obtained.

Step 3. Reduce the search step size systematically and repeat Step 2 until the step size for each of the N independent variables is less than the allowable error.

Step 4. Set the value of J equal to the maximum found and $x_1, \ldots, x_N$ equal to the coordinate values corresponding to J_{max}.

Step 5. Return control to the calling program.

The choice of the two optimization algorithms, direct search and gradient search was governed by limited experience and availability of the computer programs. Of the many methods, none has been found best for all types of problems. Other techniques are touched upon in Chapter 2. Based on a good deal of experience with direct and gradient search methods,[21,59,129] and a limited amount with the methods of Powell,[95]

Fletcher and Reeves[46] and Rosenbrock,[100,101] it is this author's opinion that convergence can usually be obtained to the true optimum with any of the methods if the step size is made small enough to allow climbing of narrow ridges. Furthermore, speed of solution is governed nearly as much by the programmers skill and subtle modifications of the technique to suit his class of problems, as by the main attributes of the optimization method. A list of methods available for solving optimization and optimal control problems is given in Table 8.1.

Comparing direct and gradient search methods to solve the split boundary value problems of Chapter 3 (up to 3 variables search), the regression problems of Chapter 5A (2 and 3 variable searches) and the 5 variable reactor optimization problems of this chapter, some general conclusions may be drawn. The gradient search was superior to the direct search for locating the region of the optimum. Convergence to a so called "optimum" was also faster with the gradient search. However, for the same minimum step size, the solutions produced by the direct search were usually somewhat better than for the gradient search. That is, a slightly higher value of the objective function was found. To achieve these results with the gradient search the minimum step size had to be reduced with a consequent increase in execution time. If a sharp change in direction of a rising ridge existed, the direct search was better at following it then the gradient search.

TABLE 8.1

METHODS AVAILABLE FOR SOLVING OPTIMIZATION AND OPTIMAL CONTROL PROBLEMS

	Reference Number
I. OPTIMAL TRAJECTORY PROBLEMS	90
A. Calculus of Variations	69,76
B. Pontryagin Maximum Principle	28,77,87, 94,104,105
C. Gradient Method in Function Space	22,23,68, 78
D. Techniques for Distributed Parameter Problems (Partial Differential Equations)	39,52
II. DISCREET OR MULTIVARIABLE OPTIMIZATION PROBLEMS	21
A. Calculus	
B. Dynamic Programming	9,14,98
C. Linear Programming	126
D. Geometric Programming	126
E. Multivariable Search Methods	
1. Gradient Search	21,129
2. Direct Search	21,59
3. Conjugate Gradients (Fletcher and Reeves)	46
4. Powell's Method	95
5. Second Variational Method	127
6. Rosenbrock's Method	100,101
F. Discrete Maximum Principle	67,89

TABLE 8.1 (Continued)

		Reference Number
III.	METHODS FOR SOLVING THE SPLIT BOUNDARY PROBLEM ARISING IN THE USE OF THE MAXIMUM PRINCIPLE AND THE CALCULUS OF VARIATIONS	
	A. All Multivariable Search Methods	
	B. Newton-Raphson Method	126
	C. Quasilinearization	81,102,103
	D. Singular Perturbation Method	47

The major factor in total execution time is the computation of the objective function, J (the function to be maximized). Only when this time was very small (less than 1 millisecond) did execution of the remaining instructions have a significant effect. Objective function evaluation required approximately 0.1 seconds for the problems of Chapters3 and 5 and between 2 and 3 seconds to obtain a set of reactor profiles. Considering all problems of the group, the optimum was generally found to within 0.01 percent of the range of all independent variables in less than fifty steps. The gradient method required between 1 and (2+N) function evaluations per step whereas the direct search required between (N+1) and (2N+1) function evaluations. However, the direct search generally required fewer steps, and often the length of each step was larger than of the gradient search.

In short, both methods were extremely valuable and complemented each other.

B. Results of Reactor Optimization

In this section, the optimization techniques described above are applied to the jacketed tubular reactor. The numerical values of the results are specific not only to a single reaction system, but also to a single reactor. Since physical interpretation of these results does have general importance, stress has been placed on insight obtained from performance and analysis of these tests rather than on quantitative results. Figure 8.2 illustrates predicted and measured concentration and temperature profiles which are nearly optimal. That is, the predicted

exit conversion of monoethyl adipate is only 0.3 percent less than the predicted optimal conversion. Optimal predicted operation is shown by the dashed curves. The reactor was not operated with the optimal shell flows, partly because of the time required for chemical analysis of reactor feedstock, and because of turnaround time* at the University of Michigan Computing Center.

Chemical analysis of reactor feedstocks was performed directly before a reactor run so that an accurate simulation could be obtained. However, the results of chemical analysis were not available for approximately 24 hours. Had computation of the optimal controls been delayed until chemical analysis was available, two days would have elapsed from feedstock analysis until reactor operation. During this time, hydrolysis of the ester solution would have been one - two percent. Consequently, the results of the optimal computation would have been in doubt. Furthermore, hot water temperature varied from day to day over a 7°F interval.

Since ester solutions were always prepared in a similar manner, the initial conditions for the previous run (No. 9) were considered a fairly good estimate for run number 10. Computation was performed first, and the reactor was run immediately after analysis of feedstocks. After the results of chemical analysis were available, the computation was

---

*Turnaround time is the total time interval between submitting a program at the computing center and obtaining the computer output. It was approximately 24 hours at the time of this work.

repeated. Reactor initial conditions for runs 9 and 10 are shown in Table 7.1. The optimal controls and final conversions to monoester are shown in Table 8.2.

TABLE 8.2

COMPARISON OF PREDICTED OPTIMAL SHELL FLOWS AND MONOESTER YIELD FOR INITIAL CONDITIONS OF RUNS 9 AND 10

	Optimal Shell Flows* (lb/hr)					Y_{R_1}(exit)
	1	2	3	4	5	
Run No. 9	0	0	435.9	600.	600.	0.6722
Run No. 10	0	0	258.9	600.	600.	0.6719

*Upper limit on each shell flow was 600 lb./hr.

The very small difference between optimal exit compositions on a mole ratio basis is due to the small difference in activation energies for the first and second saponification reactions (see Equation 5.5). Had the activation energies been equal, exit compositions of monoester would only differ due to differences in monoester present in the feed. The decrease in optimal value of shell flow number 3 was due mainly to a 4°F increase in inlet hot water temperature. A somewhat compensating effect is the five percent decrease in Y_{B_i}, inlet mole ratio of hydroxyl ion. Had Y_{B_i} been the same in both cases, optimal shell flow number 3 would have been even lower. This same phenomena, almost equal optimal conversions for different inlet

conditions, also occurred for the ideal tubular reactor problems treated in Chapter 3. (Compare Figures 3.7 and 3.9).

The fact that predicted exit conversion to monoester in run number 10 was only 0.3 percent below the optimal value despite a difference of 68 percent in shell flow number 3 from the predicted optimal shell flow, is an indication of the flat peak in monoester concentration along the reactor. At the temperature in the final section of the reactor, 180°F, the rate constant ratio k_2/k_1 was 1/4 , so that monoester saponified more slowly than it formed.

As expected the measured concentrations and temperature agreed with predictions within experimental uncertainty. Run number 10 simply provides additional evidence to support the usefulness of the plug flow model.

Figure 8.2 shows the predicted and measured concentration and temperature profiles for run number 9. Here, the optimal shell flows were calculated using the preliminary estimates of frequency factors and activation energies shown in Table 3.1. The broken curves illustrate the predicted profiles using these preliminary estimates. The preliminary values yielded reaction rate constants approximately 20 and 50 percent low for k_1 and k_2 and predicted an exit yield of monoester 19 percent high. Had the error caused predicted rate constants to be higher rather than lower than the corrected values, the results might have been more serious since the left side of the monoester trajectory is far steeper than the right side.

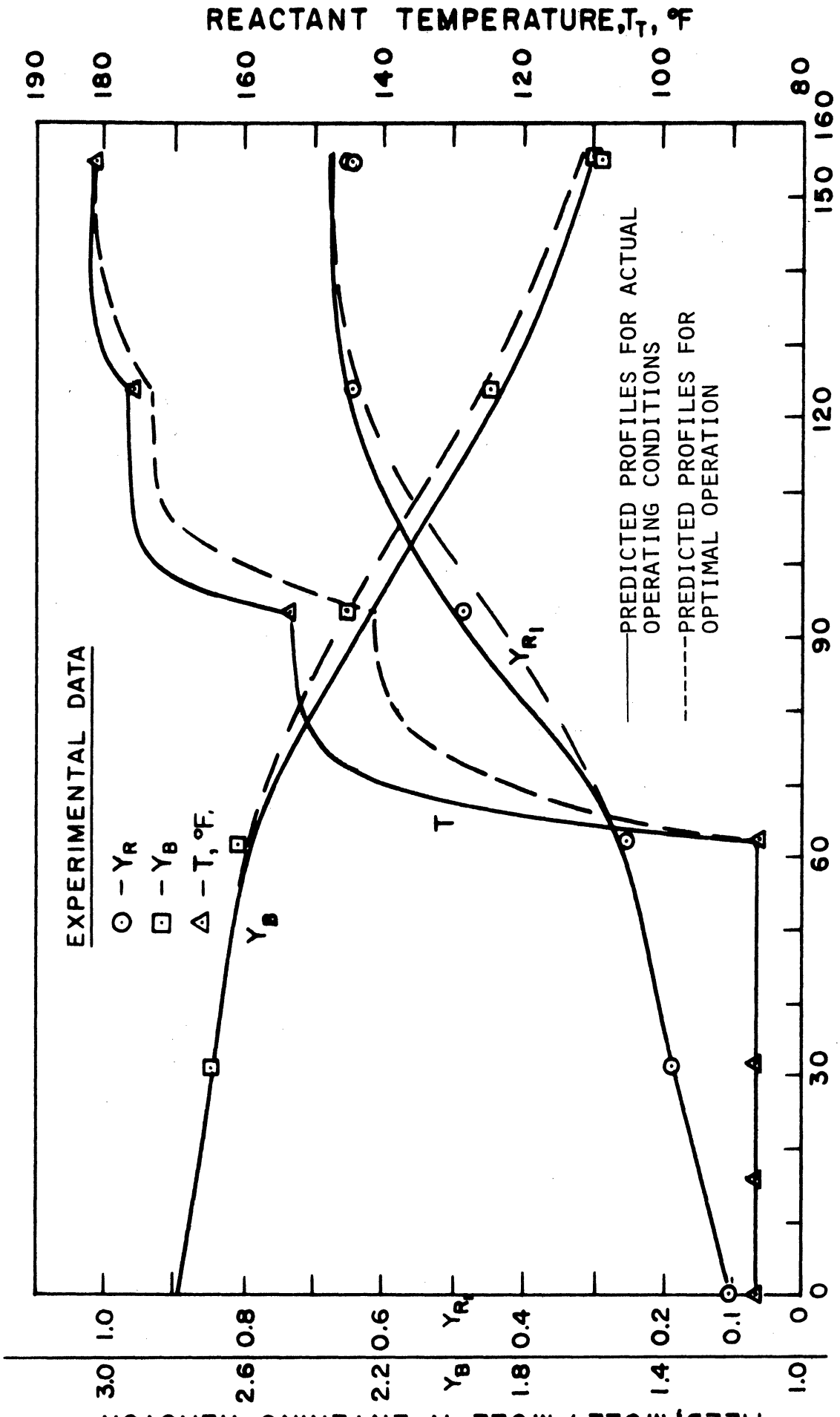

Figure 8.1. Run No. 10 Reactor Concentration and Temperature Profiles.

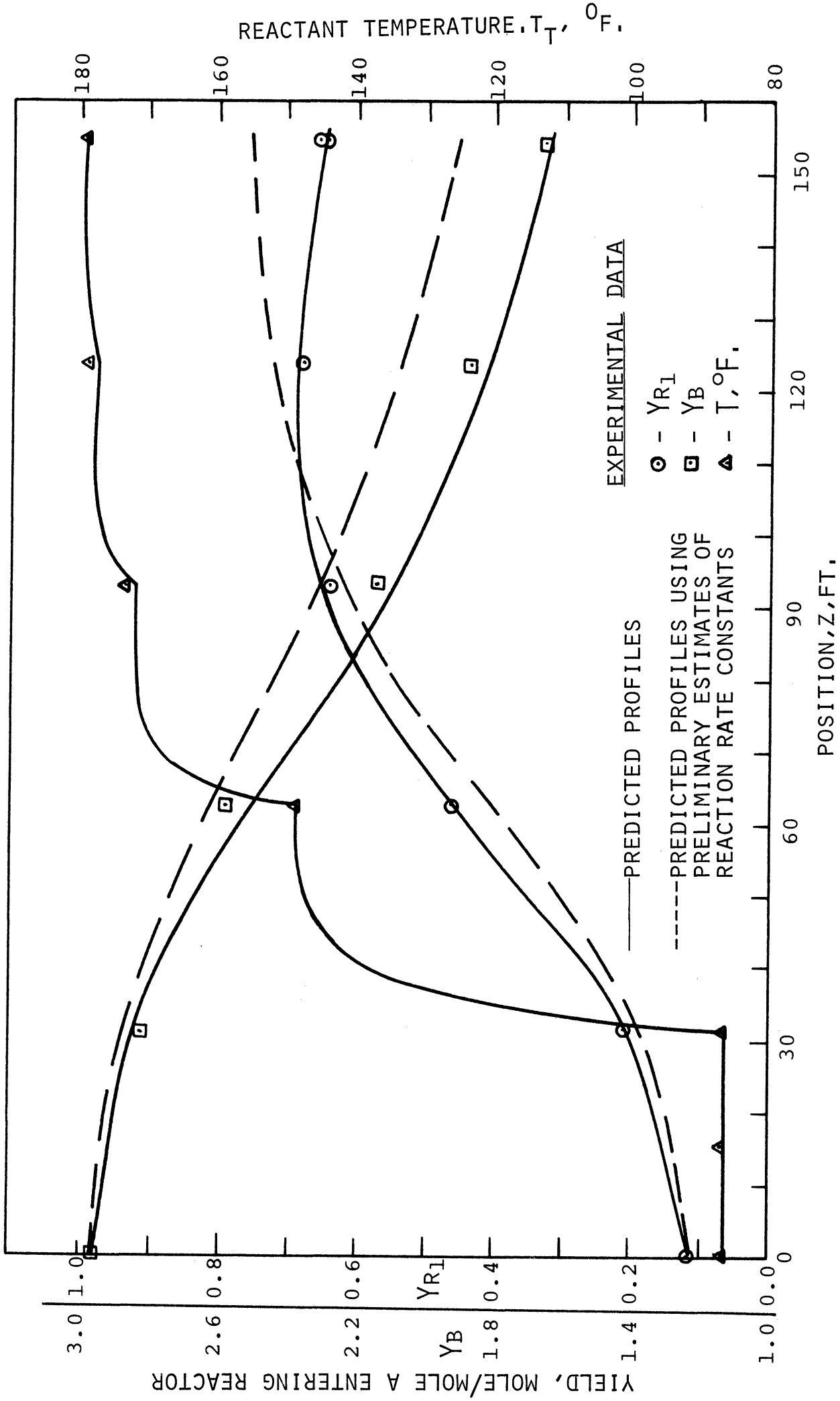

Figure 8.2. Run No. 9 Reactor Concentration and Temperature Profiles.

Table 8.3 shows the measured and predicted exit conversions of monoester for run number 11. This reactor run demonstrated the effect of variations in shell flow on monoester production about "near optimal" conditions. In run number 11 samples were taken for eight different combinations of shell flows only at the reactor exit. As before, initial estimates of the optimal shell flows (set no. 1) were somewhat in error due to errors in estimates of feedstock compositions and inlet temperatures. Set number 9 shows the values of optimal shell flows based on corrected estimates of initial conditions. Although shell flow number 3 in set 1 was 180 percent higher than the optimal setting, the loss in conversion to monoester was only 0.002 or 0.3 percent.

Perturbations in sets 2 - 6 were in increments of 60 pounds/hour about the shell flows of set number 1. The maximum predicted change in monoester conversion was only 0.15 percent, twenty times smaller than the calculated uncertainty of the measurements (three percent). The measured changes in conversion are also less than half the calculated experimental error, the maximum being only 1.4 percent of the conversion for set number 1. For sets 7 and 8, the changes in shell flow rates were 120 pounds/hour due to limitations on the flowmeters. Here the change in exit monoester conversion was more significant. Exit conversion was most sensitive to increases in flow in the first jacket section. This was expected since an increase in reactant temperature close to the reactor entrance, raises the reaction rate over the entire remaining length. Predicted descreases in conversion were 3.6 percent and

TABLE 8.3

RUN NUMBER 11--SENSITIVITY ANALYSIS

Set No.	Shell Flow Rates, pounds/hour					Y_{R_1}(exit)	
	1	2	3	4	5	Measured	Predicted
1	0	0	436	600	600	.650	.676
						$(Y_{R_1}-Y_{R_1}$(Sample 1))	
2	0	0	436	600	540	.0025	0.0
3	0	0	436	540	540	.0058	-.0001
4	0	0	436	540	600	.0018	0.0
5	0	0	496	600	600	0.0005	-.0008
6	0	0	376	600	600	0.0097	.001
7	0	120	436	600	600	-.0156	-.0126
8	120	0	436	600	600	-.0362	-.0245
9*	0	0	162	600	600	---	0.002

Initial Conditions for Run Number 11

C_{A_i} = 0.01814 $Y_{R_{1_i}}$ = 0.113, $Y_{R_{2_i}}$ = 0.00131, Y_{B_i} = 2.843

Tube Flow Rate = 197 pounds/hour

T_{T_i} = 86.9, °F T_{S_i} = 185.8, °F T_{room} = 82.1°F

* Computed Optimal Shell Flows for Initial Conditions of Run Number 11.

1.9 percent for 120 pounds/hour increases in flows of the first and second jacket sections (20 percent of maximum flow rate). Measured decreases in conversion were 5.6 percent and 2.4 percent. This analysis confirms the general insensitivity of monoester conversion to shell flow changes.

C. Comparisons with Ideal Reactor Performance

In this section the results of optimization of the jacketed reactor are compared with isothermal operation and with the optimal operation of the idealized reactor of Chapter 3. These comparisons show that the Maximum Principle is quite useful in predicting an upper bound on conversion in a real reactor. To make these comparisons, several of the solutions of Chapter 3 were repeated using the corrected estimates of activation energies and frequency factors given in Equation (5.5). The forms of all solutions remained the same as those of Chapter 3. In all cases the "optimal trajectory" is taken as that profile which maximizes the conversion to monethyl adipate at the reactor exit. A comparison of various "optimal solutions" is shown in Table 8.4. It should be noted that initial conditions of all runs were not exactly the same. However, only the initial value of Y_{R_1} has serious bearing on Y_{R_1} (exit) for optimal operation, and the largest difference in Y_{R_1} was 0.01. Initial conditions for reactor runs 9 and 10 are shown in Tables 7.1, and in Table 3.1 for all other problems.

TABLE 8.4

COMPARISON OF IDEAL AND ACTUAL OPTIMAL REACTOR OPTIMIZATION

	Problem	Y_{R1} at Reactor Exit	
		Predicted	Measured
1.	Sub Optimal Reactor Run Number 10	0.672	0.652
2.	Actual Optimal Shell Flows for Conditions of Run Number 10	0.673	
3.	Run Number 9 Predicted Optimal Operation Using Preliminary Estimate of Rate Laws	0.755	0.663
4.	Run Number 9--Corrected Rate Law	0.645	0.663
5.	Optimal Temperature Profile	0.692	
	$28°C \leq T \leq 85°C$ Set $T = 28°C$ from $t = 0$ -26.01 Sec. Set $T = 85°C$ for $t = 26.01$-38 Sec.		
6.	Optimal Heat Flux and Optimal Inlet Temperature	0.652	
	$T_i = 27.7°C$ $0 \leq q \leq 181.1$ cal./sec./ft.^{2} Set $q = 181.1$ along entire length		
7.	Optimal Isothermal Operation	0.613	
	$T = 61.8$ °C		

Referring to Table 8.4, the results of problems 1 - 4 for the jacketed reactor clearly show that large decreases from optimal conversion do not occur as a result of large deviations from optimal shell flow rates. Under the conditions of run 10, predicted exit conversion to monoester was only 0.001 less than the predicted maximum, a difference not measurable by the analytical methods used. Even for run number 9, where erroneous values of activation energies and frequency factors caused considerable overheating, the predicted loss from optimal operation was only 4.2 percent. This however was at the expense of considerably hydroxyl ion and unreacted diester compared with optimal operation. (Compare Figures 8.1 with 8.2) Had these other components been considered in the object function, run 9 would not have compared as well. Problem 5 gives the highest conversion of all of the problems considered, and also gives an upper bound for conversion in real reactors with the same residence time and temperature range. This is true because all other "optimal" solutions are possible candidates for the solution of the optimal temperature control problem.

Problem 6, the choice of a constrained heat flux profile, produces a final conversion which is six percent less than that produced with the optimal temperature profile and three percent less than that predicted for the jacketed reactor (Problem 2). The heat flux constraint, $0 \leq q \leq 181.1$ cal/sec.ft.^{2} was chosen so that with full heating, the total temperature change along the reactor would be approximately equal

to the total temperature change in the jacketed reactor operating optimally. There are certainly sections of the jacketed reactor where the heat flux is much higher than the average value. Hence, the optimal control of problem 2 is a heat flux profile outside the constraints set in problem 6.

Problem 7, the best isothermal operation, produces the lowest yield of all problems considered, This is as expected, since isothermal operation is included as possible choices in problems 5 and 6, and it may be closely approximated in the jacketed reactor.

These comparisons lead to important conclusions regarding the usefulness of the Maximum Principle for tubular reactor optimization. Since the optimal temperature problem provides an upper bound on yield in real reactors, this is a logical point of comparison for all actual tubular reactor designs. However for more complicated reaction systems, the optimal temperature profile problem is much more difficult to solve, for the following reason. As shown in the analysis of Chapter 3 (Section D and F), it was necessary to find the control in the allowable control region (either temperature or k_1) which minimized the Hamiltonian, H, at every point along the reaction path. Success was achieved with reasonably short computing times mainly because minimization of H could be accomplished in an analytical rather than a numerical fashion. That is, an explicit expression was obtained for k_1 which minimized H for all possible values of $\vec{y}$ and $\vec{\psi}$. Only the two point boundary value problem

had to be solved by trial and error. Had a numerical minimization been required at each step of the integration, not only would computing time have increased by a factor of 10-20, but the approximations necessary might have caused instabilities which would make numerical solution impossible. Failure to realize this is the major reason for difficulties reported in the literature concerning the usefulness of the Maximum Principle.

We do not imply that analytical minimization of H can be accomplished in all problems. However a method is suggested in Appendix G which guarantees this minimization for more complex reaction schemes by solving the optimal heat flux problem rather than the temperature profile problem. The use of "penalty functions" is suggested to include bounds on allowable temperature.

9. SUMMARY, CONCLUSIONS, AND RECOMMENDATIONS

A theoretical and experimental study was conducted on the optimal operation of a jacketed tubular reactor in which consecutive, second order, homogeneous, liquid phase reactions occurred in turbulent flow. The chemical reaction used to verify the applicability of the mathematical model and to illustrate optimal operation was the saponification of diethyl adipate with sodium hydroxide in aqueous solution.

The reactor consisted of ten, fifteen foot lengths of 0.25 inch O.D. by 0.025 inch wall thickness, hard drawn copper tubing. This tubing was concentric with larger diameter tubing of 0.625 inch O.D. by 0.040 inch wall thickness. All inner tubes were connected in series. Pairs of the outer tubes were connected to form five separate jacket sections. Hot water flowed through each jacket section cocurrent with reactant flow, and was used to control the reactant temperature. Because of the change in temperature along the reactor, tube Reynolds and Prandtl numbers varied from 7,800 and 5.7 at 85°F to 18,500 and 2.1 at 185°F.

Comparison of predicted concentration and temperature profiles with experimental data showed that the plug flow model satisfactorily predicted reactor performance under adiabatic operation as well as during strong heating.

The correlation of Sieder and Tate[110] was employed to predict the overall heat transfer coefficient for transfer from shell to tube.

Experimental temperature measurements agreed with predicted values to within 1°F over the temperature range: 80-180°F.

Pulses of hot water injected into a cold stream were used to charaterize axial dispersion. Analysis by the method of moments resulted in a dispersion number (D_e/vL) for the reactor equal to 0.009 Tichacek[115] showed that for this dispersion number, the decrease in yield of middle product compared with plug flow operation is less than one percent for second order consecutive reactions. Furthermore, an error analysis indicated that the calculated dispersion numbers could be high by more than 25 percent because of heat losses and the high heat capacity of reactor end fittings. This would further reduce the predicted effect of axial dispersion of reactor performance. The dispersion number obtained from the pulse testing study was 6-10 times higher than predicted by the correlation of Levenspiel[82] for flow in straight pipes. The results of Carter and Bir[27] for axial dispersion in a high pressure ethylene reactor containing twelve-180° return bends were three times higher than those given by Levenspiel. Thus, this study also indicated that reactor bends drastically increase the effective axial dispersion in tubular reactors.

From preliminary tubular reactor experiments, the values of activation energies and frequency factors in the Arrhenius law for the consecutive saponification reactions are:

$$k_{1_o} = 4.868 \times 10^6 \text{ l./g.mole/sec.} \qquad E_1 = 10{,}079 \text{ cal./g.mole}$$

$$k_{2_o} = 3.487 \times 10^3 \text{ l./g.mole/sec.} \qquad E_2 = 5964.6 \text{ cal./g.mole} \quad (9.1)$$

$$29 \leq T \leq 85°C$$

The results of preliminary batch studies designed to determine reaction rate constants at various temperatures had very large experimental uncertainties and were not used to predict performance in the tubular reactor. The batch results did, however, agree with the flow data within experimental error.

There were no reported values of reaction rate constants for the saponification of diethyl adipate in the temperature or concentration range of this study. Extrapolation of the data of this study yielded reaction rate constants much higher than the few available sets of data. The difference in the concentration range, and disagreement between the few other investigators made comparison impossible. The summary of other investigators' results is shown in Table 5.1.

Heats of reaction for the consecutive saponifications were determined by measuring temperature rises during batch adiabatic reaction. The results were:

$$(-\Delta H_1) = 10.8 \text{ kcal./g.mole}$$

$$(-\Delta H_2) = 16.3 \text{ kcal./g.mole} \quad (9.2)$$

Because the reaction mixtures in the tubular reactor studies were dilute, the heats of reaction had a minor effect in the reactor heat balance compared with wall heat flux.

A method of analysis of monoethyl adipate in the reaction mixture was developed based on selective extraction of diethyl adipate from aqueous solution using benzene. To account for the small amount of monoethyl adipate also extracted, the equilibrium distribution of monoethyl adipate between water and benzene was determined. The distribution at 25°C is given by:

$$C_{Benz} = 0.0033\ C_{Aq} \qquad (9.3)$$

where C_{Benz} and C_{Aq} are concentrations of monoethyl adipate in the benzene and aqueous phases respectively. This relationship is based on experimental data over the concentration range $C_{Aq} = 0 - 0.012$ g.mole/l.

For the experimental system, the optimal policy was defined as the set of hot water shell flow rates which maximized the yield of monoethyl adipate at the reactor exit (i.e. moles monoester leaving per mole diester entering the reactor). Inlet conditions had the following nominal values:

$C_{diester} = 0.018$ mole/l.

$C_{monoester} = 0.002$ mole/l.

$C_{OH^-} = 0.053$ mole/l.

$T_{tube} = 85°F.$

$T_{shell} = 183°F.$

Tube Flow Rate = 197pounds/hour

Shell Flow Rate Range = 0 - 600 pounds/hour

The yield of monoethyl adipate was maximized at the reactor exit by operating the reactor with no hot water flow in the first two jacket sections, intermediate flow in the third section, and maximum flows (600 pounds/hour) in the last two sections. The maximum yield of monoethyl adipate was 0.67 moles per mole of diester fed to the reactor. The optimal value of the third shell flow rate was found to be very sensitive to inlet concentrations and especially to inlet hot water temperature. However, large deviations in the third shell flow rate from the optimum produced only slight decreases in yield of monoethyl adipate.

A sensitivity analysis was conducted both experimentally and numerically to determine the effect of deviations of all shell flow rates on the optimal yield of monoethyl adipate. The yield was found to be most sensitive to increases in flows in the first and second jacket sections. The maximum predicted change in yield was a decrease of 3.6 percent corresponding to an increase of flow in the first jacket section from 0 to 120 pounds/hour. The experimental and numerical sensitivity analyses agreed within experimental error.

A theoretical study was performed to determine what contribution the boundary layer made to reactor yield. The "stagnant boundary layer model" predicted an upper bound on this effect. For the conditions of operation in this study, the stagnant boundary layer model predicted yields of monoethyl adipate less than one percent

higher than those of the plug flow model. The effective boundary layer thickness was shown to decrease with increasing Reynolds and Schmidt numbers, and to be otherwise independent of tube diameter. Consequently, the plug flow model should accurately predict reactor performance for reactions with activation energies comparable to those of this study, occurring in larger scale jacketed reactors at equal or greater Reynolds and Schmidt numbers. However, for systems possessing very high activation energies, the large increase in reaction rate with temperature will cause the boundary layer effect to be significant.

Optimal temperature profiles and optimal wall heat flux profiles were found which maximized the yield of middle product for first and second order consecutive reactions occurring in an idealized tubular reactor. The Pontryagin Maximum Principle was used to obtain these solutions. The optimal temperature profile problem provides an upper bound on yields in all real reactors with the same residence time and temperature range. Using the parameters of the experimental system, the optimal temperature profile was so called "bang-bang". The temperature was held at the lowest possible value (28°C) over the first part of the reactor, followed by a jump to the highest possible temperature (85°C) for the remainder of the reactor length. The optimal temperature profile produced a yield of 0.69 moles monoester per mole of diester entering the reactor, compared with 0.67 for optimal operation of the experimental reactor and 0.61 for optimal isothermal operation.

For the optimal wall heat flux problem, the maximum allowable heat flux was taken as the average heat flux in the experimental reactor which was operating optimally (181.1 cal./sec./ft.^{2}). The optimal policy was to set the inlet temperature at 27.7°C and to use full heating along the entire reactor length. The optimal yield was 0.65 moles monoester per mole diester entering the reactor. If the inlet temperature was raised above the optimal inlet temperature, it was best to operate adiabatically for the first part of the reactor, followed by full heating for the remainder. If the inlet temperature was reduced below the optimal inlet temperature, it was best to use full heating along the entire reactor.

Two other problems were considered for optimal operation of the idealized plug flow reactor. The first was to find the heat flux profile which produced a given yield at the reactor exit and minimized the total "amount of heating" along the reactor. The total "amount of heating" was quantitatively defined as $\int_0^{t_f} q^2 dt$ where t is reactor residence time. This integral was minimized by starting with a fairly high heat flux and gradually decreasing it until reactor operation was adiabatic at the exit. The second problem was to find the reactor heat flux profile which maximized a more general profit function:

$$J = Y_{R_1}(t_f) - a_o \int_0^{t_f} q^2 dt \qquad (9.4)$$

where $Y_{R_1}(t_f)$ is the yield of monoester and the intergral represents the total amount of heating. The constant "a_o" is proportional to the ratio of unit heating cost to unit selling price of monoester. Three different values of "a_o" chosen to illustrate high, medium, and low heating costs compared with selling price of monoester. In all cases it was best to gradually reduce heat flux along the reactor and to operate adaiabatically at the exit. When heating was inexpensive, it was profitable to improve the yield by increasing the heat load on the reactor. For the case of high heat cost, the reactor was operated with a very low heat flux. Consequently, reactant temperature and conversion remained low.

The conclusions of this research serve to draw together the results of experiment and theoretical analysis. These conclusions are presented below.

The plug flow model should be adequate to describe concentration profiles for wall heated tubular reactors under a broad range of conditions. Most tubular reactors will satisfy the sufficient conditions of Chapter 7 for applicability of the plug flow model.

The majority of previous papers on optimal tubular reactor operation have assumed the plug flow model to obtain optimal temperature profiles without considering the actual implementation of these profiles. The plug flow model was employed mainly because of its simplicity. These "paper studies" may now be relied on to give an upper bound on conversion in a broad class of wall heated tubular chemical reactors.

The determination of optimal temperature and wall heat flux profiles for the consecutive second order reactions of this study indicates that the Pontryagin Maximum Principle may be successfully applied to problems more difficult than those of the first order reaction systems previously considered. This is not to imply that the Maximum Principle can be applied in the same straightforward manner to all problems. On the contrary, keen analysis of the

mathematical equations obtained from application of the Maximum Principle will generally be paramount to successful computer solution.

For tubular reactor systems in which more than two simultaneous chemical reactions occur, the Maximum Principle will be more easily applied to determine the optimal constrained wall heat flux profile than to determine the optimal temperature profile. Although temperature enters the Hamiltonian non-linearly, wall heat flux appears linearly. Consequently, explicit determination of the optimal heat flux policy is guaranteed. This greatly simplifies the numerical solution of the two point boundary value problems.

Based on the results of this study, five recommendations are presented. The first three refer to preliminary kinetics and dispersion measurements. The final recommendations concern the plug flow model and the usefulness of the Maximum Principle.

The precise determination of reaction rate constants for complex systems is difficult because of the propagation of small systematic errors. In future studies, it is recommended that independent measurements be made of concentration profiles for at least two components of the reaction mixture.

Non-isothermal operation of a tubular reactor provides a means of determining reaction rate constants over a complete temperature range with relatively little data and in a short time compared with batch experiments. However, the apparatus is more complex than the constant temperature bath and laboratory glassware required for batch tests. If a tubular reactor is available it should definitely be employed for the measurement of reaction rate constants. Precautions must be taken regarding the validity of the plug flow assumption.

Pulses of either heat or mass may be used to characterize axial dispersion in tubular reactors. Both methods suffer small errors introduced by experimental uncertainty, especially in measurements of the "tail" section of the pulse. In addition to these common errors, the "heat" method also

contains inherent uncertainties due to heat losses to the reactor surroundings. The injection of a concentration pulse is therefore to be preferred for axial dispersion measurements.

The plug flow model should be employed to predict preformance of wall heated tubular reactors whenever boundary layer and axial dispersion effects are small. In turbulent flow, this will usually be the case. This study provides sufficient conditions on reactor Reynolds and Schmidt numbers, and on reaction activation energies to allow omission of the boundary layer correction in the plug flow model.

The optimal temperature profile problem for an idealized tubular reactor should be employed to obtain an upper bound on optimal operation in real reactors which may be simulated by a plug flow model. The allowable temperature range should include all possible temperatures in the real reactor. For complex reactions it may be very difficult if not impossible to solve this problem using the Maximum Principle. The gradient method [23,68] should then be tried, or the problem should be rephrased as an optimal heat flux problem. The constraints on heat flux should be set to include all possible heat fluxes in the real reactor. If high heat flux in the optimal idealized reactor causes reactor temperature to exceed that possible in the real reactor, the penalty function method [102,103] is suggested for modifying the problem.

APPENDICES

APPENDIX A

PROOF OF CONSTANCY OF $\psi_o(t)$ AND $\mathcal{M}(\vec{\psi}, \vec{x})$

It will now be shown, that the function $\mathcal{M}(\vec{\psi}(t), \vec{x}(t))$ $= H(\vec{\psi}, \vec{x}, \vec{u})$ and the function $\psi_o(t)$ are constant. For clarity Equations (3.2), (3.7) and (3.8) in expanded form are rewritten here:

$$\frac{dx_i}{dt} = f_i(x_1, x_2, \ldots x_n, \vec{u}) \quad i=0,1,\ldots n \tag{3.2}$$

$$H = \psi_o f_o + \psi_1 f_1 + \ldots + \psi_n f_n \tag{3.7}$$

$$\frac{dx_i}{dt} = \frac{\partial H}{\partial \psi_i}, \quad \frac{d\psi_i}{dt} = -\frac{\partial H}{\partial x_i} \quad i=0,1,\ldots n \tag{3.8}$$

Since none of the f_i contain x_o, Equation (3.8) gives for

$$i=0: \quad \frac{d\psi_o}{dt} = 0$$

Thus $\psi_o(t)$ = constant = $\psi_o(t_1)$. (A.1)

Now choose $\vec{u}$ optimally so that H is maximized at every point along the trajectory.

Differentiate (3.7) with respect to t along the trajectory:

$$\frac{dH}{dt} = \sum_{i=0}^{n} \left\{ \frac{\partial H}{\partial \psi_i} \frac{d\psi_i}{dt} + \frac{\partial H}{\partial x_i} \frac{dx_i}{dt} \right\} + \frac{\partial H}{\partial \vec{u}} \frac{d\vec{u}}{dt} \tag{A.2}$$

Substituting (3.2), and (3.8) into (A-1.2)

$$\frac{dH}{dt} = \sum_{i=0}^{n} \left\{ f_i \frac{d\psi_i}{dt} - \frac{\partial \psi_i}{\partial t} f_i \right\} + \frac{\partial H}{\partial \vec{u}} \frac{d\vec{u}}{dt} = \frac{\partial H}{\partial \vec{u}} \frac{d\vec{u}}{dt} \tag{A.3}$$

In maximizing H, $\vec{u}$ is either chosen as an interior point in U, or on a boundary. When $\vec{u}$ is interior to U, $\frac{\partial H}{\partial \vec{u}} = 0$ so that Equation (A.3) reduces to zero. Similarly if $\vec{u}$ is chosen on a boundary of U, for a finite length of time, $\frac{d\vec{u}}{dt} = 0$ and Equation (A.3) again reduces to zero. The constancy of H during a jump discontinuity in $\vec{u}$ must be examined from a different viewpoint, since the second term of Equation (A.2) is not defined for this case.

Suppose that the control $\vec{u}$ is required to change discontinuously from $\vec{u}_{max}$ to $\vec{u}_{min}$ at time t_j. By contradiction it will now be shown that at the jump point, $H(\vec{u}_{min}) = H(\vec{u}_{max})$:

Suppose that $H(\vec{u}_{min}) > H(u_{max})$: Then after the jump, $H(u_{min})$ will remain constant as shown above. The optimal trajectory, however must satisfy the necessary condition when approached from either side of the jump point. On reversing the direction of travel along the trajectory, a jump from $\vec{u}_{min}$ to $\vec{u}_{max}$ at t_j would violate the necessary condition that H be maximized. Therefore, such a trajectory would not be optimal.

Suppose that $H(\vec{u}_{min}) < H(\vec{u}_{max})$. Then a jump in $\vec{u}$ from $\vec{u}_{max}$ to $\vec{u}_{min}$ would again violate the necessary condition. Hence, if a jump is to occur in the control for example from $\vec{u}_1$ to $\vec{u}_2$, it does so at a point of the trajectory at which $H(\vec{u}_1) = H(\vec{u}_2) =$ abs max $H(\vec{u})$.

The supposition is thus completely proven. However, an additional remark is in order regarding the practical location of a jump discontinuity in $\vec{u}$. Except in relatively simple problems amenable to phase plane analysis, numerical integration is used and $\vec{u}$ is chosen equal to $\vec{u}_{min}$, $\vec{u}_{max}$ or a value which causes $\frac{\partial H}{\partial \vec{u}} = 0$,

whichever produces a larger H. The jump occurs, for example, after a step of integration when $H(\vec{u}_{min})$ becomes greater than $H(\vec{u}_{max})$. $H(\vec{u}_{min}) - H(\vec{u}_{max})$ can be made arbitrarily small by decreasing the step size, but this rapidly increases the computation time on a digital computer.

In this work, the jump was first located with a relatively large step at which time a "homing in" routine was used to pinpoint the position of the jump. When the point of discontinuity was precisely located the integration again proceeded with a large step size thereby saving computing time. An analog computer possessing the required logic or a hybrid computer might avoid this difficulty.

APPENDIX B

DETERMINATION OF AXIAL PECLET NUMBER FROM PULSE TESTING

The schematic drawing of Figure B.1 illustrates the several heat transfer fluxes between tube fluid and the wall.

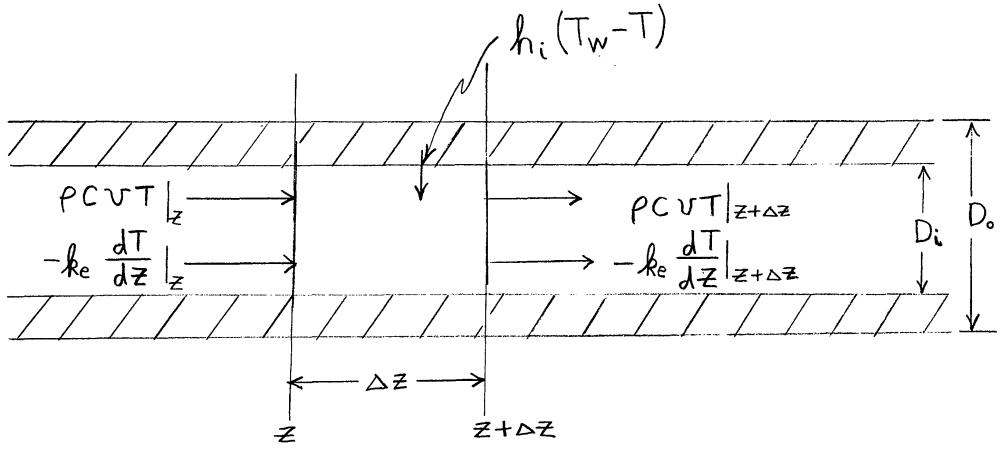

Figure B.1. Illustration of Various Heat Transfer Fluxes

Differential heat balances on tube and shell, in dimensionless form are given below:

$$-\frac{1}{Pe}\frac{\partial^2 \tau}{\partial \bar{z}^2} + \frac{\partial \tau}{\partial \bar{z}} + \frac{\partial \tau}{\partial \theta} = -b_1(\tau - \tau_w) \qquad (B.1)$$

$$\frac{\partial \tau_w}{\partial \theta} = b_2(\tau - \tau_w) \qquad (B.2)$$

where:

$$b_1 = \frac{4h_i}{D_i \rho C}\frac{L}{v} \quad , \quad b_2 = \frac{b_1 D_i}{D_o^2 - D_i^2}$$

$$Pe = \frac{vL}{D_e} \quad , \quad D_e = \frac{k_e}{\rho C} \qquad (B.3)$$

$$\bar{z} = \frac{z}{L} \quad , \quad \theta = \frac{vt}{L}$$

$$\tau = T - T_{wi} \quad , \quad \tau_w = T_w - T_{wi}$$

The required initial and boundary conditions on $\tau(\bar{z},\theta)$ are:

a. $\tau(\bar{z},0) = 0$

b. $\tau(0,\theta) = \tau_0(\theta)$

c. $\lim_{\bar{z}\to\infty} \tau(z,\theta) = 0$

d. $\tau_w(z,0) = 0$ (B.4)

Denote by $\bar{\tau}$ and $\bar{\tau}_w$ the Laplace Transforms of τ and τ_w with respect to θ .

$$\bar{\tau}(z,s) = \mathcal{L}_\theta(\tau) = \int_0^\infty e^{-s\theta}\,\tau(\bar{z},\theta)\,d\theta$$

$$\bar{\tau}_w(z,s) = \mathcal{L}_\theta(\tau_w) = \int_0^\infty e^{-s\theta}\,\tau_w(z,\theta)\,d\theta \qquad \text{(B.5)}$$

Transforming Equations (B.1) and (B.2) and applying initial conditions (B.4) a. and d. yields:

$$-\frac{1}{Pe}\frac{d^2\bar{\tau}}{d\bar{z}^2} + \frac{d\bar{\tau}}{dz} + s\bar{\tau} = -b_1(\bar{\tau} - \bar{\tau}_w) \qquad \text{(B.6)}$$

$$s\bar{\tau}_w = b_2(\bar{\tau} - \bar{\tau}_w) \qquad \text{(B.7)}$$

Solving simultaneously for $\bar{\tau}$ and $\bar{\tau}_w$:

$$\bar{\tau}_w = \frac{b_2}{s + b_2}\,\tau \qquad \text{(B.8)}$$

$$\bar{\tau} = C_1 e^{r_1' z} + C_2 e^{r_2' z} \qquad \text{(B.9)}$$

where

$$r'_{1,2} = \frac{1 \pm \sqrt{1 + \frac{4}{Pe}\left[S + b_1 - \frac{b_1 b_2}{(S+b_2)}\right]}}{2Pe^{-1}} \qquad (B.10)$$

To satisfy boundary conditions c. and d.:

$$C_1 = 0$$

$$C_2 = \bar{\tau}_o(s) \equiv \mathcal{L}_\theta\left[\tau_o(\theta)\right]$$

Equation (B.9) then becomes:

$$\bar{\tau}(z,s) = \bar{\tau}_o(s)\ \exp\left\{ \frac{1 - \sqrt{1 + 4Pe\left[S + b_1 - \frac{b_1 b_2}{(S+b_2)}\right]}}{2\,Pe^{-1}} \right\} \qquad (B.11)$$

We now make use of an identity between the moments defined in Equation (5.12) and the Laplace transform given in (B.5)

$$\mathcal{M}_n(\bar{z}) = \int_o^\infty \tau(\bar{z},\theta)\,\theta^n d\theta = \left[(-1)^n \frac{d^n}{ds^n}\bar{\tau}(\bar{z},s)\right]_{s=o} \qquad (B.12)$$

This relation may be verified by performing the required operations on the Laplace transform, $\bar{\tau}(\bar{z},s)$.

Table B.1 lists expressions for the zeroth through second moment at the zeroth and first sampling positions.

TABLE B.1

EXPRESSIONS FOR THE ZEROTH THROUGH SECOND MOMENTS

n	$\bar{z}=0$	$z=1$
0	$\mathcal{M}_0(0)=\bar{\tau}_0(0)$	$\mathcal{M}_0(1)=\bar{\tau}_0(0)$
1	$\mathcal{M}_1(0)=-\bar{\tau}_0'(0)$	$\mathcal{M}_1(1)=-\bar{\tau}_0'(0)+\bar{\tau}(0)\left[1+\frac{b_1}{b_2}\right]$
2	$\mathcal{M}_2(0)=\bar{\tau}_0''(0)$	$\mathcal{M}_2(1)=\bar{\tau}_0''(0)-2\left(1+\frac{b_1}{b_2}\right)\bar{\tau}_0'(0)+\bar{\tau}_0(0)\left\{\left(1+\frac{b_1}{b_2}\right)^2\left(1+\frac{2}{Pe}\right)+2\left(\frac{b_1}{b_2}\right)\left(\frac{1}{b_2}\right)\right\}$

Eliminating $\bar{\tau}_0'$ and $\bar{\tau}_0$ from the expression for $\mathcal{M}_1(1)$ the required expression for μ' is obtained.

$$\mu' = \frac{\mathcal{M}_1(1)-\mathcal{M}_1(0)}{\mathcal{M}_0} = \left(1+\frac{b_1}{b_2}\right) \tag{B.13}$$

Next, the expression for $\mathcal{M}_2(1)$ is simplified with the aid of all other expressions in Table B.1 and Equation (B.13). The result is:

$$\frac{\mathcal{M}_2(1)}{\mathcal{M}_0} = \frac{\mathcal{M}_2(0)}{\mathcal{M}_0} + 2\mu'\frac{\mathcal{M}_1(0)}{\mathcal{M}_0} + \mu'^2 + \frac{2}{b_2}\frac{b_1}{b_2} + \frac{2\mu'^2}{Pe} \tag{B.14}$$

from which the Peclet number may be calculated. This result may be rearranged into a somewhat more useful form by introducing central moments:

$$\mathcal{M}_n^c(\bar{z}) = \int_0^\infty \tau(\bar{z},\theta)\cdot(\theta-\mu')^n\, d\theta \qquad (B.15)$$

The transformation gives the required result:

$$\frac{\mathcal{M}_2^c(1)}{\mathcal{M}_0} - \frac{\mathcal{M}_2^c(0)}{\mathcal{M}_0} = \frac{2}{b_2}(\mu'-1) + \frac{2\mu'^2}{Pe} \qquad (B.16)$$

The only information required in addition to that obtained from the pulse tests is the value of the constant b_2 . This may be calculated from physical property data and an estimate of the tube side heat transfer coefficient.

Notice that Equation (B.16) contains only ratios of moments, and that both $\mathcal{M}_2^c$ and $\mathcal{M}_0$ are linear in τ . Therefore, any number proportional to τ such as thermocouple response or recorder pen position may be used in place of τ .

APPENDIX C

DETAILED ANALYTICAL PROCEDURE FOR DETERMINATION OF CONCENTRATIONS OF SODIUM HYDROXIDE AND MONOETHYL ADIPATE IN REACTION MIXTURE

1. Into a weighed 50 ml. Erlenmeyer flask containing 10 ml. of 0.150 N. HCl, and three drops bromthymol blue indicator solution, collect approximately 25 ml. of reaction mixture.

2. Reweigh to determine sample weight.

3. Cool to approximately 20°C.

4. Titrate to neutral with 0.1 N. NaOH. Record volume of base, normality and carbonate content.* If end point is passed, back titrate with 0.03 N. HCl. (The initial NaOH concentration may now be calculated.)

5. From this solution, pipette 25 ml. into a clean 50 ml. centrifuge tube.

6. Add to the centrifuge tube, 25 ml. of benzene. Shake for two minutes to assure complete mixing. Centrifuge until aqueous and benezene phases are completely separated.

7. Remove with a pipette as much of the benzene phase (top phase) as possible without removing the aqueous phase.

8. Repeat steps 6 and 7. (Two benzene washes remove essentially all unreacted ester and 0.66 percent of monoethyl adipate).

9. With a clean pipette, remove 20 ml. of the remaining aqueous phase and place in a 50 ml. flask.

10. Add to this flask, 10 ml. of 0.03N. NaOH. Record exact normality and carbonate content.*

---

*The carbonate content may be determined from the difference in titre when the NaOH solution is titrated using phenolphthalein and methyl orange indicators.

11. To completely saponify the monoester, allow flask to stand overnight at room temperature, at 60°C for one hour, 70°C for 40 minutes, or 80°C for 30 minutes.

12. Add two additional drops of bromthymol blue indicator.

13. Back titrate with 0.03N. HCl. Record volume of HCl and normality. (The original monoester concentration may now be calculated.)

Calculation of base and monoester compositions were performed on a General Electric Model 225 computer operated in the time shared mode from a remote terminal. This proved to be very convenient since results became available very soon after the chemical analysis was completed. Using the nomenclature in Table C.1, the computer program, ANALM shown in Figure C.1 gives the required calculations to obtain compositions from the titration data. Concentrations of unreacted ester and disodium adipate are also calculated assuming plug flow in the reactor. The program is written in the Basic language.

TABLE C.1

NOMENCLATURE FOR COMPUTER PROGRAM ANALM

Symbol	Meaning
A	Mole ratio of diethyl adipate, mole/mole initially present.
AO	Initial conc. of diethyl adipate.
B	Mole ratio of NaOH, mole/mole A initially present.
BO	Initial NaOH concentration., mole/l.
B1	Normality of NaOH in step 4 of analytical procedure mole OH^-/l.
B2	Normality of NaOH in step 10, mole OH^-/l.
C1	Carbonate content of NaOH in step 4, as equivalent moles OH^-/l.
C2	Carbonate content of NaOH in step 10, as equivalent moles OH^-/l.
D1	Density of reactor sample, g/ml .
H1	Normality of HCl in step 4., mole/l.
H2	Normality of HCl in step 1., mole/l.
H3	Normality of HCl in step 13., mole/l.
P	Position along reactor at which sample was taken, ft.
R	Reactor run number.
R1	Mole ratio of monoethyl adipate, mole/mole A initially present.
R2	Mole ratio of sodium adipate, mole/mole A initially present.
S	Sample number.
V	Sample volume calculated by computer, ml.
V1	Volume of NaOH in step 4.

TABLE C.1 (CONT'D)

Symbol	Meaning
V2	Volume of HCl in step 4., ml.
V3	Volume of HCl in step 13., ml.
V4	Volume of HCl in step 1., ml.
V5	Volume of HCl in step 10., ml.
W	Weight of sample. Difference of weights obtained in steps 1 and 2, grams.

```
ANALM     20:39      WED.---09/27/67

10 READ D1,B1,H1,B2,V5,H3,V4,H2,C1,C2
15 READ A0,B0,R0,R3,C0
16 PRINT "A0="A0"MOLE/LITER"
17 PRINT "CONCENTRATIONS= MOLE/MOLE A ENTERING REACTOR"
18 PRINT "A0="1.0,"B0="B0/A0,"R10="R0/A0,"R20="R3/A0
20 READ R,S,P,W,V1,V2,V3
30 LET V=W/D1
40 LET B= (V2*H1+V4*H2-V1*(B1+C1)-V*C0)/V
50 LET R1=1.0066*(V5*B2-V3*H3)*(V+V1+V2+V4+.18)/(20.*V)
60 LET A=(R0+2.*A0-B0+B-R1)/2.
70 LET R2=R2/A0
76 LET R2=R2/A0
77 LET B=B/A0
78 LET R1=R1/A0
79 LET A=A/A0
80 PRINT "RUN NO."R; "SAMPLE"S;"POS.="P"FT."; "SAMPLE VOL.="V"ML."
100 PRINT "A="A;"R1="R1;"R2="R2;"B="B
105 PRINT
110 GO TO 20
120 DATA 0.9974,0.1004,0.03,0.02997,10.0,0.03,10.0,0.150
125 DATA 0.0016,8.38E-4
130 DATA 0.01796,0.05469,0.00186,8.17E-5
135 DATA 0.00172
140 DATA 7,2,30,25.5612,1.21,0.04,8.38
150 DATA 7,3,60,25.1059,1.51,0.14,7.88
160 DATA 7,4,90,26.2476,1.69,0.06,7.45
170 DATA 7,5,120,22.8983,3.70,0.11,7.27
180 DATA 7,6,150,27.4961,3.06,0.09,5.41
190 DATA 7,7,150,26.9984,3.27,0.05,5.50
200 DATA 7,8,30,21.0152,3.82,0.05,5.00
300 END
```

APPENDIX D

BATCH KINETIC AND HEAT OF REACTION DATA

TABLE D.1

EXPERIMENTAL SODIUM HYDROXIDE CONCENTRATION--TIME DATA

Sample Number	Reaction Time, Seconds	C_B mole/l. x 10^2
	Run Number 1 29°C	
1	180.6	7.031
2	180.8	6.803
5	150.9	7.194
6	151.4	7.277
7	180.6	7.161
8	149.9	7.410
9	150.3	7.371
10	110.9	7.594
11	110.0	7.587
12	111.4	7.577
13	86.5	7.960
14	90.3	7.837
16	80.8	7.860
17	80.0	7.910
18	40.6	8.360
19	40.2	8.459
20	24.7	8.693
21	25.3	8.593
22	26.3	8.693
23	25.7	8.709
24	15.3	8.829
25	14.2	8.969
27	13.95	8.986
28	14.4	8.966
29	40.8	8.543
	Run Number 2 39.8°C	
33	60.2	7.523
34	60.3	7.380
35	59.8	7.616
36	80.0	7.167
37	80.8	7.256
38	80.4	7.219
39	100.0	7.037
40	100.2	6.996
41	101.3	7.010
42	40.3	7.828
43	40.9	7.920
44	40.6	7.715
45	40.4	7.811
46	25.8	8.119
47	25.9	8.146
48	25.5	8.112
49	130.3	6.788
50	17.8	8.266
51	130.5	6.764
52	17.8	8.266
53	15.2	8.475
54	14.4	8.533
	Run Number 3 46.1°C	
56	32.6	7.756
57	32.4	7.708
58	33.0	7.691
59	50.4	7.277
60	52.2	7.205
61	51.8	7.249
62	16.8	8.071
63	16.8	8.071
64	14.8	8.334
65	16.0	8.225
66	15.8	8.197
67	41.4	7.444
68	41.7	7.492
69	40.9	7.585
70	66.7	7.171

TABLE D.1 (Continued)

Sample Number	Reaction Time,	C_B mole/l. x 10^2
	Run Number 3 Continued	
71	65.1	7.078
72	65.1	7.119
73	80.5	6.852
74	81.0	6.842
	Run Number 4 51.6°C	
75	70.9	6.795
76	71.4	6.774
77	60.4	6.921
78	60.4	6.870
79	60.8	6.938
80	48.7	7.185
81	48.9	7.127
82	42.6	7.304
83	36.4	7.390
84	36.5	7.387
85	36.5	7.397
86	24.5	7.787
87	24.9	7.674
88	24.5	7.671
89	11.9	8.352
90	11.5	8.263
91	11.6	8.194
92	12.3	8.338
	Run Number 5 46.1°C	
2	21.0	7.879
3	30.7	7.452
4	40.6	7.141
5	51.5	7.019
6	60.8	6.783
7	69.7	6.731
8	10.6	8.208
9	15.9	7.926
10	80.8	6.713
11	100.5	6.333
12	120.4	6.206
13	140.6	6.159
14	162.1	6.055

Sample Number	Reaction Time, Seconds	C_B mole/l. x 10^2
	Run Number 5 Continued	
15	41.2	7.296
16	30.8	7.412
17	80.0	6.615
18	20.8	7.759
19	60.7	7.015
	Run Number 6 68.9°C	
1	11.5	2.052
2	21.3	1.904
4	32.3	1.728
5	41.7	1.536
6	61.6	1.412
7	91.6	1.270
8	151.3	0.9599
9	230.8	0.8116
10	300.4	0.7004
	Run Number 7 85.0°C	
1	10.3	1.901
2	20.7	1.636'
3	34.9	1.374
4	50.2	1.142
5	101.3	0.8571
6	66.2	1.029
7	85.3	0.9270
8	120.0	0.8421
9	150.2	0.7597
11	180.1	0.6499
12	210.4	0.5950
13	240.3	0.6174
14	280.4	0.5425
15	17.3	1.718
16	25.5	1.484

TABLE D.1 (Continued)

Sample Number	Reaction Time, Seconds	C_B mole/l. x 10^2	C_{R_1} mole/l. x 10^2
	Run Number 8 57.8°C		
1	51.3	1.313	0.8687
2	50.6	1.331	0.8662
3	30.9	1.592	0.7461
4	70.9	1.109	0.9350
5	111.7	0.8647	0.9926
6	140.4	0.7624	1.0024
7	180.3	0.5960	0.9828
8	221.5	0.5080	0.9527

TABLE D.2

INITIAL CONDITIONS FOR BATCH KINETICS RUNS IN TABLE D.1

Run Number	Temp.°C	Initial Concentrations mole/l.x10^2			
		C_{A_i}	C_{B_i}	$C_{R_{1_i}}$	$C_{R_{2_i}}$
1	29.2	1.358	9.223	0.276	0.012
2	39.8	1.380	8.986	0.257	0.011
3	46.1	1.359	8.975	0.275	0.011
4	51.6	1.450	9.046	0.188	0.0080
5	46.1	1.475	8.730	0.150	0.011
6	68.9	1.101	2.410	0.112	0.0061
7	85.0	1.095	2.370	0.128	0.0069
8	57.8	1.398	2.326	0.238	0.0088

TABLE D.3

EXPERIMENTAL TEMPERATURE PROFILE FOR HEAT OF REACTION DETERMINATION

Reaction Time, Sec. Run Number 1	Temp.°C	Reaction Time, Sec. Run Number 2	Temp.°C
30	24.17	16	25.655
60	24.215	70	25.760
90	24.250	120	25.815
140	24.30	170	25.860
190	24.34	220	25.890
240	24.37	270	25.915
290	24.39	320	25.933
340	24.408	370	25.950
390	24.426	420	25.962
440	24.438	470	25.973
490	24.455	520	25.980
540	24.462	570	25.990
590	24.470	620	25.996
640	24.480	670	26.00
690	24.485	720	26.005
740	24.490	770	26.010
790	24.500	820	26.013
840	24.500	870	26.02
890	24.510	920	26.02
940	24.510	970	26.02
990	24.514		

TABLE D.4

INITIAL CONDITIONS FOR HEAT OF REACTION DETERMINATION IN TABLE D.3

Run Number	Initial Conditions**			
	T, °C*	C_A	C_B	C_{R_1}
	mole/l. x 100			
1	24.137	1.678	7.410	0.2265
2	25.658	1.681	7.410	0.2265

* The initial temperature was calculated from the heat of dilution and initial temperatures of ester and NaOH solutions.

** Heat Capacity of Dewar Flask = 41.1 cal./°C
Heat Capacity of Reaction Mixture = 154.29 cal./°C
Reaction Mixture Volume = 154.29 ml.

APPENDIX E

RATE EQUATIONS FOR SAPONIFICATION IN THE PRESENCE OF CARBONATE

In this appendix, the rate equations are derived for saponification of diethyl adipate in the presence of carbonate. Carbonate ion exists in equilibrium with bicarbonate and carbonic acid. In basic solution, the carbonic acid concentration is neglible so that only the carbonate - bicarbonate equilibrium is considered:

$$CO_3^{=} + H_2O \overset{K_H}{\rightleftharpoons} HCO_3^{-} + OH^{-} \qquad (E.1)$$

The hydrolysis constant K_H is the quotient of the equilibrium constants for the reactions:

$$H_2O \overset{K_w}{\rightleftharpoons} OH^{-} + H^{+}$$

$$HCO_3^{-} \overset{K_2}{\rightleftharpoons} CO_3^{=} + H^{+} \qquad (E.2)$$

Equilibrium data for these reactions at various temperatures are given by Roques.[99]

The differential Equations (5.3) describing the rate of change of diester and monoester remain unchanged but Equation (5.4) giving the hydroxide concentration must be modified. The algebraic equation which now related the change in OH^{-} concentration with other species is:

$$C_{B_i} - C_B = 2\left(C_{A_i} - C_A\right) - \left(C_{R_1} - C_{R_{1i}}\right) - \left(C_{HCO_3^-} - C_{HCO_{3_i}^-}\right) \qquad (E.3)$$

Denoting the total carbonate (eq./l.) by C_i a carbonate balance yields:

$$2C_{CO_3^=} + C_{HCO_3^-} = C_i \qquad (E.4)$$

Finally the hydrolysis constant for reaction (E.1) is given by:

$$\frac{[C_B][C_{HCO_3^-}]}{[C_{CO_3^=}]} = K_H \qquad (E.5)$$

Equations (E.4) and (E.5) were solved for $C_{HCO_3^-}$ in terms of C_B. The results was substituted into (E.3) to eliminate $C_{HCO_3^-}$. The quadratic equation thereby formed was solved for C_B taking the positive square root in the quadratic formula since the negative root gave a physically meaningless negative solution. The required result is:

$$C_B = \frac{2C_1 - K_H + \sqrt{(2C_1 - K_H)^2 + 8K_H(C_1 + C_i)}}{4} \qquad (E.6)$$

where

$$C_1 = C_{B_i} - 2(C_{A_i} - C_A) + (C_{R_1} - C_{R_{1i}}) - C_{HCO_{3i}^-} \qquad (E.7)$$

$C_{HCO_{3i}^-}$ is found by letting $C_B = C_{B_i}$ in (E.5) and eliminating $C_{CO_3^=}$ with (E.4). This calculation yields:

$$C_{HCO_{3i}^-} = \frac{C_i K_H}{2C_{B_i} + K_H} \qquad (E.8)$$

APPENDIX F

DETAILS OF ERROR ANALYSIS FOR RATE CONSTANT DETERMINATION

Batch Kinetic Experiments

The expression used to calculate points along the hydroxide concentration profile was:

$$C_B = \frac{V_2 \cdot H_2 - V_3 \cdot (C_3 + B_3) - C_1 V_1}{(V + V_1)} \qquad (F.1)$$

The meaning, nominal value and possible error of the symbols are listed in Table F.1.

TABLE F.1

SUMMARY OF BATCH KINETICS ERROR ANALYSIS

Symbol	Meaning	Nominal Value	Possible Error
V	volume of ester solution, ml.	25	$\pm$ 0.5%
V_1	volume of NaOH solution to start reaction, ml.	4.65	$\pm$ 0.1
C_1	total carbonate content of above NaOH, eq/l.	.003-0.01	$\pm$ 50%
V_2	volume of HCl solution to quench reaction, ml.	4.90	$\pm$ 0.1
H_2	normality of above HCl, mole/l.	0.150-0.6	$\pm$ 1%
V_3	volume of NaOH solution in back titration, ml.	2.5-9.0	$\pm$ 0.03
B_3	normality of above NaOH, mole/l.	0.1	$\pm$ 1%
C_3	total carbonate of above NaOH, eq/l.	.002	$\pm$ 50%

Regression of Tubular Reactor Data

The expressions used to calculate points along the sodium hydroxide and monoethyl adipate profiles are given below:

$$C_B = \left(V_2 \cdot H_1 + V_4 \cdot H_2 - V_1(B_1 + C_1) - V\,C_o\right) \Big/ V \qquad (F.2)$$

$$C_{R_1} = \frac{1.0066}{20.0}\left(V_5 \cdot B_2 - V_3 \cdot H_3\right)\left(V + V_1 + V_2 + V_4 + 0.18\right) \qquad (F.3)$$

The meaning of all symbols are given in Appendix C, Table C.1, where the analysis procedure is described. The nominal values and possible errors are listed in Table F.2.

TABLE F.2

SUMMARY OF ERROR ANALYSIS FOR DETERMINATION OF KINETIC CONSTANTS FROM TUBULAR REACTOR RUN NO. 3

Symbol	Value	Possible Error
B_1	0.1997 mole/l.	± 1%
B_2	0.02962 mole/l.	± 1%
C_o	0.00165 eq./l.	± 50%
C_1	0.00156 eq./l.	± 50%
H_1	0.03 mole/l.	± 1%
H_2	0.150 mole/l.	± 1%
H_3	0.03 mole/l.	± 1%
V_1	1.74-8.32 ml.	± 0.03

TABLE F.2 (CONT'D)

Symbol	Value	Possible Error
V_2	0.09-0.74 ml.	± 0.02
V_3	5.0-6.9 ml.	± 0.03
V_4	10.0 ml.	± 1%
V_5	10.0 ml.	± 1%

TABLE F.3

CALCULATED CHANGES IN CONCENTRATION PROFILE DATA
DUE TO ASSUMED ERRORS IN TABLE F.2
TUBULAR REACTOR RUN NO. 3*

Sampling Position Feet	Y_B** Calc. Value of Y_B	Y_B** Change Pos. (% of Calc. Value)	Y_B** Change Neg. (% of Calc. Value)	Y_{R_1}** Calc. Value of Y_{R_1}	Y_{R_1}** Change Pos. (% of Calc. Value)	Y_{R_1}** Change Neg. (% of Calc. Value)
30	2.699	5.0	4.5	0.4287	8.5	8.5
30	2.681	5.9	5.4	0.4286	9.7	9.7
30	2.723	5.9	5.4	0.4292	9.8	9.8
60	2.279	6.9	6.3	0.6658	5.9	5.8
60	2.274	6.3	5.8	0.6522	5.6	5.6
90	1.959	7.8	7.3	0.6996	5.5	5.6
90	1.941	9.4	8.9	0.6943	6.4	6.4
120	1.737	9.5	9.0	0.6637	5.9	5.8
150	1.579	8.9	9.2	0.5822	7.0	7.1
150	1.645	10.5	10.4	0.5990	7.7	7.7

*Errors for other runs are comparable.

**Y_i = mole i per mole A entering reactor.

APPENDIX G

USE OF THE MAXIMUM PRINCIPLE FOR MORE COMPLEX REACTIONS

To illustrate the major shortcoming of the Maximum Principle, we describe a somewhat more complex problem than was considered in Chapter 3.

Given a chemical reaction which proceeds as shown below:

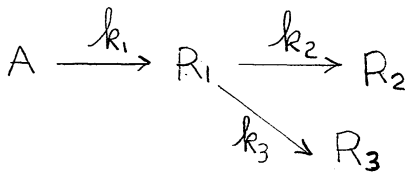

(G.1)

We pose the same problem as in Chapter 3, Section D. The reaction is to occur in a plug flow tubular reactor of known residence time. How shall the temperature profile be chosen along the reactor length in the range $T_* \leq T \leq T^*$ to maximize the conversion of "A" to intermediate "B" ? The reactions are all assumed to be first order, and as before, overall density is constant. Taking reactor residence time, $t = \frac{x}{L}$ as the independent variable, differential equations which describe the system are:

$$\frac{dY_1}{dt} = -k_1 Y_1 = f_1 \tag{G.2}$$

$$\frac{dY_2}{dt} = k_1 Y_1 - (k_2 + k_3) Y_2 = f_2 \tag{G.3}$$

where:

Y_1 = mole A/mole A entering in feed

Y_2 = mole R_1/mole A entering in feed

The reaction rate constants are of the Arrhenius form.

$$k_i = k_{i_0} \exp\left\{-E_i/RT\right\} \quad , \quad i = 1, \ldots, 3 \tag{G.4}$$

The Hamiltonian is then given by:

$$H = \sum_{i=1}^{2} \psi_i f_i = k_1 \gamma_1 (\psi_2 - \psi_1) - k_2 \gamma_2 \psi_2 - k_3 \gamma_2 \psi_2 \tag{G.5}$$

Expressing k_2 and k_3 in terms of k_1 instead of T ,

$$k_2 = k_{2_0} \left(\frac{k_1}{k_{1_0}}\right)^{E_2/E_1} \tag{G.6}$$

$$k_3 = k_{3_0} \left(\frac{k_1}{k_{1_0}}\right)^{E_3/E_1} \tag{G.7}$$

Substituting (G.6) and (G.7) into (G.5), we obtain:

$$H = k_1 \gamma_1 (\psi_2 - \psi_1) - C_1 \gamma_2 \psi_2 k_1^{E_2/E_1} - C_2 \gamma_2 \psi_2 k_1^{E_3/E_1} \tag{G.8}$$

where

$$\begin{aligned} C_1 &= k_{2_0} k_{1_0}^{-E_2/E_1} \\ C_2 &= k_{3_0} k_{1_0}^{-E_3/E_1} \end{aligned} \tag{G.9}$$

An attempt to analytically find the value of k_1 in $k_{1_*} \leq k_1 \leq k_1^*$ which minimizes H is doomed to failure in all but special cases (i.e. $E_2 = E_1$ or $E_3 = E_1$). Attempts to include this minimization in the computer program which also solves the split boundary value problem**

**The analysis was not continued far enough to show the adjoint equations and split boundary value problem. They are similar to those of Chapter 3.

will certainly greatly increase computing time and may also lead to the instability and to very poor convergence. We now suggest that restating the problem as one of choosing the optimal heat flux profile will avoid this problem.

To equations (G.2) and (G.3) add a differential heat balance:

$$\frac{dY_3}{dt} = C_3 \sum_{i=1}^{3} r_i(-\Delta H_i) + C_4 q_f \qquad \text{(G.10)}$$

Y_3 = reactant temperature

r_i = volumetric reaction rate of the ith reaction

$(-\Delta H_i)$ = heat of reaction of the ith reaction

q_f = wall heat flux into the reactor

C_3, C_4 = positive constants

The problem may now be restated as follows. Choose the heat flux along the reactor such that $q_{f*} \le q_f \le q_f^*$ and Y_2 is maximized at the reactor exit.

The Hamiltonian is then given by:

$$H = -k_1 Y_1 \Psi_1 + \left[k_1 Y_1 - (k_2 + k_3) Y_2\right] \Psi_2 + \left[C_3 \sum_{i=1}^{3} r_i(-\Delta H_i)\right] \Psi_3 + C_4 \Psi_3 q_f \qquad \text{(G.11)}$$

It is linear in the control variable q_f, and the proper control to minimize the Hamiltonian is easily found as shown in Chapter 3 sections D and F. The values of q_{f*} and q_f^* should be set at the minimum and maximum possible in the real reactor. This will guarantee that the choice of

heat flux profiles will include all those possible in the real reactor, and will provide an upper bound on exit conversion. If the solution of this problem causes temperature to leave the allowable region, the problem can be modified with the aid of penalty functions. A clear exposition on the use of penalty functions is given by Rothenberger and Lapidus.[103]

APPENDIX H

CALIBRATION CURVES

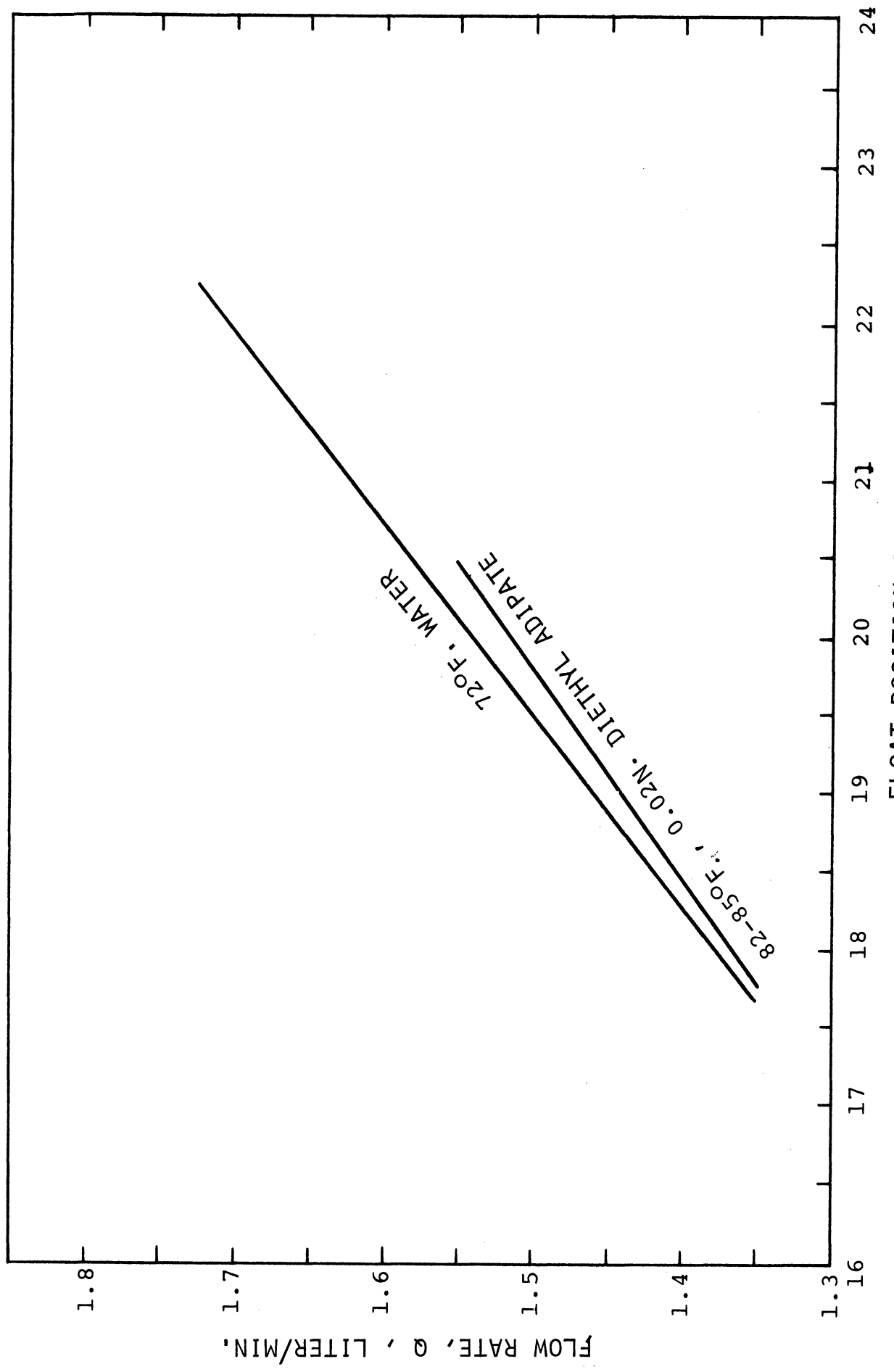

Figure H.1. Ester Flow Meter Calibration.

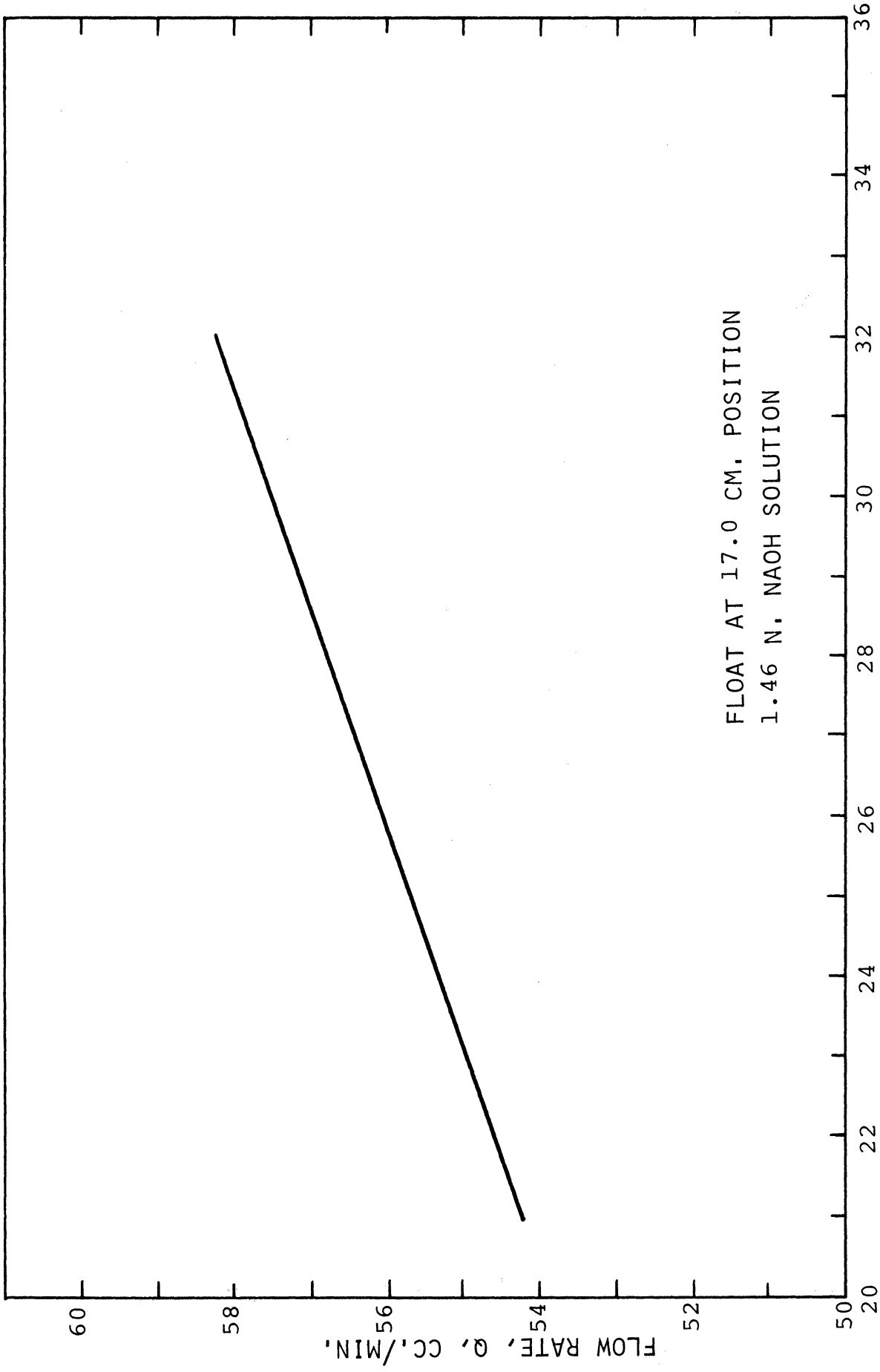

Figure H.2. Sodium Hydroxide Flow Meter Calibration.

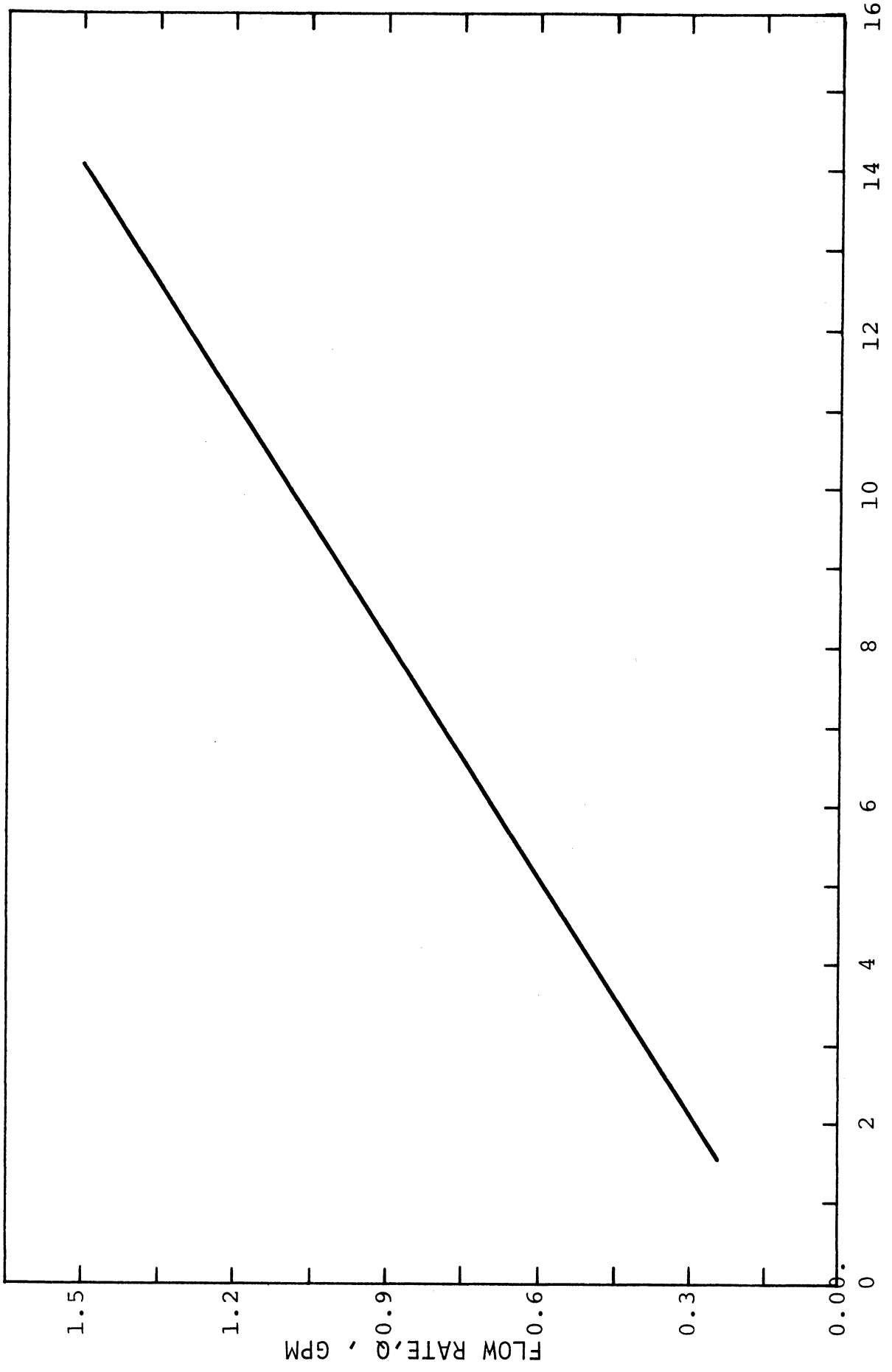

Figure H.3. Hot Water Flow Meter Calibrations.

BIBLIOGRAPHY

1. Adler, J. and Vortmeyer, D. "Effect of Axial Diffusion on the Optimum Yield of Tubular Reactors. I." Chem. Eng. Sci. 18 (1963), 99-108.

2. Adler, J. and Vortmeyer, D. "Effect of Axial Diffusion on the Optimum Yield of Tubular Reactors. II." Chem. Eng. Sci. 19, No. 6 (1964), 413-422.

3. Ahlgen, T. D. and Stevens, W. F. "Process Optimization in Presence of Errors." I. and E. C. Process Design and Development. 5, No. 3 (July, 1966), 290-297.

4. Ahn, Y. K. Models of Flow Reactor Systems and Their Optimal Performances. Ph.D. Thesis. Kansas State University, 1966.

5. Ames, W. F. "Canonical Forms for Nonlinear Kinetic Differential Equations". I. and E. C. Fundamentals. 1, No. 3 (August, 1962), 214-217.

6. Annable, D. "Application of the Tempkin Kinetic Equation to Ammonia Synthesis in Large Scale Reactors". Chem. Eng. Sci. 1 (1952), 145-154.

7. Aris, R. Proc. of Royal Soc. (London) A245 (1958), 268-277.

8. Aris, R. "Studies in Optimization". Chem. Eng. Sci. 13, No. 1 (August, 1960), 18-29.

9. Aris, R. The Optimal Design of Chemical Reactors, A Study in Dynamic Programming. New York: Academic Press, 1961.

10. Ball, W. E. and Groenweghe, L. C. D. "Determination of Best Fit Rate Constants in Chemical Kinetics". I. and E. C. Fundamentals. 5, No. 2 (1966), 181-184.

11. Baron, T. et al. "Reaction Kinetics in a Tubular Reactor". Chem. Eng. Progr. 48 (1952), 125-132.

12. Batten, J. J. "Possible Error in Measurement of Rate Constants". Australian J. Appl. Sci. 12 (March, 1961), 11-22.

13. Beek, J. "Design of Packed Catalytic Reactors." Advances in Chem. Eng. 3, New York: Academic Press (1963).

14. Bellman, R. E. Dynamic Programming, Princeton University Press, 1957.

15. Bilous, O. and Amundson, N. R. "Optimum Temperature Gradients in Tubular Reactions". Chem. Eng. Sci. 5 (1956), 81-92, 115-126.

16. Bilous, O. and Amundson, N. R. "Chemical Reactor Stability and Sensitivity Effect of Parameters on Sensitivity of Empty Tubular Reactors". A.I.Ch.E. Journal. 2 (1956), 117-126.

17. Bird, R. B., Stewart, W. E. and Lightfoot, E. N. Transport Phenomena. John Wiley and Sons, 1960.

18. Bischoff, K. B. "Mixing in Tubular Reactor with Return Bends", A.I.Ch.E. Journal. 10, No. 4 (1964), 584.

19. Bischoff, K. B. "A Note on Boundary Conditions for Flow Reactors." Chem. Eng. Sci. 16 (1961), 131-133.

20. Blum, E. H. and Luus, R. "Thermodynamic Consistency of Reaction Rate Expressions." Chem. Eng. Sci. 19, No. 4 (1964), 322.

21. Boas, A. H. "Optimizing Multi-variable Functions." Chem. Eng. (March, 1964), 97-104.

22. Breakwell, J. V. "Optimization of Trajectories." J. Ind. and Appl. Math. 7 (1959), 215-247.

23. Bryson, A. E. and Denham, W. F. "A Steepest Ascent Method for Solving Optimal Programming Problems." J. Appl. Mech. 29, No. 2 Series E (June, 1962), 247-257.

24. Calderbank, P. H. "Contact Process Converter Design." Chem. Eng. Progr. 49, No. 11 (November, 1953).

25. Carberry, J. J. "First Order Rate Processes and Axial Dispersion in Packed Bed Reactors." Can. J. Chem. Eng. 36, No. 5 (October, 1958), 207-209.

26. Carberry, J. J. and Wendel, M. M. "A Computer Model of the Fixed Bed Catalytic Reactor." A.I.Ch.E.J. 9 No. 1, 129-133.

27. Carter, D. and Bir, W. G. "Axial Mixing in Tubular High Pressure Reactors." Chem. Eng. Progr. 58, No. 3 (March, 1962), 40-43.

28. Chang, S. S. L. "Optimal Control in Bounded Phase Space." Automatika, 1, (1962), 55-57.

29. Chen, T. C. and Ceaglske, N. H. "Optimum Cross Current Extraction with Miscible Solvents." I. and E. C. Fundamentals 5, No. 3 (August, 1966), 422-426.

30. Chu, Chieh and Hougen, O. A. "Optimization of Nitric Oxide Plant." Chem. Eng. Progr. 57, No. 6 (1961), 51-58.

31. Colburn, A. P. "Mean Temperature Difference and Heat Transfer Coefficients in Liquid Heat Exchangers." Ind. and Eng. Chem. 25, (1933), 873.

32. Coste, J. et al. "Taylor Diffusion in Tubular Reactors." Can. J. Chem. Eng. 39 (1961), 149-151.

33. Coutie, G. A. and Box G. E. P. "Application of Digital Computers in the Exploration of Functional Relationships." Proceedings Institute E. Eng. (London), 103B (1956), 100.

34. Curl, R. L. and Mc Millan, M. L. "Accuracy in Residence Time Measurements." A.I.Ch.E. Journal 12, No. 4 (July, 1966), 819-822.

35. Dankwerts, P. V. "Effect of Incomplete Mixing on Homogeneous Reactions." Chem. Eng. Sci. 8 (1958), 93-102.

36. Dankwerts, P. V. "Continuous Flow Systems." Chem. Eng. Sci. 2 (1953), 1-13.

37. Denbigh, K. G. "Instantaneous and Overall Reaction Yields." Chem. Eng. Sci. 14 (Jan., 1961), 25-38.

38. Denbigh, K. G. Chemical Reactor Theory. Cambridge Univ. Press, 1965.

39. Denn et. al. "Optimization of a Class of Distributed Parameter Systems." I. and E. C. Fundamentals 5, No. 1 (February, 1966), 59-66.

40. DiBella, C. W. and Stevens, W. F. "Process Optimization by Non-Linear Programming." I. and E. C. Process Design and Development. (January, 1966), 16-20.

41. Douglass, J. M. and Bischoff, K. B. "Variable Density Effects and Axial Mixing in Chemical Reactors." I. and E. C. Process Design and Development. 3, No. 2 (April, 1964), 130-133.

42. Douglass, J. M. and Eagleton, L. C. "Analytical Solutions of Some Adiabatic Reactor Problems." Ind. Eng. Chem. 1, No. 2 (May, 1962), 116-119.

43. Fabuss, B. et al. "Tables Simplify Analysis of Non-Isothermal Reactors." Chem. Eng. 70, No. 8 (April, 1963), 153-156.

44. Fan, L. T. and Ahn, Y. K. "Critical Evaluation of Boundary Conditions for Tubular Flow Reactors." I. and E. C. Process Design and Development. 1, No. 3 (1962), 190-195.

45. Fan, L. T. and Bailie, R. C. "Axial Diffusion in Isothermal Tubular Flow Reactors." Chem. Eng. Sci. 13 (1960), 63.

46. Fletcher, R. and Reeves, C. M. "Function Minimization by Conjugate Gradients." Computer Journal. 7, No. 2 (1964), 149-154.

47. Freeman, L. B. and Houghton, G. "Singular Perturbations of Non-linear Boundary Value Problem Arising in Chemical Flow Reactors." Chem. Eng. Sci. 21, No. 11 (November , 1966), 1011-1024.

48. Friedman, M. H. A Study of Consecutive Competitive Reaction Systems. Ph.D. Thesis, University of Michigan, Ann Arbor, Michigan, 1960.

49. Frost, A. A. and Pearson, R. G. Kinetics and Mechanisms; a Study of Homogeneous Chemical Reactions. New York: John Wiley and Sons, 1953.

50. Frost, A. A. and Schwemer, W. C. "The Kinetics of Competitive Consecutive Second Order Reactions - The Saponification of Ethyl Adipate and of Ethyl Succinate." J. Am. Chem. Soc. 74 (1952), 1268.

51. Geissman, T. A. Principles of Organic Chemistry. San Francisco: W. H. Freeman and Co., 1959, 246-247.

52. Gray, R. D. Two Dimensional Effects in Optimal Tubular Reactor Design. Ph.D. Thesis, University of Delaware, 1965.

53. Havorka, R. B. and Kendall, H B. "Tubular Reactor at Low Flow Rates." Chem. Eng. Progr. 56, No. 8 (August, 1960), 58-62.

54. Hawthorn, R. D. "Effect of Radial Temperature Variation in Pipes." A.I.Ch.E. Journal. 6 (1960), 443.

55. Hoarse, M. R. "Determining True Residence Time In Flow System Reactors." Ind. Eng. Chem. 53, No. 3 (March, 1961), 197-198.

56. Hoelscher, H. E. "Non-Uniform Residence Time and the Production of Intermediates in Tubular Reactors." A.I.Ch.E.J. 9, No. 4 (July, 1963), 569-571.

57. Hoelscher, H. E. "Reaction Engineering ... A Bibliography and Literature Guide." Chem. Eng. Progr. Technical Manual, A.I.Ch.E. New York, 1964.

58. Hoffman, R., Astheimer, J. "Effect of Mixing on Output of an Isothermal Heterogeneous Tubular Reactor." Chem. Eng. Sci. 18 (1963), 643.

59. Hooke, R. and Jeeves, T. A. "Direct Search Solution of Numerical and Statistical Problems." J. Assoc. Computing Machinery. 8, No. 2 (April, 1961), 212-219.

60. Horn, F. "Optimale Temperatur und Konzentnationer laüfer." Chem. Eng. Sci. 14 (January, 1961), 77-88.

61. Hougen, O. Watson, K. and Ragatz, R. Chemical Process Principles. 3, New York: John Wiley and Sons, 1958.

62. Ingold, C. K. et al. "The Mechanism and Constitutional Factors Controlling the Hydrolysis of Carboxylic Esters." J. Chem. Soc. (1930), 1032-1057; (1931), 2170-2179.

63. Jackson, R. "A Generalized Variational Treatment of Optimization Problems in Complex Chemical Plants." Chem. Eng. Sci. 19. No. 4 (1964), 253.

64. Jackson, R. "Optimum Startup Procedure for an Autothermic Reaction." Chem. Eng. Sci. 21 (March, 1966), 241-261.

65. Johnson, C. H. J. "Hydrogenation of Carbon in a Tubular Reactor." Australian J. Appl. Sci. 14, No. 4 (December, 1963), 322-339.

66. Katz, S. "Best Temperature Profiles in Plug Flow Reactors." Annals N. Y. Acad. Sci. 84 (1960), 441-478.

67. Katz, S. "Best Operating Points for Staged Systems." I. and E. Fundamentals. 1 (1962), 226-240.

68. Kelly, H. J. "Gradient Theory of Optimal Flight Paths." American Rocket Soc. 30 (October, 1960), 947-954.

69. Kipiniak, W. Dynamic Optimization and Control: A Variational Approach. New York: MIT Press and John Wiley and Sons, 1961.

70. Klinkenberg, A. "Distribution of Residence Times in a Cascade of Mixed Vessels with Backmixing." I. and E. C. Fundamentals. 5, No. 2 (May, 1966), 283.

71. Kno, M. T. and Rubin, D. I. "Optimization Study of Chemical Processes." Can. J. of Chem. Eng. 40, No. 4 (August, 1962), 152-156.

72. Koppel, L. B. "Sampled Data Control of Unstable Processes." I. and E. C. Fundamentals. 5, No. 3 (August, 1966).

73. Kramers, H. and Westerterp, K. Elements of Chemical Reactor Design and Operation. Netherlands University Press, 1963.

74. Krasovskii, N. N. "Optimal Control in Regular Dynamical Systems." Russian Mathematical Surveys. 20, No. 3 (May-June, 1965).

75. Lapidus, L. "On the Dynamics of Chemical Reactors." Chem. Engr. Progr. Symposium Series 57, No. 36 (1961).

76. Lawden, D. F. Optimal Trajectories for Space Navigation. London and Washington: Butterworths Inc., 1963.

77. Lee, E. B. "An Approximation to Linear Bounded Phase Coordinate Control Problems." J. Math. Analysis and Application. 13, No. 3 (March, 1966), 550-564.

78. Lee, E. S. "Optimization by a Gradient Technique." I. and E. C. Fundamentals. 3, No. 4 (November, 1964), 373-380.

79. Lee, E. S. "Optimization by Pontryagin's Maximum Principle on the Analog Computer." A.I.Ch.E. Journal. 10, No. 3 (May, 1964), 309-315.

80. Lee, E. S. "Optimum Design and Operation of Chemical Processes." Ind. Eng. Chem. 55, No. 8 (August, 1963).

81. Lee, E. S. "Quasi-linearization of Non-Linear Boundary Value Problems and Optimization." Chem. Eng. Sci. 21 (February, 1966), 183-194.

82. Levenspiel, O. Chemical Reaction Engineering. New York: John Wiley and Sons, 1965.

83. Levenspiel, O. and Bischoff, K. B. "Patterns of Flow in Chemical Process Vessels." Advances in Chemical Engineering. Vol. 4, New York: Academic Press, 1963.

84. Lloyd, A. and Amundson, N. "Experimental Reduction of Ferric Oxide in a Tubular Reactor." Ind. Eng. Chem. 53 (1961), 19-22.

85. Lynn, S. et al. "Material Transport in Turbulent Gas Streams: Radial Diffusion in a Circular Conduit." A.I.Ch.E. Journal. 3, No.1 (1957), 11-15.

86. Mah, R. S. and Aris, R. "Optimal Policies for First Order Consecutive Reversible Reactions." Chem. Eng. Sci. 19, No. 8 (1964), 541-555.

87. Marcus, L. and Lee, E. B. "On the Existence of Optimal Controls." J. Basic Eng. 84 (1962), 13-22.

88. Mickley, H. S. et al. Applied Mathematics in Chemical Engineering. New York: McGraw-Hill (1957), 193-198.

89. Neustadt, E. "Discrete Time Optimal Control Systems." International Symposium of Non-Linear Differential Equations and Non-Linear Mechanics. New York: Academic Press (1963), Lasalle and Lefschetz editors.

90. Parker, W. A. Comparison of Techniques of Optimal Control of a Chemical Process. Ph.D. Thesis, University of Tennessee, 1966.

91. Pauls, A. C. et al. "Instrumentations Role in Reactor Response Studies." I.S.A. Journal. 7, No. 11 (November, 1960), 46-51.

92. Perry, J. H. Chemical Engineers' Handbook. 3rd Ed., New York: McGraw-Hill (1950), 374.

93. Petersen. E. E. Chemical Reaction Analysis. Englewood Cliffs: Prentice Hall, 1965.

94. Pontryagin, L. S. et al. Mathematical Theory of Optimal Processes. New York: John Wiley (1962).

95. Powell, M. J. D. "An Efficient Method for Finding the Minimum of a Function of Several Variables without Calculating Derivatives." Computer Journal. 7, No. 2 (1964), 155-162.

96. Raines, G. E. and Corrigan, T. E. "The Use of Axial Dispersion Model to Predict Conversions of First and Second Order Reactions." Chem. Eng. Progr. Symposium Series, 63, No. 72, 1967.

97. Reid, R. and Sherwood, T. Properties of Gases and Liquids. New York: McGraw-Hill, 1958.

98. Roberts, S. M. "Dynamic Programming and Lagrangian Multipliers." I. and E.C. Fundamentals. 2 (1963), 224-228, 231-235.

99. Roques, Henri. "Contribution A L'Etude Statique et Cinetique de Systems Gaz Carbonique." Carbonate Annales de Spéléologie. XIX, No. 2 (1964), 286-287.

100. Rosenbrock, H. H. "An Automatic Method for Finding the Greatest or Least Value of a Function." Computer J. 3, No. 3 (October, 1960), 175-184.

101. Rosenbrock, H. H. and Storey, C. Computational Techniques for Chemical Engineers. Oxford: Pergamon Press, 1966.

102. Rothenberger, B. F. Quasilinearization as a Numerical Method for the Solution of Optimal Control Problems With and Without Constraints. Ph.D. Thesis, Princeton University, 1966.

103. Rothenberger, B. F. and Lapidus, L. "Quasilinearization and State Constraints Systems." A.I.Ch.E. Journal. 13, No. 5, 982-988.

104. Roxin, E. "A Geometric Interpretation of Pontryagin's Maximum Principle." in International Symposium on Non-linear Differential Equations and Non-linear Mechanics. Lasalle and Lefschetz editors, New York: Academic Press, 1963.

105. Rozonoer, L. T. "L. S. Pontryagin Maximum Principle in the Theory of Optimum Systems." Auto and Remote Control. 20, No. 10 (October, 1959), 1288-1302; No. 11 (November, 1959), 1405-1421; No. 12 (December, 1959), 1517-1532.

106. Satterfield, C. N. and Young, R. S. S. "Diffusion and Heterogeneous Reaction in a Tubular Reactor." I. and E. C. Fundamentals. 2 (1963), 291-328.

107. Shatkhan, F. A. "Application of the Maximum Principle to the Optimization of Parallel Chemical Reactions." Auto. and Remote Control. 25, No. 3 (1964), 344.

108. Siebenthal, C. D. and Aris, R. "Application of Pontryagin's Maximum Principle to Control of CSTR." Chem. Eng. Sci. 19, No. 10 (October, 1964), 729-747.

109. Siebenthal, C. D. and Aris, R. "Studies in Optimization Part VII Application of Pontryagin's Method to Control of Batch and Tubular Reactors." Chem.Eng. Sci. 19, No. 10 (October, 1964), 747-761.

110. Sieder, E. N. and Tate, G. E. Ind. Eng. Chem. 28 (1936), 1429-1435.

111. Simpkins, C. R. Dynamics and Control of Tubular Chemical Reactors. Ph.D. Thesis, University of Delaware, 1966.

112. Smith, J. W. Gowen, R. A. and Wasmund, B. "Diffusion Coefficients and Temperaure Profiles for Turbulent Heat Transfer to Water in Pipes." A.I.Ch.E. Fifty-ninth Annual Meeting-Symposium 10. December, 1966.

113. Spencer, J. L. The Effect of Axial Mixing on a Tubular Chemical Reactor. Ph.D. Thesis, University of Pennsylvania, 1961.

114. Taylor, G. I. Proceedings of the Royal Society. A223 (1954), 446; A225 (1954), 473; A219 (1953), 186.

115. Tichacek, L. J. "Selectivity in Chemical Reactors." A.I.Ch.E. Journal. 9, No. 3 (May, 1963), 394-399.

116. Tou, J. Modern Control Theory. New York: McGraw-Hill, 1963.

117. Tomovic, R. Sensitivity Analysis of Dynamic Systems. New York: McGraw-Hill, 1963.

118. Van de Vusse, J. G. and Voetter, H. "Optimum Pressure and Concentration Gradients in Tubular Reactors." Chem. Eng. Sci. 14 (January, 1961), 90-100.

119. Van Heerden, C. "Autothermic Processes - Properties of Reactor Design." Ind. Eng. Chem. 45 (1953), 1242-1247.

120. Van Kreuelen, D. W. "Selectivity of Consecutive Reactions." Chem. Eng. Sci. 14 (1961), 58-71.

121. Weger, E. and Hoelscher, H. E. "Rate Studies in Tubular Reactors." A.I.Ch.E. Journal. 3 (1957), 153-156.

122. Wehner, J. F. and Wilhelm, R. H. Chem. Eng. Sci. 6 (1956), 89-98.

123. Wei, J. and Prater, C. D. "The Structure and Analysis of Complex Reaction Systems." Advances in Catalysis. Vol. 13, New York: Academic Press, 1962.

124. Weinstein, H. and Adler, R. J. "Micromixing Effects in Continuous Chemical Reactors." Chem. Eng. Sci. 22, No. 1 (January, 1967), 65-77.

125 Westheimer, F. H., Jones, W. A. and Lad, R. A. "Electrostatic Influence of Substituents on Reaction Rates." J. Chem. Phys. 10 (1942), 478-484.

126. Wilde, D. J. and Beightler, C. S. Foundations of Optimization. Englewood Cliffs, New Jersey: Prentice Hall Inc., 1967.

127. Wilhelm, R. H. "Progress Towards the A Priori Design of Chemical Reactors." Pure and Appl. Chem. 5 (1962), 403.

128. Wood, R. D. and Stevens, W. F. "Optimum Volume Ratios for Maximum Residence Time in CSTR Sequences." Chem. Eng. Sci. 19, No. 6 (June, 1964), 426-429.

129. Zellnick, H. E., Sondack, N. E. and Davis, R. S. "Gradient Search Optimization." Chem. Eng. Progr. 58, No. 8 (August, 1962), 35-41.